FEASIBILITY STUDY OF THE UNIVERSITY OF UTAH TRIGA REACTOR POWER UPGRADE IN RESPECT TO CONTROL ROD SYSTEM

by

Avdo Cutic

A thesis submitted to the faculty of
The University of Utah
in partial fulfillment of the requirements for the degree of

Master of Science

in

Nuclear Engineering

Department of Civil and Environmental Engineering

The University of Utah

December 2012

The University of Utah Graduate School

STATEMENT OF THESIS APPROVAL

The thesis of Avdo Cutic

has been approved by the following supervisory committee members:

Tatjana Jevremovic	, Chair	May 18,2012
		Date Approved
Dong-Ok Choe	, Member	May 18, 2012
		Date Approved
Haori Yang	, Member	May 18, 2012
		Date Approved

and by Paul Tikalsky , Chair of

the Department of Civil and Environmental Engineering

and by Charles A. Wight, Dean of The Graduate School.

ABSTRACT

The objectives of this thesis are twofold: to determine the highest achievable power levels of the current University of Utah TRIGA Reactor (UUTR) core configuration with the existing three control rods, and to design the core for higher reactor power by optimizing the control rod worth. For the current core configuration, the maximum reactor power, eigenvalue k_{eff}, shutdown margin, and excess reactivity have been measured and calculated. These calculated estimates resulted from thermal power calibrations, and the control rod worth measurements at various power levels. The results were then used as a benchmark to verify the MCNP5 core simulations for the current core and then to design a core for higher reactor power. This study showed that the maximum achievable power with the current core configuration and control rod system is 150kW, which is 50kW higher than the licensed power of the UUTR. The maximum achievable UUTR core power with the existing fuel is determined by optimizing the core configuration and control rod worth, showing that a power upgrade of 500 kW is achievable. However, it requires a new control rod system consisting of a total of four control rods. The cost of such an upgrade is $115,000.

CONTENTS

LIST OF FIGURES

LIST OF TABLES

ACKNOWLEDGEMENTS

My greatest gratitude goes to Dr. Tatjana Jevremovic for her unconditional support and guidance during my graduate school years. Also, I would like to express my gratitude to Dr. Dong-OK Choe and Dr. Haori Yang for their support and guidance. In addition, I would like to thank my school friends, Philip Babitz, Jason Rapich, Todd Sherman, Andrey Rybalkin, Christian Amevi Adjei, and Can Liao, for their help with my schoolwork.

CHAPTER 1

INTRODUCTION

1.1. Motivation

The University of Utah TRIGA Reactor (UUTR) was licensed on October 31, 2012 to operate at a maximum power of 100kW for the next 20 years. This is an adequate power level when considering a wide range of experiments such as sample irradiation, neutron activation analysis (NAA), cadmium ratio experiments, some studies on irradiation damage to materials, analysis of the radiation effects on various electronic devices, and very basic experiments pertaining to biological and medical studies. However, a higher reactor power would open up a plethora of new opportunities for expanding current use of the reactor facility. A higher reactor power would provide a higher neutron flux. It will significantly shorten the irradiation time of samples during NAA, material irradiation, and provide opportunities for designing new experiments such as but not limited to fast neutron studies, designing a fast neutron pencil beam, new types of experiments pertaining to material science and engineering, biology and medical studies, and many more. The higher reactor power will also provide more opportunities to broaden training and education, and further our collaboration with the industry sector.

1.2. Thesis Objectives

Thesis objectives are summarized as follows:

1. Investigate the current UUTR (called the "24B") core configuration by determining the highest attainable power level with the existing control rod system.

2. Experimentally determine the worth of each currently existing control rod, the core excess reactivity, and the shut down margins.

3. Experimentally measure the temperature coefficient of the fuel during regular UUTR operation and extrapolate for higher power levels.

4. Use N-Particle Monte Carlo Neutron Transport Code (MCNP5) to determine the worth of each control rod, the core excess reactivity, the shut down margins, and temperature coefficient of the fuel; evaluate these parameters for the current core configuration and new core configurations leading to higher UUTR core power levels.

5. Propose new core configurations and new control rods system design if needed for the highest attainable core power given the available fuel elements.

6. Determine the cost associated with a feasible reactor power upgrade.

1.3. Organization of the Thesis

The University of Utah TRIGA Reactor is described in Chapter 2. In Chapter 3, the measured control rod worth of the current UUTR is detailed. In Chapter 4, the relationship between control rod position (reactivity insertion) and reactor power is described. The experimentally determined relationship between the fuel temperature, reactivity insertion, and reactor power is described in Chapter 5. In Chapter 6, the numerical estimates of the relationship between reactivity insertion, reactor power, and fuel temperature and comparisons to experimental values are

presented. A summary of the experimental values and the numerical calculations based on MCNP5 is given in Chapter 6. Chapter 7 concludes with the maximum achievable reactor power of the current UUTR control rod system. In Chapter 8, three UUTR power upgrade designs are described. Chapter 9 summarizes the economical and monetary requirements of the three new UUTR higher power reactor designs. Chapter 10 describes the sources of error of all calculations that were shown in this thesis.

CHAPTER 2

UNIVERSITY OF UTAH TRIGA REACTOR

2.1. Introduction

TRIGA (Training, Research, Isotope, General Atomics) is a pool-type research reactor specifically designed to be used by educational and research institutions for training and research [1]. The TRIGA reactor uses light water as a coolant and moderator and does not produce electricity [2]. Its fuel is made with zirconium hydride incorporated into a uranium matrix; this mixture creates a large prompt negative temperature coefficient causing a large negative reactivity insertion [1], which shuts down the reactor if the fuel temperature is increased during a sudden power excursion. Therefore, by inherent design, the TRIGA reactors are passively safe and cannot suffer from a core meltdown.

2.2. UUTR Reactor Core Configuration

The University of Utah TRIGA Reactor (UUTR) went critical for the first time in September 30, 1975. The UUTR is an in-ground pool-type research reactor of hexagonal core geometry licensed to operate at 100kW. The upper and lower grid plates of the core are designed to hold the fuel elements and are supported by the side plates. The upper and lower plates are 1.905cm (0.75in) plate 6061-T6 aluminum while the side plates are 0.635cm (0.25in) thick. In total, 127 locations for fuel elements (or moderators, or reflectors) are arranged in concentric rings labeled "A" thru "G"; each consecutive ring has a larger diameter and thus a number of

locations available for fuel elements. Each top location has a diameter of 3.83cm (1.505in) and a hexagonal lattice pitch of 4.369cm (1.72inch). The lower location, however, has only a 0.635cm (0.25in) diameter hole that allows the inserted pin to be held securely in place [3].

The current "24B" UUTR core configuration is shown in Figure 2-1. In addition to fuel elements in the core, there are 12 graphite reflector elements and 12 heavy water reflector elements; all are placed in the "F" or "G" rings. The current core configuration has three control rods: regulation located at "D1", safety located at "D7", and shim located at "D13". Instrumented fuel elements, located in "C4" and "D11", are used for fuel temperature measurements. The Pu-Be source is present in the core while it is shut down and during its startup; it is stored in location "G19". Four sample irradiation sites facilities (ports) are available in the core: the central irradiator (CI) located in "A1", pneumatic irradiator (PI) located in "D4", fast neutron irradiation facility (FNIF), and the thermal irradiator (TI) [3].

2.3. UUTR Fuel Elements

UUTR fuel contains a nominal 8.5 weight percent of U-235 of less than 20% enrichment. The two types of fuel element cladding are stainless steel and aluminum. Both fuel types have graphite chip inserts on the top and bottom in order to minimize neutron leakage. The current "24B" core configuration requires 78 fuel elements to reach criticality [4].

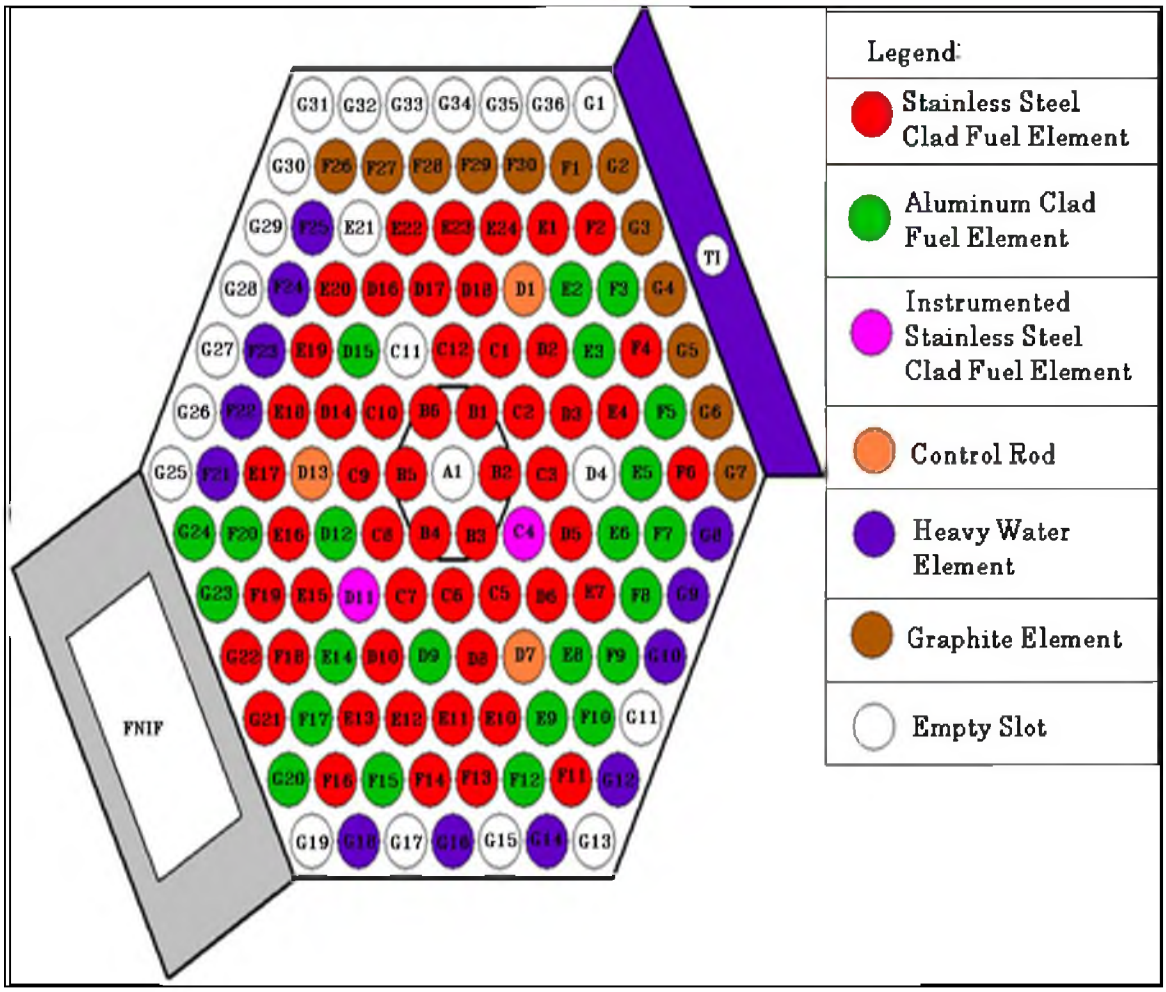

Figure 2-1. Schematic of UUTR Configuration "24B"

2.4. D_2O and Graphite Reflector Elements

The 12 graphite reflector elements and 12 heavy water reflector elements are encompassed in aluminum cladding. The purpose of a reflector in the core is to minimize neutron leakage from the core, hence increasing the k_{eff} without increasing the size of the core. The physical size of the reflector elements is identical to that of the fuel elements.

2.5. UUTR Control Rods

The UUTR core contains three control rods, each located in the "D" ring, as shown in Fig. 2-1. Each rod varies in its negative reactivity or the worth. The safety,

shim, and regulation rods have worth of $2.25, $1.51, and $0.27, respectively. These values must be reevaluated every 12 months [5].

The UUTR control rods are composed of aluminum clad boron carbide with each rod having its own driver (Fig. 2-2). The driver consists of a rack & pinion drive motor, a potentiometer – to measure percent position, and an electromagnet – which holds the rod to the driver shaft and limit switches and which indicates the rod's upper and lower limit positions. A scram signal cuts the current to the electromagnet and releases the rods into the core. Once the rods are dropped, a small spring protects the rods from being damaged at the bottom of the drop. Control rod insertion cannot exceed $0.30/sec. It takes about 77 seconds to lower a rod 100%. The rods must not take more than 2 seconds to drop during a scram. Experiments indicate that the UUTR control rods take about 0.9 seconds to fully drop. The control rods must be visually inspected every 2 years through control rod inspection done during fuel inspection. Figure 2-2 shows the control rod drive [4].

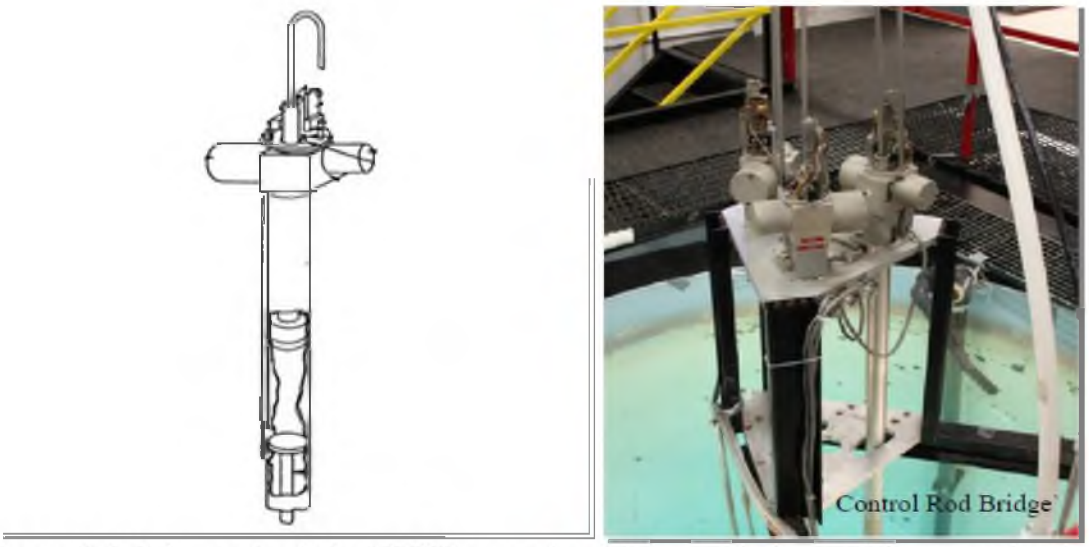

Figure 2-2. Schematic of the UUTR control rod drive and photo of the control rod bridge

The shim and safety control rods are identical in their dimensions, with height of 109.22cm and diameter of 2.223cm. Concurrently, the regulation rod is 109.22cm in height, and has a diameter of 0.635cm. The regulation, shim and safety rods are located in “D1”, “D7”, and “D13”, respectively, Fig. 2-1. All three control rods are held into place by an electromagnet. The power to the electromagnets is supplied by the reactor console. In the event of scram, the power to the magnets is cut off, and as a result of gravity, the control rods fall and become fully inserted into the core [4].

CHAPTER 3

UUTR CONTROL ROD WORTH MEASUREMENTS

3.1. Introduction

It is important to accurately determine the worth of each control rod of the current UUTR control rod system. In this chapter, the control rod worth, the measurements of the core excess reactivity, and the shut down margin are described and measured. In addition, the methods used to determine the value of each control rod are explained.

3.2. UUTR Core Excess Reactivity

The reactor core excess reactivity is defined as additional reactivity, which is available right at the point when the reactor has been brought critical from a subcritical state [6]. Figure 3-1 illustrates the principle of reactivity balance in a research reactor. The available excess reactivity is required in order to compensate for the negative reactivity inserted into the core due to experiments, fuel burn up, production of fission product poisons such as xenon and samarium, and the power defect due to the negative temperature coefficient of fuel [6].

3.3. Shut Down Margin

The shut down margin (SDM) is defined as the amount of negative reactivity that would be inserted into the core during a steady state critical condition in the event of a scram disregarding the most valuable rod [7].

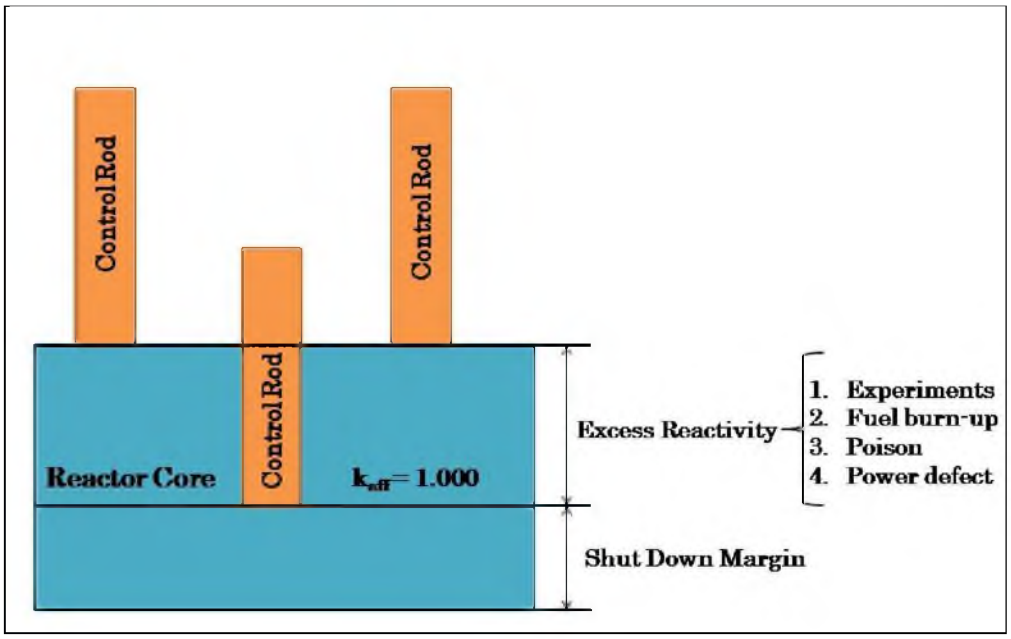

Figure 3-1. Schematic of reactivity balance in a research reactor

The most valuable rod is the control rod that has the ability to insert the highest amount of reactivity by itself – which turns out to be the safety control rod for the UUTR. The shut down margin is calculated by:

$$SDM = \rho_{TOTAL} - \rho_{MVR} - \rho_{EX} \tag{3.1}$$

where:

ρ_{TOTAL} = Reactivity of all Rods

ρ_{MVR} = Most Valuable Rod (safety rod)

ρ_{EX} = Core Excess Reactivity

3.4. Control Rod Drop Method

The dollar worth of each control rod is determined by a rod drop experiment; an experiment is performed at least semiannually at the UUTR. The rod drop method is the most widely used to determine the control rod worth. At the beginning

of the rod drop experiment, the control rod, whose worth is to be measured, is fully withdrawn from the core. Then, the UUTR is brought critical at a power of 1kW. One kilowatt of power is high enough to allow for measuring the control rod worth. At the same time, this power level is low enough to neglect Xenon poisoning and the effect of temperature coefficient. In other words, the UUTR is in a cold critical condition, which means that it is Xenon free while the fuel and water temperatures are below 40°C [8].Once the power of 1kW is stabilized, the magnetic disconnect switch holding the control rod is pressed, releasing only the measuring control rod into the core. During this procedure, the power levels are graphed with respect to time by using an internally developed computer program [8]. This computer program was developed in order to solve the Inhour equation and the relative neutron flux simultaneously [8]. Finally, the power level graph is analyzed and the control rod worth is determined. This procedure is repeated for every control rod. At the end of the experiment, a numerical table is produced giving the values of each control rod. The measured control rod worth, shut down margin, and excess reactivity for the past 10 years are summarized in Table 3-1 [6].

3.5. Integral Control Rod Worth

The integral control rod worth of each control rod can be derived based on the results derived from the rod drop experiment. The reactivity insertion of each control rod follows a sine curve [6, 9]:

$$\rho(\$) = A * sin^2\left(\frac{\pi * x}{2 * H}\right) = A * sin^2\left(\frac{\pi * (\%OUT)}{2}\right) \quad (3.2)$$

Table 3-1. UUTR semiannually measured control rod worth

Date of Experiment	Safety Control Rod ($)	Shim Control Rod ($)	Regulation Control Rod($)	Shut Down Margin ($)	Excess Reactivity ($)	Total Control Rod Worth ($)
Aug 16, 2001	2.230	1.560	0.240	0.791	1.013	4.030
Aug 27, 2003	2.223	1.503	0.280	1.012	0.771	4.006
Apr 2, 2004	2.923	1.713	0.300	1.135	0.879	4.936
Aug 26, 2004	2.208	1.493	0.280	0.975	0.798	3.981
Nov 17, 2005	2.198	1.494	0.283	0.967	0.810	3.975
Feb 24, 2005	2.200	1.460	0.263	1.113	0.610	3.923
Aug 4, 2005	2.190	1.467	0.270	1.119	0.618	3.927
Nov 9, 2005	2.230	1.415	0.267	1.074	0.608	3.912
Dec 27, 2005	2.227	1.553	0.273	1.006	0.761	4.053
Feb 17, 2006	2.227	1.557	0.237	1.068	0.758	4.021
Aug 25, 2006	2.017	1.463	0.270	0.983	0.751	3.750
Nov 8, 2006	2.120	1.053	0.263	0.996	0.771	3.436
Feb 22, 2007	2.173	1.547	0.273	1.033	0.787	3.993
Aug 28, 2007	2.510	1.700	0.276	1.126	0.850	4.486
Jan 24, 2008	2.173	1.457	0.207	0.855	0.838	3.837
Feb 25, 2008	2.173	1.493	0.273	0.967	0.800	3.939
Aug 27, 2008	2.290	1.563	0.293	0.991	0.865	4.146
Feb 24, 2009	2.170	1.553	0.323	1.020	0.856	4.046
Aug 26, 2009	2.297	1.587	0.290	0.744	1.137	4.174
Dec 18, 2009	2.293	1.517	0.277	1.027	0.586	4.087
Feb 22, 2010	2.263	1.530	0.277	1.172	0.635	4.070
Apr 30, 2010	2.243	1.550	0.287	1.018	0.819	4.080
Feb 18, 2011	2.232	1.543	0.283	0.981	0.845	4.058
Aug 13, 2011	2.293	1.543	0.290	0.948	0.884	4.126
AVERAGE	**2.254**	**1.513**	**0.274**	**1.005**	**0.794**	**4.041**
Standard Deviation	**0.166**	**0.119**	**0.023**	**0.102**	**0.127**	**0.264**

where:

ρ *($)* = cumulative reactivity inserted of control rod

A = total worth of the control rod

x = position of the control rod

H = total height of the control rod

%OUT = percent of the control rod withdrawn out of the core

As the rod is withdrawn from the lower part of the core, cumulative reactivity is inserted at a slower rate due to a lower neutron flux. However, reactivity insertion per unit length of control rod will start to increase with each incremental raise towards the center of the core. The rate of reactivity insertion is the highest at the center of the core where the flux is the highest. As the control rod continues to be raised towards the top of the core, the reactivity insertion will start to decrease due to decreasing neutron fluxes [6]. Values of reactivity inserted into the core versus control rod position are shown in Figure 3-2. These values were obtained by utilizing equation (3.2) and by using the average values of each control rod from Table 3-1.

3.6. Control Rod Shadowing Effect

Control rod shadowing is an effect where the position or the repositioning of one control rod causes a reactivity change in another control rod. This effect is evident in the UUTR because the safety and the shim control rods are identical in size; they also have the same boron content, yet their worth is different; this is because the neutron flux is higher around the safety rod as compared to the shim control rod, as seen in Figure 3-3. The worth of a control rod is a direct function of the thermal neutron flux and the thermal diffusion length to which the control rod is exposed [6, 9].

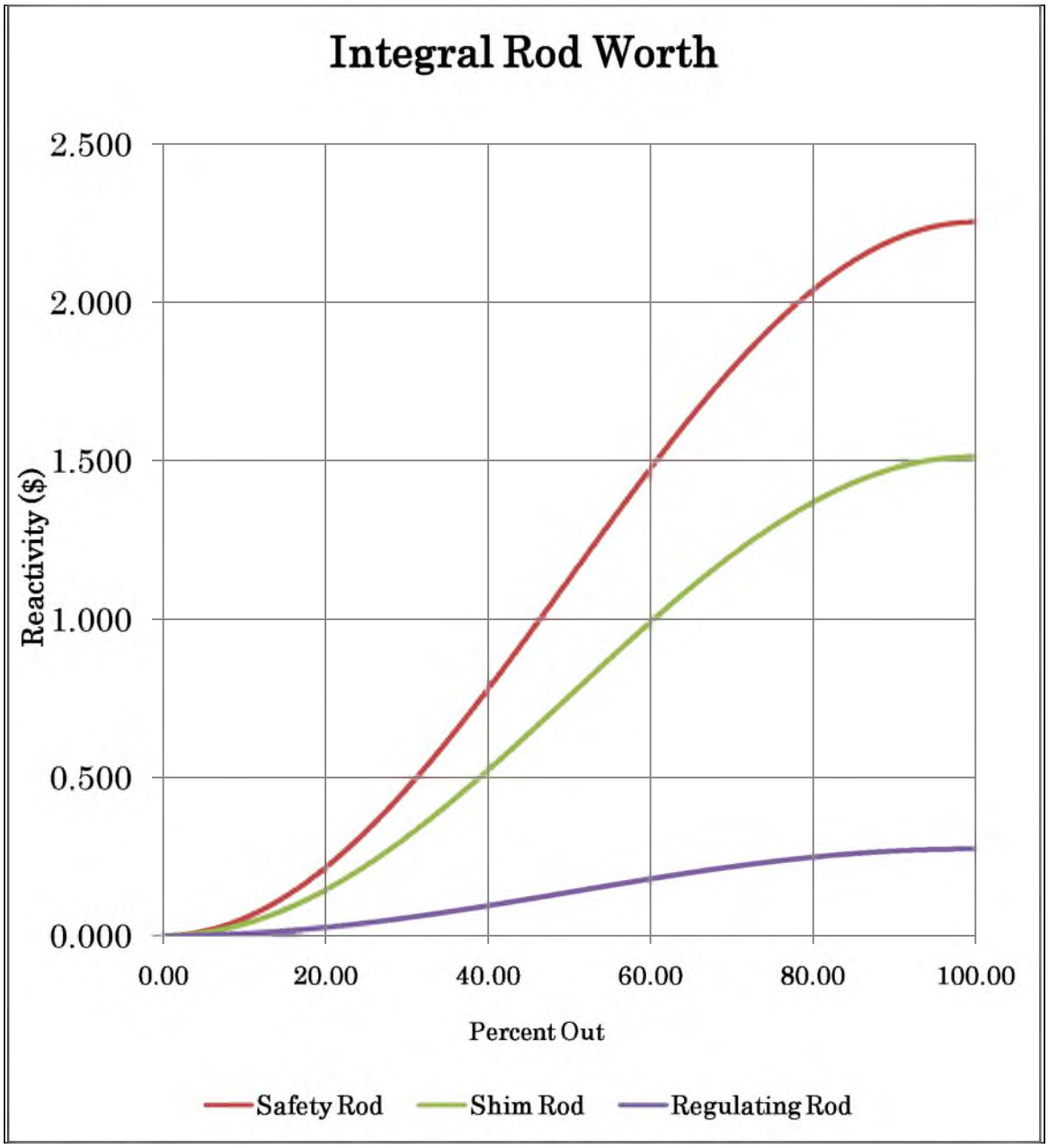

Figure 3-2. Safety, shim, and regulation integral control rod worth in UUTR

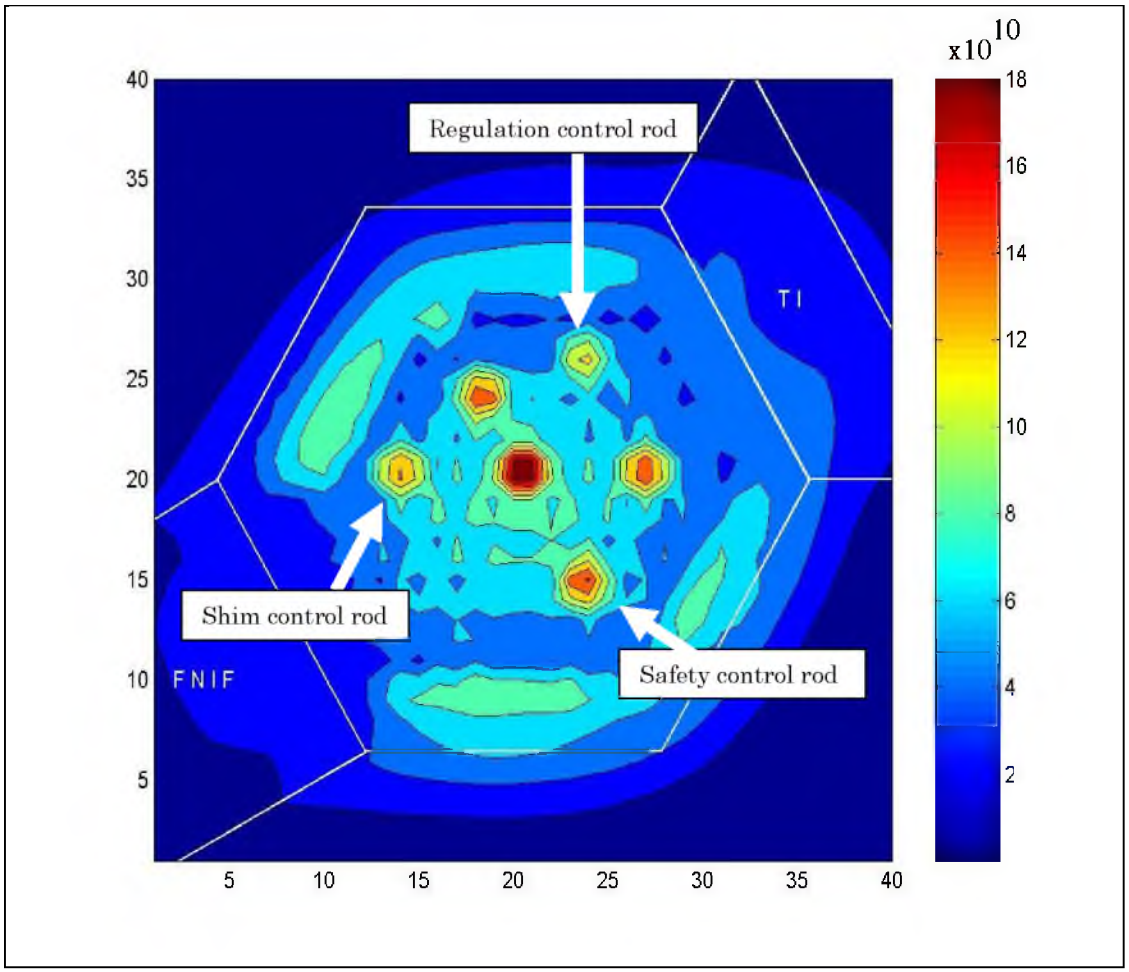

Figure 3-3. Illustration of the control rod shadowing effect

To illustrate the control rod shadowing effect, Figure 3-3 clearly shows that the safety control rod is exposed to the highest thermal flux compared to the other control rods; as a result, this control rod has the highest dollar value. On the other hand, the regulation control rod is exposed to the lowest thermal flux value as compared to the safety control rod and shim control rod and therefore has the lowest dollar value.

CHAPTER 4

REACTIVITY INSERTION EXPERIMENTS

4.1. Introduction

It has been shown that the reactor power is proportional to reactivity inserted [10].Five reactivity insertion experiments are conducted. The main objective of these experiments is to confirm and validate the already established relationship between the reactivity insertion and reactor power. Another objective of these experiments is to confirm the shape of the integral control rod curve [11]. Once this relationship between reactivity insertion and UUTR reactor power is examined, a curve fit could then be used to forecast higher powers with respect to control rod position, thus providing information on the maximum practical power of the UUTR with the existing control rod system [12].

4.2. Experimental Procedure

Initially, data from the UUTR log books [13] is used to determine the average values of reactivity insertion with respect to reactor power. Table 4-1 shows the average reactor power vs. control rod position or reactivity inserted. The change in reactivity [$\Delta\rho$ (\$)] is defined by:

$$\Delta\rho\,(\$) = R_2\,(\$) - R_1\,(\$) \tag{4.1}$$

Table 4-1. Average cumulative reactivity insertion vs. UUTR power

Safety Control Rod (% out)	100	$2.254		
Regulation Control Rod (% out)	65.3	$0.200		
Reactor Power (kW)	Shim Control Rod (% out)	Shim Control Rod Reactivity($)	$\Delta\rho$ ($)	Cumulative Inserted Reactivity ($)
1	50.9	0.778	----------	3.232
10	54.1	0.853	0.076	3.308
20	57.3	0.928	0.075	3.383
30	60.6	1.004	0.075	3.458
40	63.0	1.057	0.053	3.511
50	64.9	1.098	0.041	3.552
60	67.8	1.158	0.060	3.612
70	70.0	1.201	0.043	3.655
80	72.4	1.246	0.045	3.700
90	75.1	1.293	0.047	3.747

where:

R_1($) = Cumulative Reactivity Inserted before power increase

R_2($) = Cumulative Reactivity Inserted after power increase

As shown in Table 4-1, when the safety control rod is 100% out, the reactivity insertion into the core corresponds to $2.254. When the regulation control rod is 65.3% out, the reactivity insertion is $0.2 into the core. In order to bring the UUTR to 1kW of power, the shim control rod has to be withdrawn to 50.9% out --this provides reactivity insertion of $0.778 and a cumulative inserted reactivity if $3.232.The cumulative reactivity insertion contributed by all three control rods at their respective positions are listed in Table 4-1 for each power level [14].

Newly developed experimental tests at the UUTR described as runs A thru E (Table 4-2) are used to examine and confirm this relationship between reactivity insertion and reactor power as shown in Table 4-1. The experimental runs differ by the control rod position in the core, as shown in Table 4-2.

4.3. Reactivity Insertion Experiments

The reactivity insertion experiments results are summarized in Table 4-3 through Table 4-8. These show the reactor power compared to the measured shim control rod percent out and the expected shim control rod percent out, which is based on data obtained from reactor operations log books [13].Concurrently, the measured cumulative reactivity insertion is compared with the expected value, which is also obtained from log book data. Operational log books are UUTR facility's internal documents that are used to record the reactor power, control rod position, fuel temperature, and other measures during UUTR operations. The reactivity insertion experiments are used to confirm the relationship between the reactivity insertion and reactor power. Therefore, the terms "expected value" or "predicted value" refer to the values that were determined to be the average values from the UUTR operation log books.

Table 4-2. Experimental setup of reactivity insertion experiments at UUTR

	Run A	Run B	Run C	Run D	Run E
Safety Control Rod	100%	100%	100%	100%	100%
Regulation Control Rod	20%	40%	60%	80%	vary
Shim Control Rod	vary	vary	vary	vary	vary

Table 4-3. Results of Run A, safety control rod at 100% out, regulation control rod at 20% out

Power (kW)	Measured Shim Control Rod (% out)	Predicted Shim Control Rod (% out)	Shim Control Rod Percent Difference	Measured Cumulative Inserted Reactivity ($)	Cumulative Reactivity Inserted Log Books ($)	Cumulative Inserted Reactivity Percent Difference
1	57.1	58.5	2.4%	3.204	3.232	0.9%
10	60.7	61.5	1.3%	3.286	3.308	0.7%
20	63.5	65.0	2.3%	3.348	3.383	1.0%
30	66.4	68.8	3.4%	3.409	3.458	1.4%
40	69.3	71.5	3.1%	3.467	3.511	1.2%
50	71.8	74.0	3.0%	3.515	3.552	1.0%
60	74.5	77.0	3.2%	3.563	3.612	1.4%
70	77.3	80.5	4.0%	3.609	3.655	1.3%
80	80.3	84.0	4.4%	3.653	3.700	1.3%
90	84.5	88.8	4.8%	3.694	3.747	1.4%

The percent difference is defined as the absolute percent difference between the predicted values (as determined from the log books) and the measured values during the reactivity insertion experiments.

$$Percent\ Difference = \left|\left(\frac{V_p - V_m}{V_p}\right) * 100\%\right| \quad (4.2)$$

where:

V_p = Predicted value as per averages taken from log books

V_m = Value that was measured

Table 4-4. Results of Run B, safety control rod at 100% out, regulation control rod at 40% out

Power (kW)	Measured Shim Control Rod (% out)	Predicted Shim Control Rod (% out)	Shim Control Rod Percent Difference	Measured Cumulative Inserted Reactivity ($)	Cumulative Reactivity Inserted Log Books ($)	Cumulative Inserted Reactivity Percent Difference
1	55.5	54.8	1.3%	3.231	3.232	0.0%
10	58.5	58.0	0.9%	3.308	3.308	0.0%
20	61.8	61.0	1.2%	3.377	3.383	0.2%
30	65.3	64.0	2.0%	3.444	3.458	0.4%
40	68.0	66.8	1.8%	3.503	3.511	0.2%
50	70.3	69.3	1.4%	3.554	3.552	0.0%
60	73.0	71.6	2.0%	3.597	3.612	0.4%
70	76.0	74.3	2.3%	3.647	3.655	0.2%
80	78.8	77.0	2.3%	3.693	3.700	0.2%
90	82.0	80.0	2.5%	3.738	3.747	0.2%

Table 4-5. Results of Run C, safety control rod at 100% out, regulation control rod at 60% out

Power (kW)	Measured Shim Control Rod (% out)	Predicted Shim Control Rod (% out)	Shim Control Rod Percent Difference	Measured Cumulative Inserted Reactivity ($)	Cumulative Reactivity Inserted Log Books ($)	Cumulative Inserted Reactivity Percent Difference
1	50.5	52.0	2.9%	3.216	3.232	0.5%
10	53.6	55.0	2.5%	3.288	3.308	0.6%
20	56.8	57.8	1.6%	3.365	3.383	0.5%
30	59.6	61.5	3.1%	3.429	3.458	0.8%
40	62.1	64.0	3.0%	3.486	3.511	0.7%
50	64.5	66.0	2.3%	3.541	3.552	0.3%
60	66.9	68.5	2.3%	3.594	3.612	0.5%
70	69.5	71.0	2.1%	3.645	3.655	0.3%
80	71.8	73.5	2.3%	3.688	3.700	0.3%
90	74.4	76.3	2.4%	3.738	3.747	0.3%

Table 4-6. Results of Run D, safety control rod at 100% out, regulation control rod at 80% out

Power (kW)	Measured Shim Control Rod (% out)	Predicted Shim Control Rod (% out)	Shim Control Rod Percent Difference	Measured Cumulative Inserted Reactivity ($)	Cumulative Reactivity Inserted Log Books ($)	Cumulative Inserted Reactivity Percent Difference
1	46.6	49.0	4.9%	3.183	3.232	1.5%
10	50.0	52.0	3.8%	3.263	3.308	1.4%
20	53.3	55.0	3.1%	3.342	3.383	1.2%
30	56.3	58.3	3.3%	3.412	3.458	1.3%
40	58.8	60.8	3.2%	3.470	3.511	1.2%
50	61.1	62.8	2.6%	3.552	3.552	0.0%
60	63.7	65.0	2.0%	3.579	3.612	0.9%
70	66.0	67.5	2.2%	3.628	3.655	0.7%
80	68.3	69.8	2.1%	3.675	3.700	0.7%
90	71.0	72.0	1.4%	3.727	3.747	0.5%

Table 4-7. Results of Run E Part 1; safety control rod at 100% out

Power (kW)	Measured Regulation Control Rod (% out)	Predicted Regulation Control Rod (% out)	Regulation Control Rod Percent Difference	Measured Shim Control Rod (% out)	Predicted Shim Control Rod (% out)	Shim Control Rod Percent Difference
1	20.0	20.0	0.0%	56.0	58.3	3.9%
10	30.0	30.0	0.0%	59.3	60.3	1.7%
20	40.0	40.0	0.0%	60.7	62.0	2.1%
30	50.0	50.0	0.0%	61.9	63.5	2.5%
40	60.0	60.0	0.0%	62.5	64.0	2.3%
50	70.0	70.0	0.0%	63.1	64.1	1.6%
60	80.0	80.0	0.0%	63.8	65.5	2.6%
70	90.0	90.0	0.0%	64.7	66.6	2.9%
80	90.0	90.0	0.0%	67.1	68.9	2.6%
90	90.0	90.0	0.0%	69.9	71.3	2.0%

Table 4-8. Results of Run E Part 2; safety control rod at 100% out

Power (kW)	Measured Cumulative Inserted Reactivity ($)	Cumulative Reactivity Inserted Log Books ($)	Cumulative Inserted Reactivity Percent Difference
1	3.178	3.232	1.7%
10	3.284	3.308	0.7%
20	3.355	3.383	0.8%
30	3.424	3.458	1.0%
40	3.479	3.511	0.9%
50	3.530	3.552	0.6%
60	3.576	3.612	1.0%
70	3.614	3.655	1.1%
80	3.664	3.700	1.0%
90	3.720	3.747	0.7%

4.4. UUTR Power vs. Reactivity Insertion

The reactor power vs. reactivity insertion data sets are used to extrapolate for higher power levels of the current "24B" core configuration. This is based on historical averages, which were obtained from the UUTR log books as well as the results obtained from reactivity insertion experiments. Table 4-9, Table 4-10, and Table 4-11 show the measured reactivity insertion values, as well as the average cumulative reactivity insertion values for various UUTR power levels from the reactivity insertion experiments as well as values taken from UUTR operation log books. These data are then plotted in Figure 4-1 and extrapolated for higher reactor powers. It is shown in Figure 4-1 that the maximum attainable reactor power for the current UUTR control rod system is 150kW +/-5kW. This turns out to be 50kW higher than licensed power of the current UUTR. The 5kW variance comes from the fact that when the data set is extrapolated for higher powers, the accuracy of the final value turns out to be within 5kW.

Table 4-9. Reactivity insertion vs. UUTR power level; results from Run A, Run B, and Run C

Power (kW)	Measured Cumulative Reactivity Inserted Run A ($)	Measured Cumulative Reactivity Inserted Run B ($)	Measured Cumulative Reactivity Inserted Run C ($)
1	3.204	3.231	3.216
10	3.286	3.308	3.288
20	3.348	3.377	3.365
30	3.409	3.444	3.429
40	3.467	3.503	3.486
50	3.515	3.554	3.541
60	3.563	3.597	3.594
70	3.609	3.647	3.645
80	3.653	3.693	3.688
90	3.694	3.738	3.738

Table 4-10. Reactivity insertion vs. UUTR power level results from Run D, Run E, and UUTR operations log books

Power (kW)	Measured Cumulative Reactivity Inserted Run D ($)	Measured Cumulative Reactivity Inserted Run E ($)	Measured Cumulative Reactivity Inserted Log Books ($)
1	3.183	3.178	3.232
10	3.263	3.284	3.308
20	3.342	3.355	3.383
30	3.412	3.424	3.458
40	3.470	3.479	3.511
50	3.552	3.530	3.552
60	3.579	3.576	3.612
70	3.628	3.614	3.655
80	3.675	3.664	3.700
90	3.727	3.720	3.747

Table 4-11. Reactivity insertion vs. UUTR power level; average cumulative reactivity insertion taken from all Runs and Log books

Power (kW)	Average Cumulative Reactivity Insertion ($)
1	3.207 +/- 0.023
10	3.289 +/- 0.017
20	3.362 +/- 0.016
30	3.429 +/- 0.019
40	3.486 +/- 0.018
50	3.541 +/- 0.015
60	3.587 +/- 0.018
70	3.633 +/- 0.019
80	3.679 +/- 0.018
90	3.727 +/- 0.019

The average Cumulative Reactivity Insertion ($) is defined as the average of Measured Cumulative Reactivity Inserted from Run A, B, C, D, E, and operational log books. The error is explained as the standard deviation of these values taken from Run A, B, C, D, E, and operational log books.

During thermal power calibrations of the UUTR, any difference below 5% is acceptable. This means that the accuracy of the measurement of reactor power is 5%. As can be seen, the difference between predicted value and the measured value is less than 5% for all measurements, which is well within the acceptable ranges.

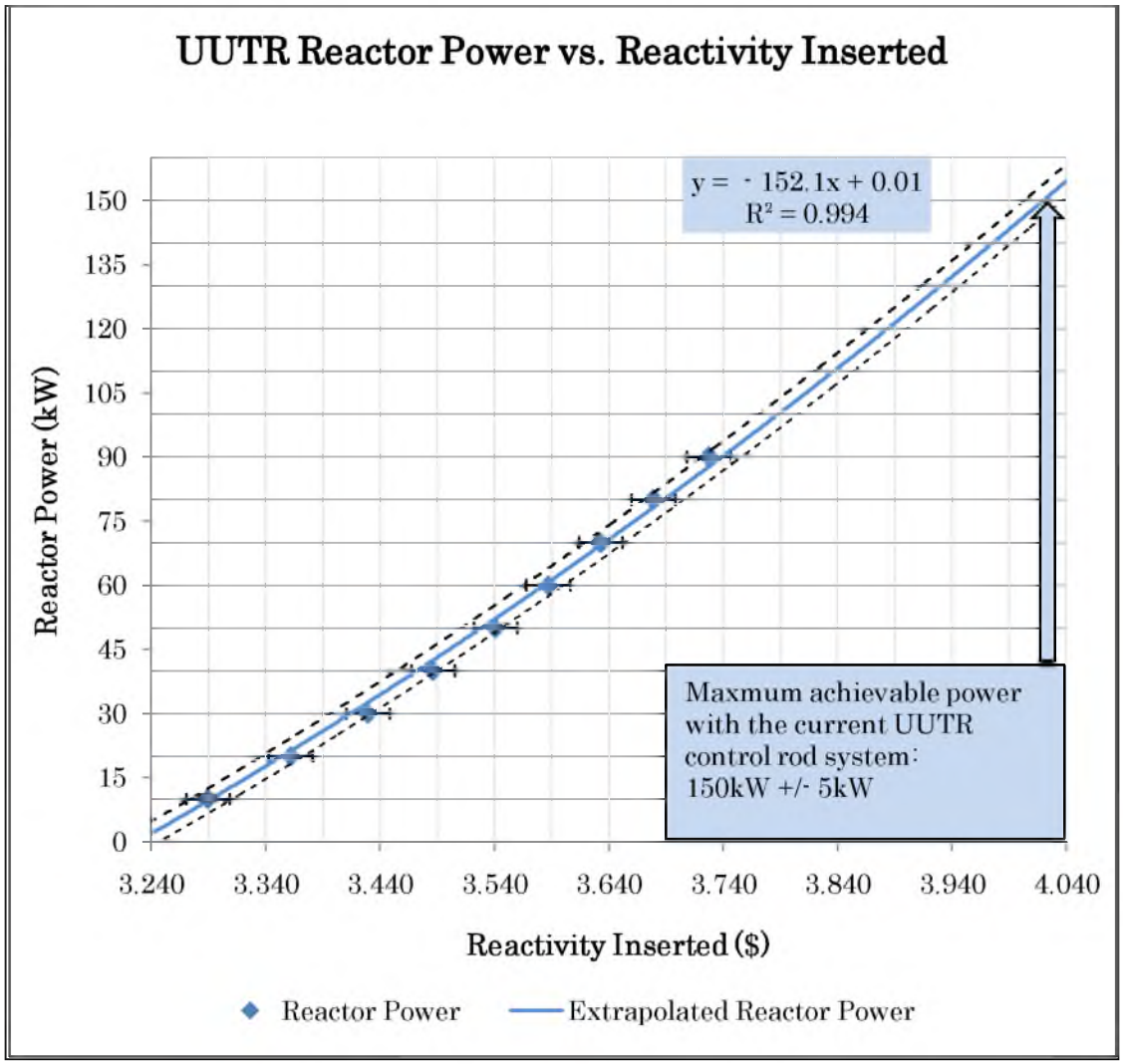

Figure 4-1. UUTR Reactor Power vs. Reactivity Insertion

CHAPTER 5

UUTR FUEL TEMPERATURE COEFFICIENT

5.1. Introduction

The fuel temperature coefficient is defined as the change in reactivity over the change in temperature of fuel [12]. One of the main safety features of the UUTR fuel is the strong negative fuel temperature coefficient [10]. This is accomplished by the incorporation of Uranium-Zirconium-Hydride (UZrH) alloy as reactor fuel. When positive reactivity is added into the reactor through the withdrawal of control rods, the power of the reactor will start to increase [15, 16]. As a result, the fuel temperature will increase. Simultaneously, the temperature of the Zirconium-Hydride (ZrH) in the fuel matrix will increase. The high concentration of hydrogen mixed within the fuel will increase the energy of the incoming neutrons (also known as up-scattering) and therefore decrease the fission rates in the fuel [17, 18]. This is because a rise in fuel temperature will increase the probability that a thermal neutron (0.025eV) will gain energy after interacting with the ZrH matrix and therefore escape out of the fuel rather than fission due to the increased mean free path for interaction [16].This, then, will decrease the power of the reactor immediately and in turn, inherently control the reactor power [19, 20].

The temperature coefficient can be obtained by the formula [9, 21]:

$$\alpha\left(\frac{\Delta k}{\mathrm{K}}\right) = \frac{d\rho}{dT} = \frac{k_2 - k_1}{k_2 * k_1 * (T_2 - T_1)} \tag{5.1}$$

where:

α = reactivity coefficient

ρ = reactivity

T_1= fuel temperature at k_1

T_2 = fuel temperature at k_2

k_1 = initial k_{eff} before reactivity insertion

k_2 = final k_{eff} after reactivity insertion

The dollar negative temperature coefficient can further be determined with [22]:

$$\alpha\left(\frac{\$}{\mathrm{K}}\right) = \frac{\alpha}{\beta_{eff}} \tag{5.2}$$

where:

α = reactivity coefficient

α(\$/K) = reactivity coefficient in dollars

β_{eff}= effective delayed neutron fraction in the core [23]

5.2. UUTR Fuel Temperature During Operation

The UUTR has a total of two instrumented fuel elements located in the "C-4" and "D-11" rings. Each instrumented fuel element has three K-type thermocouples capable of measuring temperature during regular operations. During every reactor run, the fuel temperature is recorded every time the power is stabilized. The temperature of the "C-4" and "D-11" fuel elements at each power level is shown in Table 5-1. There is a linear relationship that can be noted between the temperature

Table 5-1. C-4 and D-11 fuel element temperature (°C) at each corresponding reactor power

Power (kW)	Temperature (Celsius)											
	Run A		Run B		Run C		Run D		Run E		Average	
	D-11	C-4	D-11	C-4	D-11	C-4	D-11	C-4	D-11	C-4	D-11	C-4
1	25	25	27	26	30	29	29	28	28	28	**28**	**27**
10	35	37	37	38	39	42	38	40	38	40	**37**	**39**
20	46	49	46	51	47	63	47	52	47	52	**47**	**53**
30	55	61	55	62	56	64	56	63	56	64	**56**	**63**
40	63	71	62	71	63	73	63	72	63	72	**63**	**72**
50	70	80	69	80	69	80	70	80	71	81	**70**	**80**
60	78	87	76	88	77	88	78	89	78	89	**77**	**88**
70	85	86	83	95	83	96	85	97	86	97	**84**	**94**
80	92	104	90	104	90	103	91	105	92	105	**91**	**104**
90	98	112	96	112	97	113	99	113	99	114	**98**	**113**

of the"C-4" and "D-11" fuel elements and reactor power. This is because reactor power is directly proportional to fission rate, which in turn is directly proportional to fuel element temperature. This relationship is illustrated in Figure 5-1.

5.3. UUTR Negative Temperature Coefficient

Any amount of reactivity insertion into the reactor will result in a reactor power increase. Hence, reactor power is a function of the amount of reactivity inserted [8].

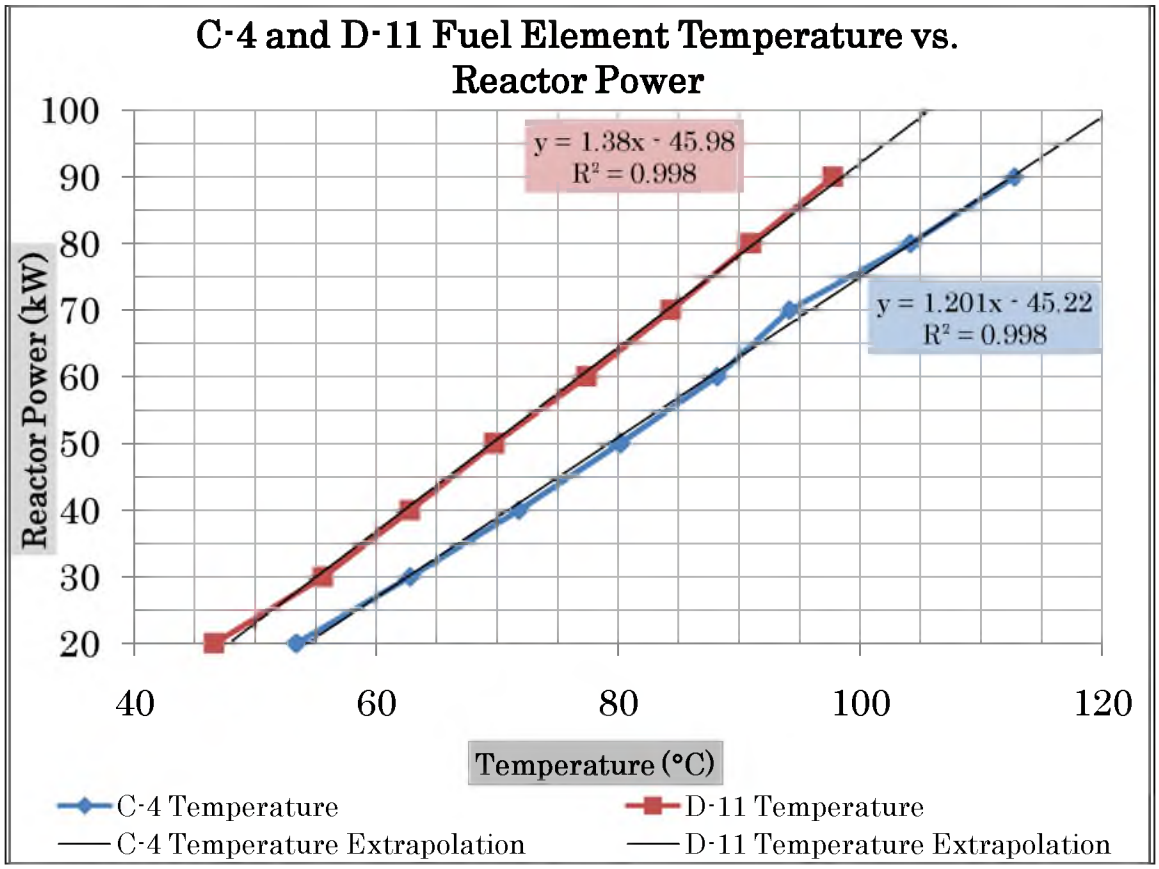

Figure 5-1. C-4 and D-11 fuel element temperatures vs. UUTR power

It has been shown in Chapter 4 that, during the reactivity insertion experiments, the power of the UUTR does not continually increase after positive reactivity has been inserted. In fact, the reactor power starts to level off and stabilizes after the fuel temperature has increased. This is because of the strong negative temperature coefficient of the UUTR fuel [8, 19]. The temperature coefficient can be obtained by measuring the change in reactivity and dividing that value by the change in temperature, as illustrated in equation 5.1. The increase in fuel temperature adds a negative amount of reactivity that is equal to the reactivity inserted into the reactor by the withdrawal of the control rods. Table 5-2 and Table 5-3 show the negative temperature coefficient of the "C-4" and "D-11" fuel element.

Table 5-2. Negative temperature coefficient of C-4 fuel element

C-4 Fuel Elements (C-Ring)					
Reactor Power (kW)	Average Cumulative Reactivity Inserted ($)	Average "C-4" Fuel Element Temperature (°C)	ΔT_{C-4} (°C)	$\Delta\rho$($)	α_{C-4} ($/K)
1	3.207	27.2			
10	3.289	39.4	12.2	0.082	-0.00673
20	3.362	54.0	14.6	0.072	-0.00494
30	3.429	62.8	8.8	0.068	-0.00770
40	3.486	71.8	9.0	0.057	-0.00630
50	3.541	80.2	8.4	0.055	-0.00649
60	3.587	88.2	8.0	0.046	-0.00578
70	3.633	94.2	6.0	0.046	-0.00768
80	3.679	104.2	10.0	0.046	-0.00458
90	3.727	112.8	8.6	0.048	-0.00564

Table 5-3. Negative temperature coefficient of D-11 fuel element

D-11 Fuel Element (D-Ring)					
Reactor Power (kW)	Average Cumulative Reactivity Inserted ($)	Average "D-11" Fuel Element Temperature (°C)	ΔT_{D-11} (°C)	$\Delta\rho$($)	α_{D-11} ($/K)
1	3.207	27.8			
10	3.289	37.4	9.6	0.082	-0.00855
20	3.362	46.6	9.2	0.072	-0.00784
30	3.429	55.6	9.0	0.068	-0.00753
40	3.486	62.8	7.2	0.057	-0.00787
50	3.541	69.8	7.0	0.055	-0.00779
60	3.587	77.4	7.6	0.046	-0.00608
70	3.633	84.4	7.0	0.046	-0.00658
80	3.679	91.0	6.6	0.046	-0.00695
90	3.727	97.8	6.8	0.048	-0.00713

The effects of the negative temperature are considered at fuel temperatures above 40°C [6, 24]. Therefore, one can measure the temperature effects during regular UUTR operations at all temperatures above 40°C and average these values to derive the average negative temperature coefficient of the UUTR of the "C-4" and "D-11" fuel elements. Table 5-4 shows the average temperature coefficient values for the UUTR.

5.4. UUTR MCNP5 Simulations of Temperature Coefficient

MCNP5 simulations are performed in order to numerically confirm the negative temperature coefficient trend for higher fuel temperatures [25]. The k_{eff} of the UUTR is calculated at temperatures of 300K, 600K, 900K, and 1200K. The U-235, U-238, and Zr-H cross section values which vary with temperature are taken into account through the S(α,β) treatment [26]. The resulting k_{eff} is plotted vs. the fuel temperature [27].The k_{eff} values correspond to all control rods out. Table 5-5 and Figure 5-2 show the MCNP5 calculated negative temperature coefficient vs. temperature of the UUTR. The MCNP5 calculations of the negative temperature coefficient correspond closely to the results of the UUTR safety analysis report [4]. All k_{eff} eigenvalue calculations are performed with 450 Million particles on a Pentium Core 2 Quad Q6600.

The error in the MCNP5 calculated k_{eff} eigenvalue is the stochastic error associated with the Monte Carlo sampling method and given along with the result of the MCNP5 calculation as k_{eff} +/- error. The error associated with the $\Delta\rho$ and α_F is the result of propagation of error, which will be explained in more detail in Chapter 10.

Table 5-4. Average negative temperature coefficient

α_{C-4} ($/K) (C-Ring)	-0.0061 +/- 0.00115
α_{D-11} ($/K) (D-Ring)	-0.0072 +/- 0.00066

Table 5-5. MCNP5 results of negative temperature coefficient vs. temperature

Temperature (K)	k_{eff}	$\Delta\rho$ ($)	α_F ($/K)
300	1.00650 +/- 0.00004		
600	0.97393 +/- 0.00004	-4.29275 +/- 0.00249	-0.01431 +/- 0.00249
900	0.94864 +/- 0.00004	-3.53654 +/- 0.00319	-0.01179 +/- 0.00319
1200	0.91097 +/- 0.00004	-5.63183 +/- 0.00217	-0.01877 +/- 0.00217

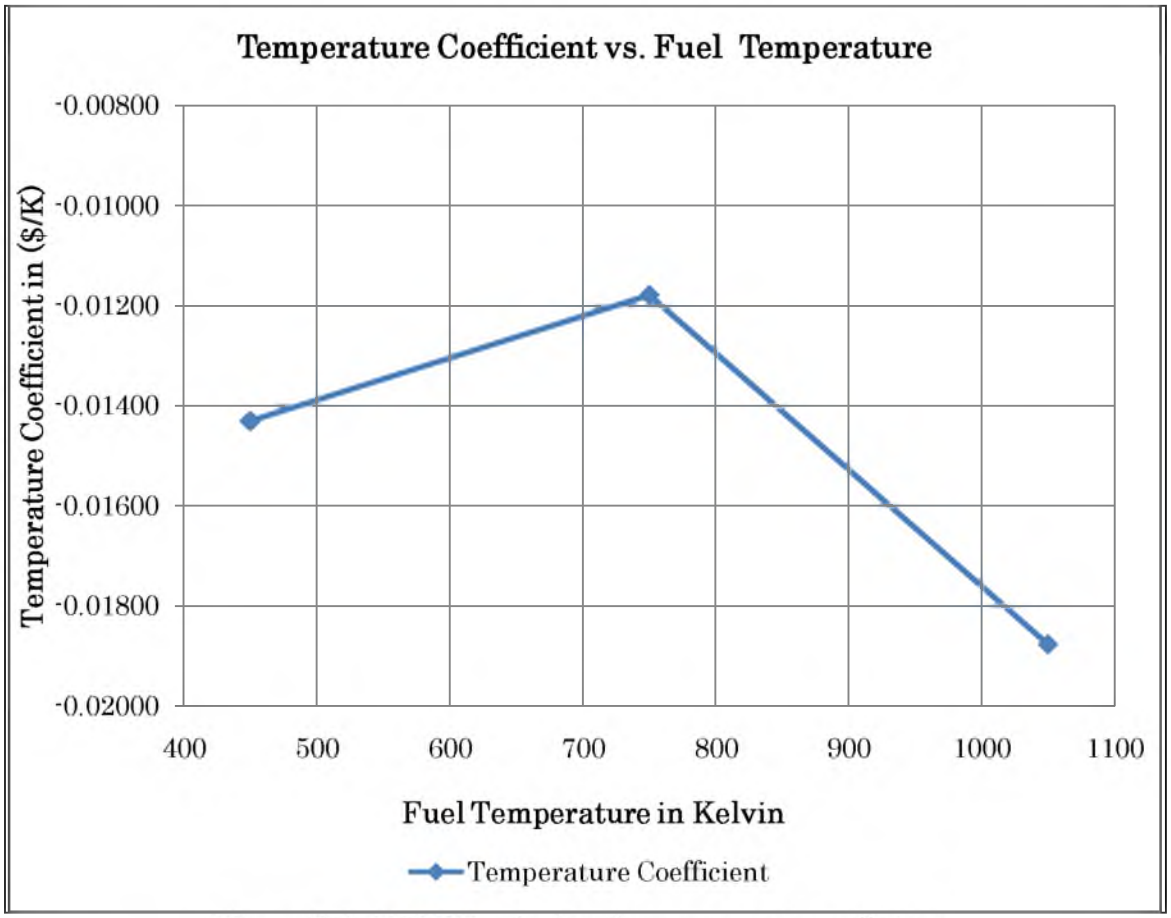

Figure 5-2. MCNP5 calculated temperature coefficient

5.5. Discussion

The fuel elements temperature is proportional to fuel elements power, which in turn is proportional to reactor power. As the control rods are withdrawn, positive reactivity is inserted. As a result, the reactor power increases, the fuel element temperature increases, causing a negative reactivity insertion in return, as seen in Table 5-2 and Table 5-3. MCNP5 simulations also confirm this trend at higher fuel temperatures, leading to the conclusion that there is a continuous trend in negative reactivity insertion with respect to fuel element temperature increase.

CHAPTER 6

NUMERICAL CALCULATIONS

6.1. Introduction

The MCNP5 [28] is used to examine the current UUTR core design for higher power levels in order to establish the understanding of the accuracy of the MCNP5 model. The core criticality, reactivity insertion, control rod worth, core excess reactivity, shut down margin, and negative temperature coefficient are calculated and compared to the experimental data obtained in Chapter 5.

6.2. Monte Carlo N-Particle Transport Code

The Monte Carlo N-Particle Transport Code, also known as MCNP5, is a Monte Carlo method that simulates transport of neutrons, photons, and electrons, or coupled neutron/photon/electron transport [26, 29]. It can be used for a wide variety of nuclear interaction simulations such as nuclear detector design, radiation shielding, particle accelerator targets, etc. [30]. In addition, MCNP5 can be used to design fission, fusion reactors, as well as criticality calculations [31]. The neutron libraries used for all simulations presented in this thesis include the ENDF/B-V.0 for some of the metallic elements and argon, and ENDF-VI.I&II [27, 32] for the uranium fuel and all other components such as graphite reflectors, fuel cladding, and aluminum casing [33].All presented UUTR computer simulations are carried out on an Intel Pentium Core 2 Quad Q6600 with 2.4GHz processors.

6.3. MCNP5 Calculation of the UUTR Control Rod Worth

Initially, the k_{eff} is calculated using MCNP5 with all control rods out considering both the prompt and delayed neutrons. Then, the k_p is calculated with all control rods out by only including the prompt neutrons. From there, the delayed neutron fraction β_{eff} is derived by [4, 23]:

$$\beta_{eff} = 1 - \frac{k_p}{k_{eff}} \tag{6.1}$$

where:

k_p= computed eigenvalue contributed by prompt neutrons only.

k_{eff} = computed eigenvalue contributed by prompt and delayed neutrons.

The amount of reactivity insertion contributed by a single control rod, also known as the control rod worth, can then be calculated by comparing the k_{eff} eigenvalue when the control rod is fully inserted with the k_{eff} eigenvalue when the control rod is fully withdrawn [24, 34]. The worth of the corresponding control rod is calculated by the difference in reactivity [4]:

$$\rho(\$) = \frac{\left[\frac{(k-k_{eff})}{k*k_{eff}}\right]}{\beta_{eff}} \tag{6.2}$$

where:

k = calculated system eigenvalue with all control rods out.

k_{eff} = calculated system eigenvalue with the corresponding control rod fully inserted.

The shut down margin is derived by:

$$\rho_{SDM}(\$) = \frac{\left[\frac{(1-k_{SR})}{k_{SR}}\right]}{\beta_{eff}} \tag{6.3}$$

where:

k_{SR} = calculated eigenvalue with shim and regulation fully inserted into the core while the safety control rod is fully withdrawn.

The core excess reactivity is calculated by:

$$\rho_{EX} = \frac{\left[\frac{(k-1)}{k}\right]}{\beta_{eff}} \tag{6.4}$$

where:

k= calculated system eigenvalue with all control rods out

6.4. MCNP5 Simulation of the UUTR During Operations

The MCNP5 was used to calculate the k_{eff} for each reactor power level ranging between 1kW to 90kW. The control rod positions were taken from log books [6] as well as from the reactivity insertion experiments.

Table 6-1 presents the MCNP5 k_{eff} calculation result of each corresponding control rod position. Table 6-2 shows the control rod worth of the safety control, the shim control rod, and the regulation control rod. In addition, the excess reactivity and the shut down margin are presented. Table 6-3 shows the k_{eff} vs. reactor power.

Table 6-1. MCNP5 k_{eff} of each corresponding control rod position. IN position corresponds to fully inserted control rod of the current UUTR core. OUT position corresponds to fully withdrawn control rod. (450 million particles)

Safety control rod	Shim control rod	Regulation control rod	k_{eff}			CPU Time (days)
IN	IN	IN	0.97599	+/-	0.00004	5.05
OUT	IN	IN	0.99260	+/-	0.00004	3.95
IN	OUT	OUT	0.99174	+/-	0.00004	5.79
OUT	IN	OUT	0.99526	+/-	0.00004	3.87
OUT	OUT	IN	1.00417	+/-	0.00004	4.56
OUT	OUT	OUT	1.00650	+/-	0.00004	4.78
OUT	OUT	OUT	0.99871	+/-	0.00004	3.75
		β_{eff}	0.00774	+/-	0.00008	

Table 6-2. MCNP5 calculated UUTR control rod worth of the current UUTR core. Calculation done with 450 million particles

MCNP5 Simulation	ρ (Δk/k)			ρ ($)		
Safety control rod	0.01479	+/-	0.00006	1.9105	+/-	0.0211
Shim control rod	0.01122	+/-	0.00006	1.4497	+/-	0.0167
Regulation control rod	0.00231	+/-	0.00006	0.2979	+/-	0.0079
Total Rod Worth	**0.02831**	**+/-**	**0.00017**	**3.6581**	**+/-**	**0.0456**
Excess Reactivity	0.00646	+/-	0.00011	0.8232	+/-	0.0089
Shut Down Margin	0.00746	+/-	0.00011	0.9503	+/-	0.0089

Table 6-3. MCNP5 k_{eff} calculation at each corresponding power level. The shim position is varied; the safety control rod is fully withdrawn at 100% out; the regulation rod is at 65.3% out.

Reactor Power (kW)	k_{eff}			Shim control rod (% out)	$\Delta\rho$ ($/K)
1	0.99968	+/-	0.00004	50.9	
10	1.00032	+/-	0.00004	54.1	0.0827
20	1.00081	+/-	0.00004	57.3	0.0632
30	1.00139	+/-	0.00004	60.6	0.0748
40	1.00178	+/-	0.00004	63.0	0.0502
50	1.00216	+/-	0.00004	64.9	0.0489
60	1.00250	+/-	0.00004	67.8	0.0437
70	1.00291	+/-	0.00004	70.0	0.0527
80	1.00314	+/-	0.00004	72.4	0.0295
90	1.00360	+/-	0.00004	75.1	0.0590

6.5. MCNP5 Simulation of the UUTR Temperature Coefficient

The MCNP5 input file was constructed in a way to simulate the position of each control rod for each power level. At the end of each run, the k_{eff} eigenvalue was recorded. Table 6-3 shows the k_{eff} at each power level. In addition, the negative temperature coefficient is calculated [35]. Table 6-4 and Table 6-5 show the MCNP5 determined temperature coefficient.

Table 6-6 shows the average temperature coefficients of the "C-4" and "D-11" fuel element and compares them to the MCNP5 calculation. The MCNP5 simulations match very closely to the experimental data. This suggests that MCNP5 simulations are a good predictor of reactor behavior and can be used to examine the current UUTR core configuration at higher powers [36, 37]. In addition, MCNP5 can reliably be used to design a core configuration for power upgrade [29, 37].

6.6. MCNP5 Analysis of the UUTR Neutron Flux

The total, fast, and thermal neutron flux are derived and plotted in order to illustrate the shape of the neutron flux for reactor power level of 100kW. An analysis of the fuel element power distribution per fuel ring is presented in Table 6-7. Concurrently, the peaking factors at the corresponding reactor power are revealed in Figure 6-1. Figure 6-2 shows the 3D view of the pin power distribution in kilowatts when the reactor is operating at 100 kilowatts. Figure 6-3 shows the top view of the pin power distribution per pin in kilowatts when the reactor is operating at a power of 100 kilowatts. Despite the UUTR fuel element being a round cylinder, the pin power distribution is represented as a hexagonal arrangement in Figures 6-2 and 6-3. This was done in order better represent localized power distributions of the core.

Table 6-4. MCNP5 calculation of the UUTR temperature coefficient of "C-4"

Power (kW)	k_{eff}			"C-4" Fuel Element Temperature (°C)	ΔT_{C-4} (°C)	$\Delta\rho$ ($\Delta k/k$)	α_{C-4} ($\Delta k/K$)	α_{C-4} (\$/K)
1	0.99968	+/-	0.00004	27.2				
10	1.00032	+/-	0.00004	39.4	12.2	0.000640	0.000052	-0.00678
20	1.00081	+/-	0.00004	54.0	14.6	0.000489	0.000034	-0.00433
30	1.00139	+/-	0.00004	62.8	8.8	0.000579	0.000066	-0.00850
40	1.00178	+/-	0.00004	71.8	9.0	0.000389	0.000043	-0.00558
50	1.00216	+/-	0.00004	80.2	8.4	0.000379	0.000045	-0.00582
60	1.00250	+/-	0.00004	88.2	8.0	0.000338	0.000042	-0.00547
70	1.00291	+/-	0.00004	94.2	6.0	0.000408	0.000068	-0.00878
80	1.00314	+/-	0.00004	104.2	10.0	0.000229	0.000023	-0.00295
90	1.00360	+/-	0.00004	112.8	8.6	0.000457	0.000053	-0.00686

Table 6-5. MCNP5 calculation of the UUTR temperature coefficient of "D-11"

Power (kW)	k_{eff}			"D-11" Fuel Element Temperature (°C)	ΔT_{D-11} (°C)	$\Delta\rho$ ($\Delta k/k$)	α_{D-11} ($\Delta k/K$)	α_{D-11} (\$/K)
1	0.99968	+/-	0.00004	27.8				
10	1.00032	+/-	0.00004	37.4	9.6	0.00064	0.000067	-0.00861
20	1.00081	+/-	0.00004	46.6	9.2	0.00049	0.000053	-0.00687
30	1.00139	+/-	0.00004	55.6	9.0	0.00058	0.000064	-0.00831
40	1.00178	+/-	0.00004	62.8	7.2	0.00039	0.000054	-0.00698
50	1.00216	+/-	0.00004	69.8	7.0	0.00038	0.000054	-0.00699
60	1.00250	+/-	0.00004	77.4	7.6	0.00034	0.000045	-0.00575
70	1.00291	+/-	0.00004	84.4	7.0	0.00041	0.000058	-0.00753
80	1.00314	+/-	0.00004	91.0	6.6	0.00023	0.000035	-0.00448
90	1.00360	+/-	0.00004	97.8	6.8	0.00046	0.000067	-0.00868

Table 6-6. Measured and MCNP5 calculated UUTR temperature coefficient. MCNP5 calculations were done with 450 million particles on a Pentium Quad 2 Core Q6600

α_{C-4} (\$/K)	Measured	-0.0061	+/-	0.00115
	MCNP5	-0.0061	+/-	0.00186
α_{D-11} (\$/K)	Measured	-0.0072	+/-	0.00066
	MCNP5	-0.0069	+/-	0.00135

Table 6-7. Fuel element power distribution per fuel ring at 100kW reactor power

Ring	Number of Fuel Pins	Maximum Power Per Fuel Pin P_{max} (kW/pin)	Minimum Power Per Fuel Pin P_{min} (kW/pin)	Average Power Per Fuel Pin P_{avg} (kW/pin)	Ratio (P_{max} / P_{min})	Ratio (P_{max} / P_{avg})
B	6	2.019	1.886	1.980	1.071	1.020
C	11	1.891	1.497	1.717	1.263	1.101
D	14	1.811	1.196	1.474	1.514	1.229
E	23	1.443	0.934	1.179	1.545	1.224
F	19	1.207	0.764	0.947	1.580	1.275
G	5	0.788	0.612	0.700	1.288	1.126
Total	78	2.019	0.612	1.282	3.299	1.575

6.6.1. MCNP5 UUTR Core Analysis at 100kW

Core analysis of the UUTR at 100kW reactor power is shown in this subsection through figures and tables. Matlab program is used to plot the flux [38]. Figure 6-4 shows the 3D view of the total neutron flux distribution at a reactor power of 100kW. Figure 6-5 is a top view of the total neutron flux distribution of the UUTR at a reactor power of 100kW. Figure 6-6 shows the 3D view of the fast neutron flux distribution at a reactor power of 100kW. Figure 6-7 is a top view of the fast neutron flux distribution of the UUTR at a reactor power of 100kW. Figure 6-8 shows the 3D view of the thermal neutron flux distribution at a reactor power of 100kW. Figure 6-9 is a top view of the thermal neutron flux distribution of the UUTR at a reactor power of 100kW.

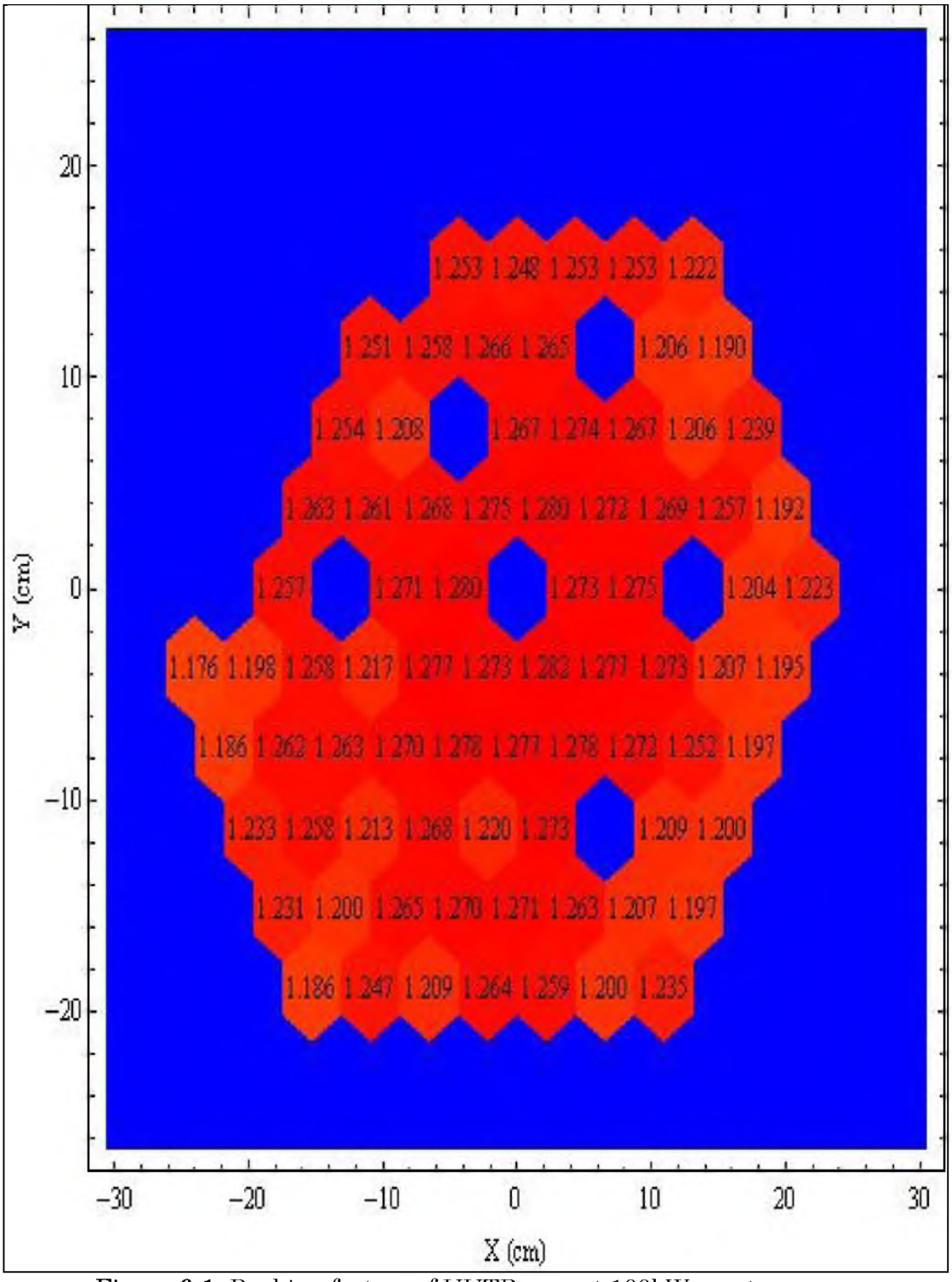

Figure 6-1. Peaking factors of UUTR core at 100kW reactor power

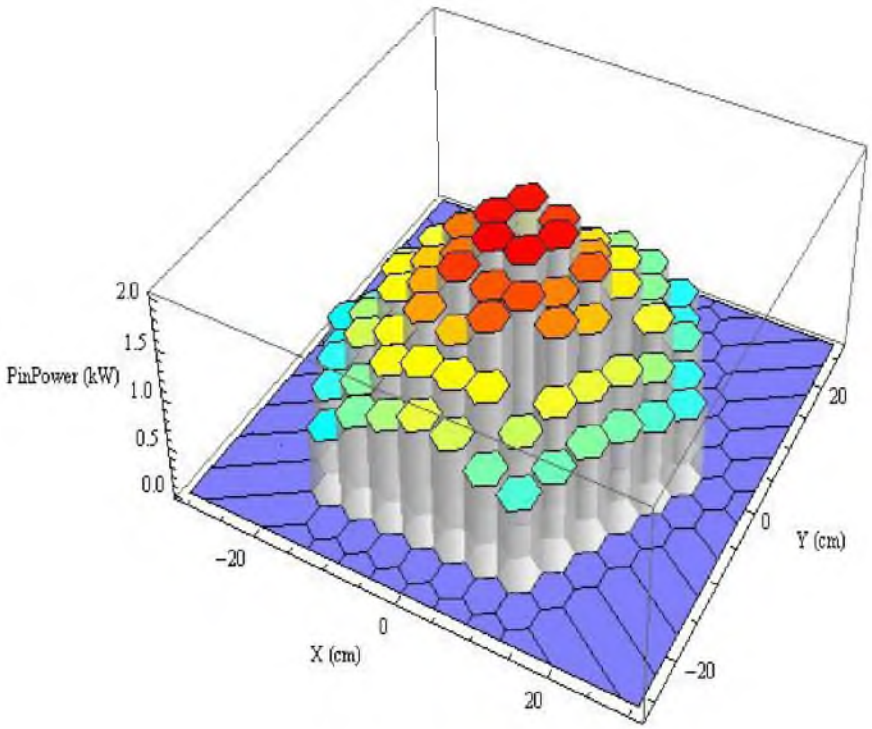

Figure 6-2. 3D view of UUTR pin power distribution in kilowatts at 100kW reactor power

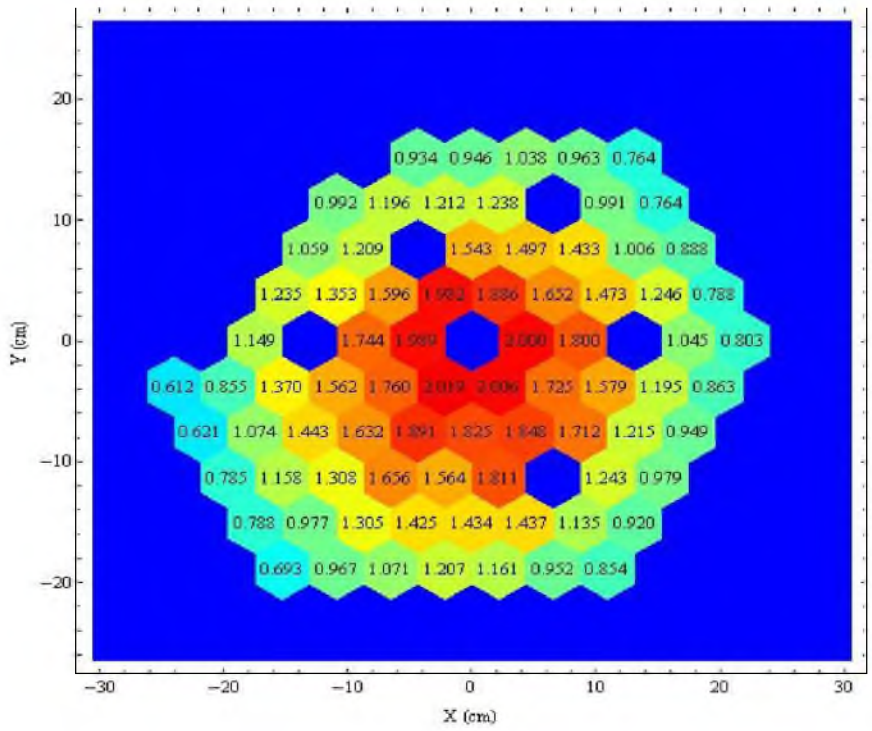

Figure 6-3. Top view of UUTR pin power distribution in kilowatts at 100kW reactor power

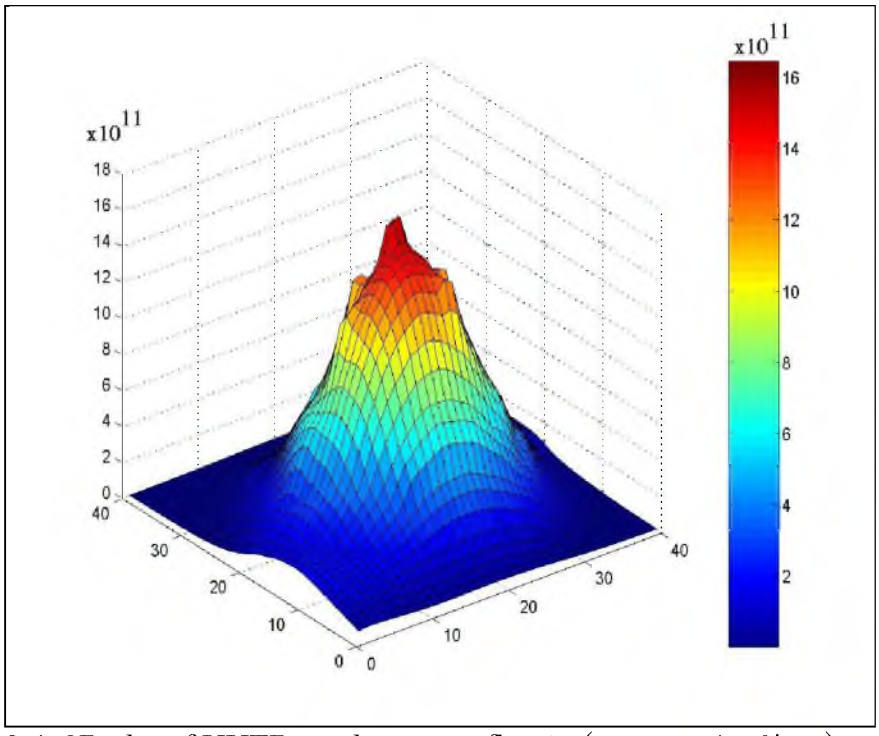

Figure 6-4. 3D plot of UUTR total neutron flux in (neutrons/cm^2*sec) at 100kW reactor power for all neutron energies

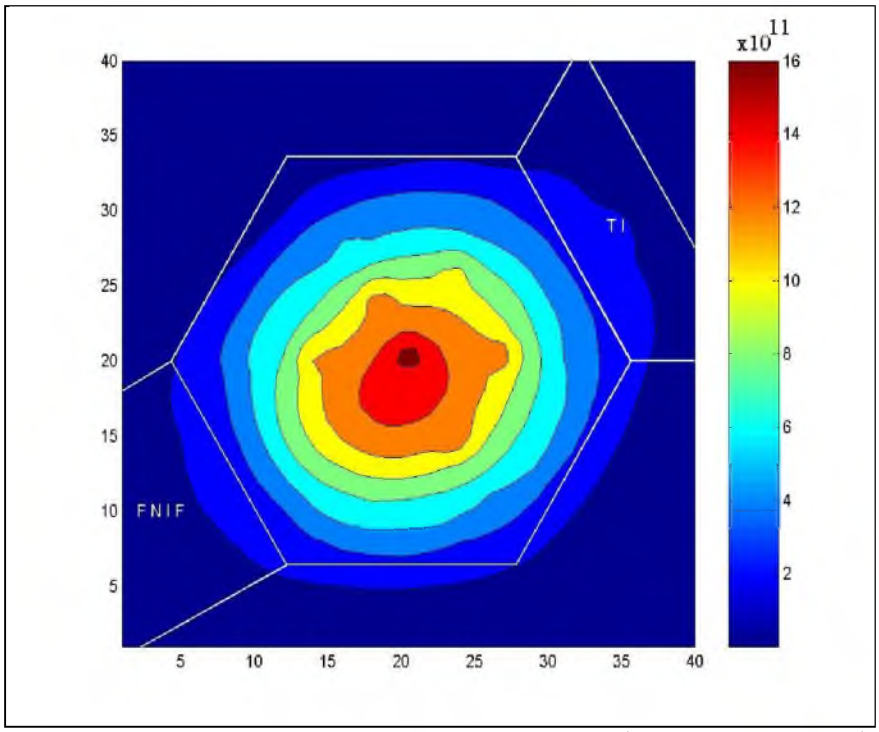

Figure 6-5. Contour plot of UUTR total neutron flux in (neutrons/cm^2*sec) at 100kW reactor power for all neutron energies

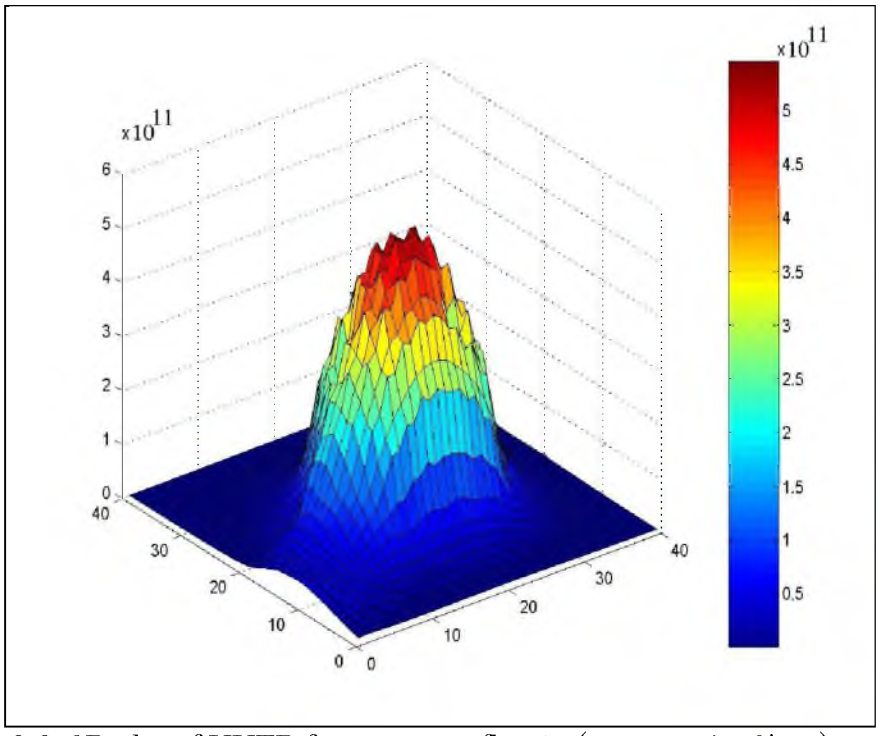

Figure 6-6. 3D plot of UUTR fast neutron flux in (neutrons/cm^2*sec) at 100kW reactor power for neutron energies above 100keV

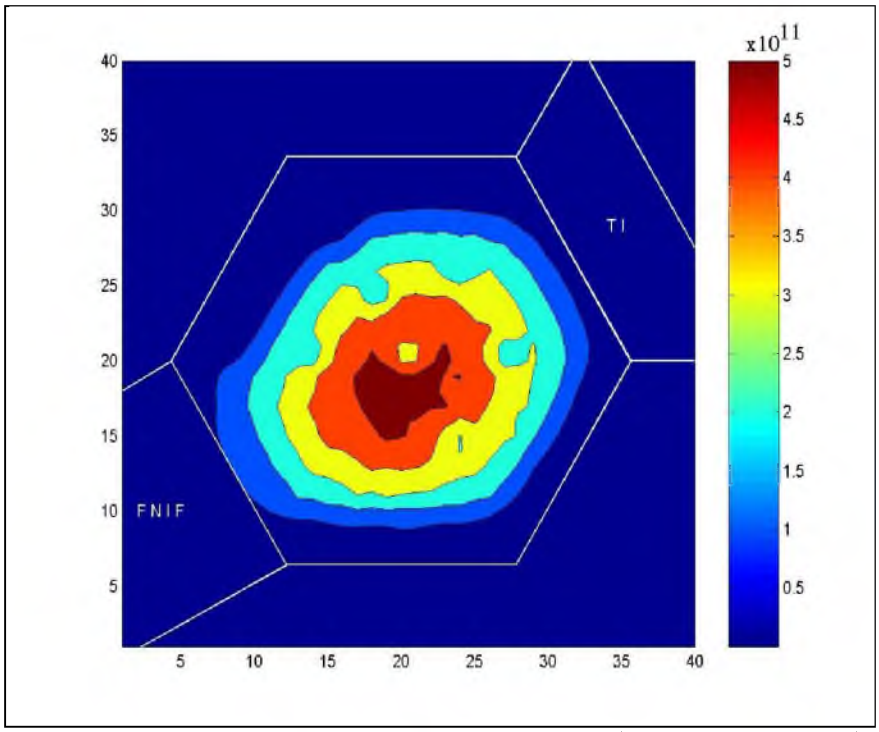

Figure 6-7. Contour plot of UUTR fast neutron flux in (neutrons/cm^2*sec) at 100kW reactor power for neutron energies above 100keV

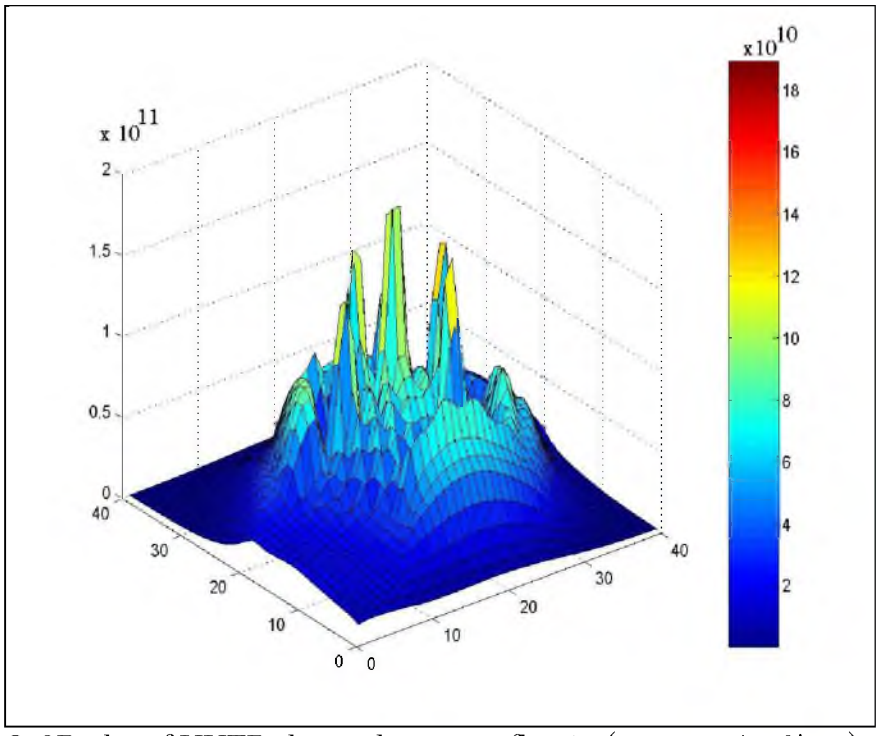

Figure 6-8. 3D plot of UUTR thermal neutron flux in (neutrons/cm^2*sec) at 100kW reactor power for neutron energies below 0.025eV

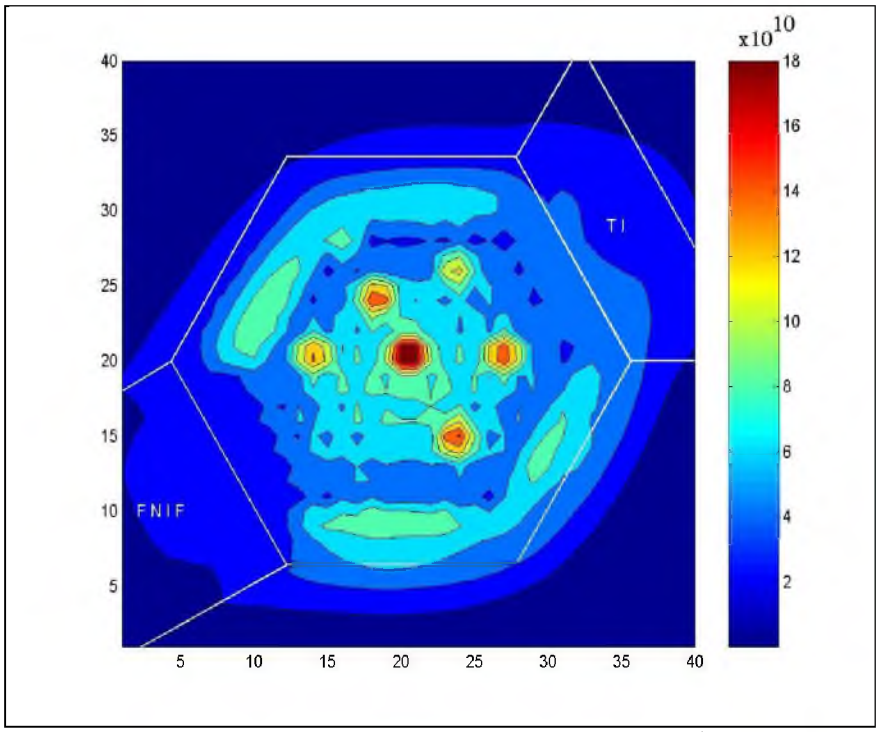

Figure 6-9. Contour plot of UUTR thermal neutron flux in (neutrons/cm^2*sec) at 100kW reactor power for neutron energies below 0.025eV

6.6.2. MCNP5 UUTR Core Analysis at 150kW

Core analysis of the UUTR at 150kW reactor power is shown in this subsection through figures and tables. Table 6-8 represents the fuel element power distribution per fuel ring at 150kW reactor power. Figure 6-10 shows the peaking factors of the UUTR core at 150kW reactor power. Figure 6-11 shows the 3D pin power distribution of the core at 150kW. Figure 6-12 shows the top view of pin power distribution in kilowatts at 150kW reactor power. Matlab program is used to plot the flux [39]. Figure 6-13 shows the 3D view of the total neutron flux distribution at a reactor power of 150kW. Figure 6-14 is a top view of the total neutron flux distribution of the UUTR at a reactor power of 150kW. Figure 6-15 shows the 3D view of the fast neutron flux distribution at a reactor power of 150kW. Figure 6-16 is a top view of the fast neutron flux distribution of the UUTR at a reactor power of 150kW. Figure 6-17 shows the 3D view of the thermal neutron flux distribution at a reactor power of 150kW. Figure 6-18 is a top view of the thermal neutron flux distribution of the UUTR at a reactor power of 150kW.

Table 6-8. Fuel element power distribution per fuel ring at 150kW reactor power

Ring	Number of Fuel Pins	Maximum Power Per Fuel Pin P_{max} (kW/pin)	Minimum Power Per Fuel Pin P_{min} (kW/pin)	Average Power Per Fuel Pin P_{avg} (kW/pin)	Ratio (P_{max} / P_{min})	Ratio (P_{max} / P_{avg})
B	6	3.029	2.829	2.970	1.071	1.020
C	11	2.836	2.246	2.575	1.263	1.101
D	14	2.716	1.794	2.210	1.514	1.229
E	23	2.164	1.401	1.768	1.545	1.224
F	19	1.811	1.145	1.421	1.582	1.274
G	5	1.183	0.917	1.050	1.290	1.127
Total	78	3.029	0.917	1.923	3.303	1.575

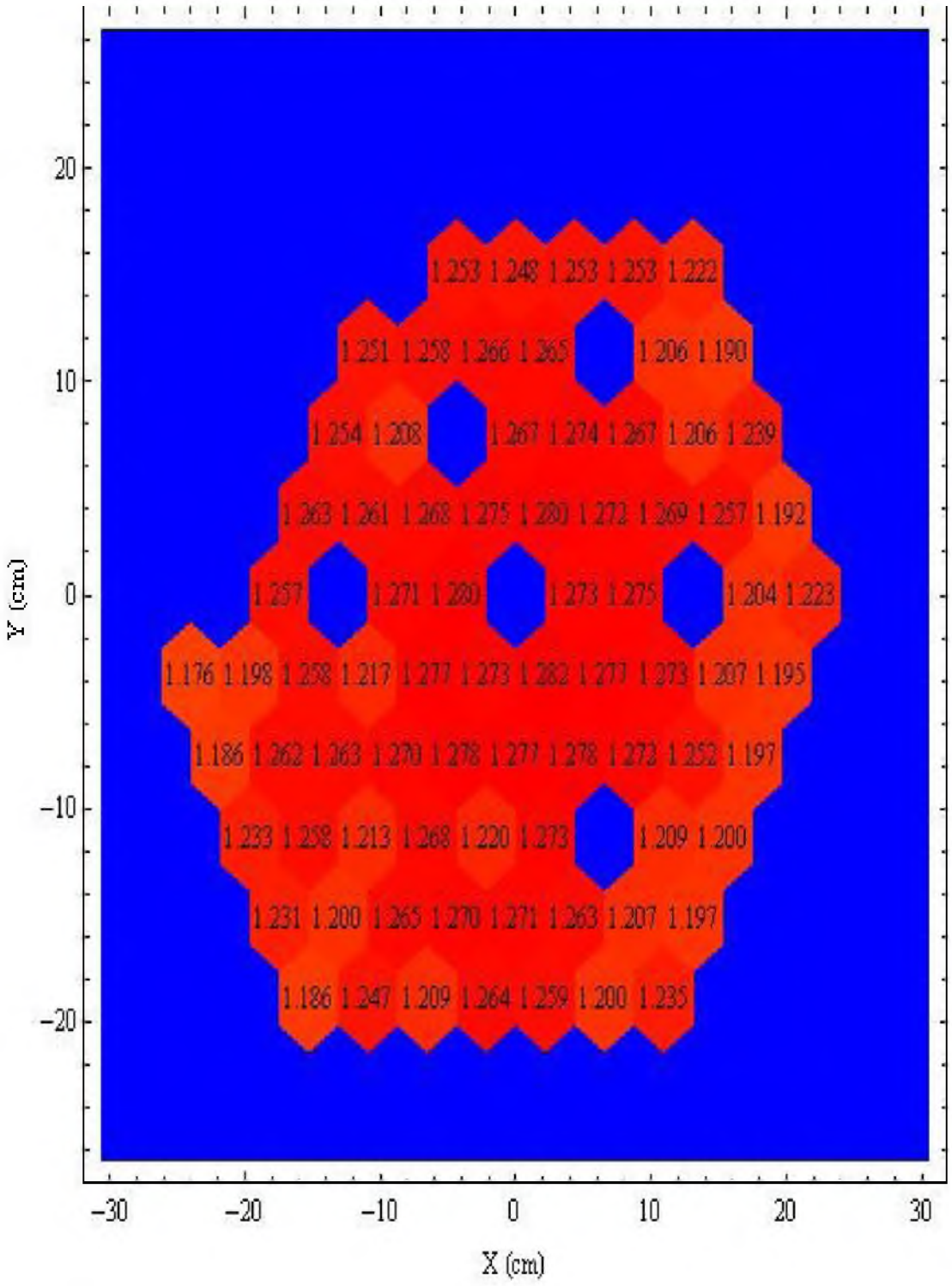

Figure 6-10. Peaking factors of UUTR core at 150kW reactor power

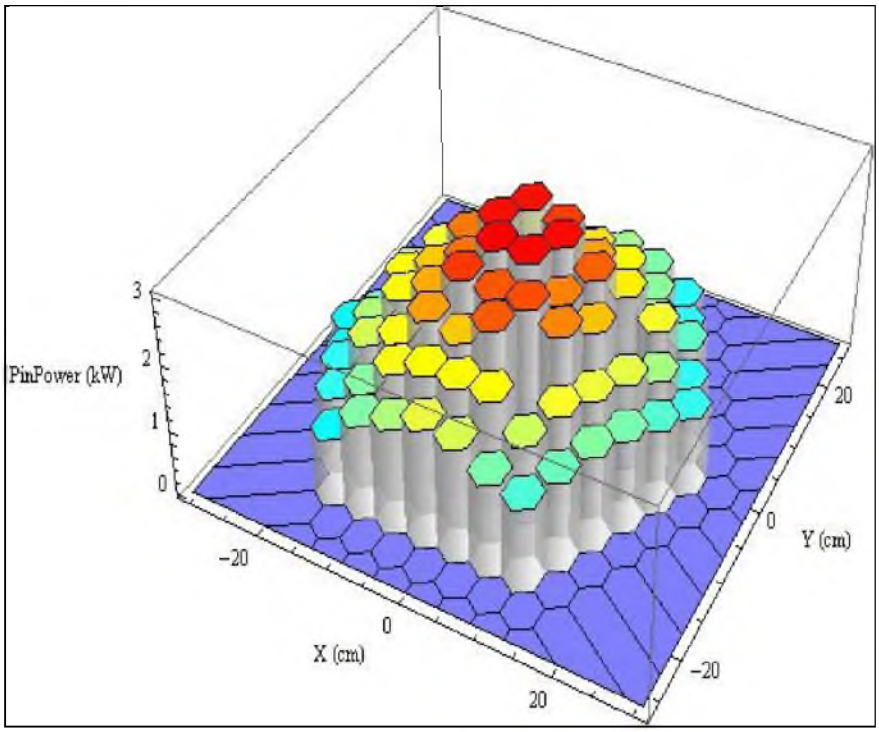

Figure 6-11. 3D view of UUTR pin power distribution in kilowatts at 150kW reactor power

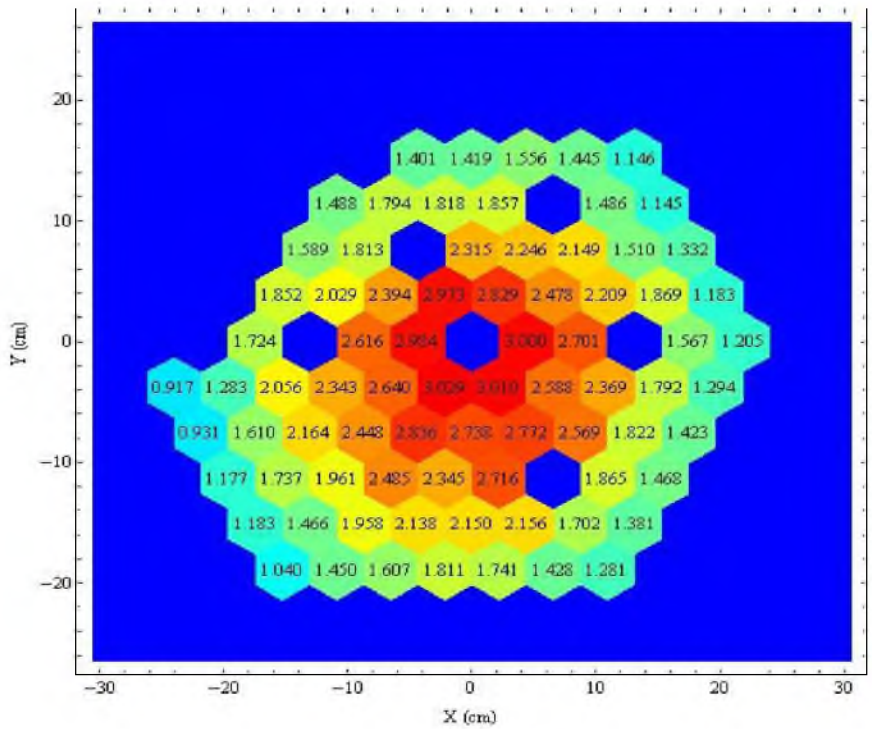

Figure 6-12. Top view of UUTR pin power distribution in kilowatts at 150kW reactor power

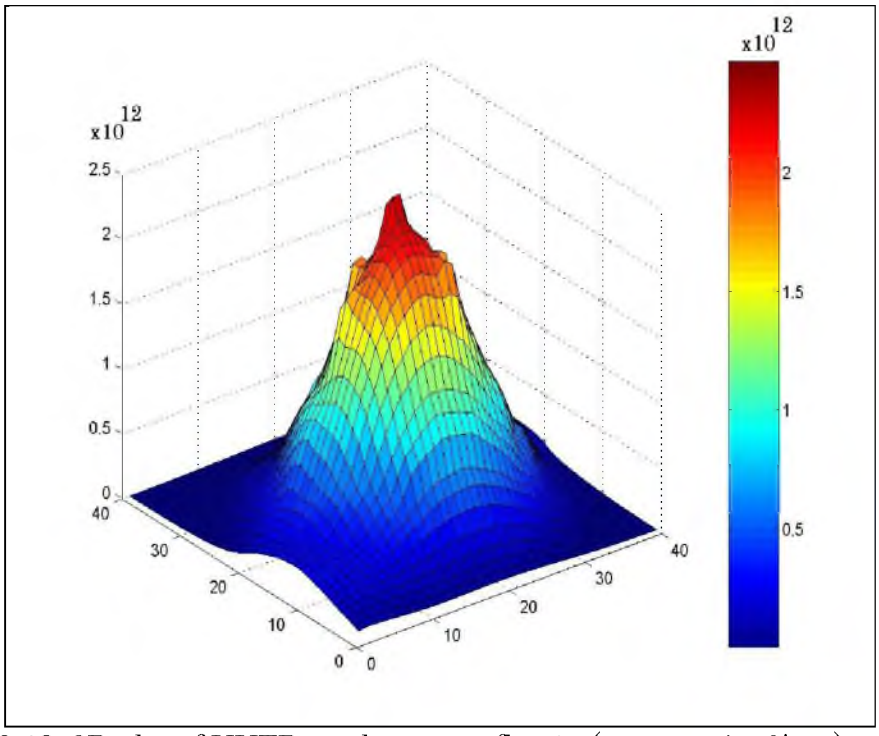

Figure 6-13. 3D plot of UUTR total neutron flux in (neutrons/cm^2*sec) at 150kW reactor power for all neutron energies

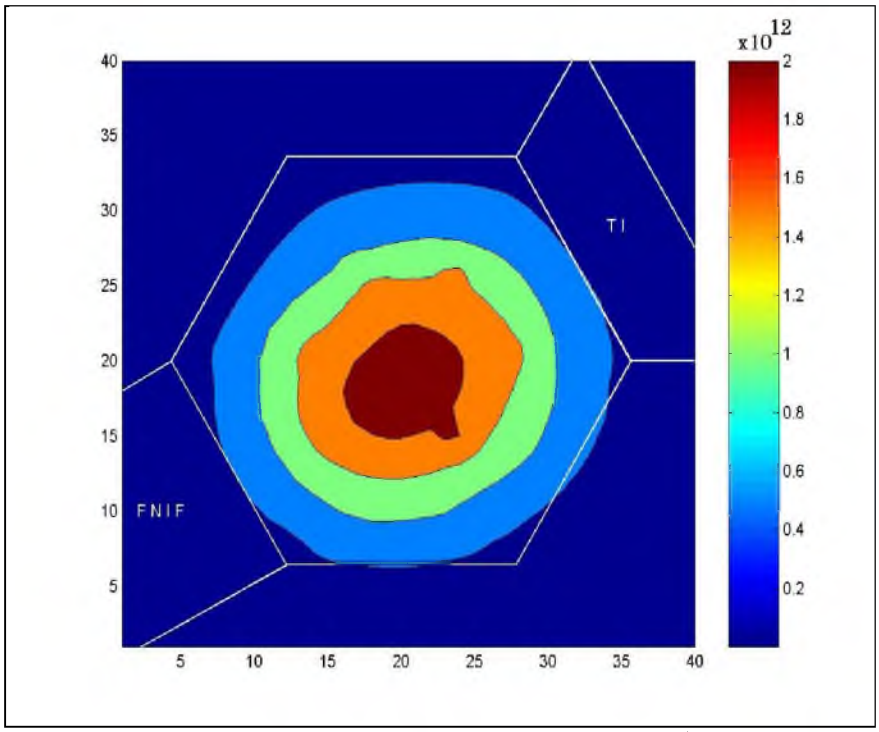

Figure 6-14. Contour plot of UUTR total neutron flux in (neutrons/cm^2*sec) at 150kW reactor power for all neutron energies

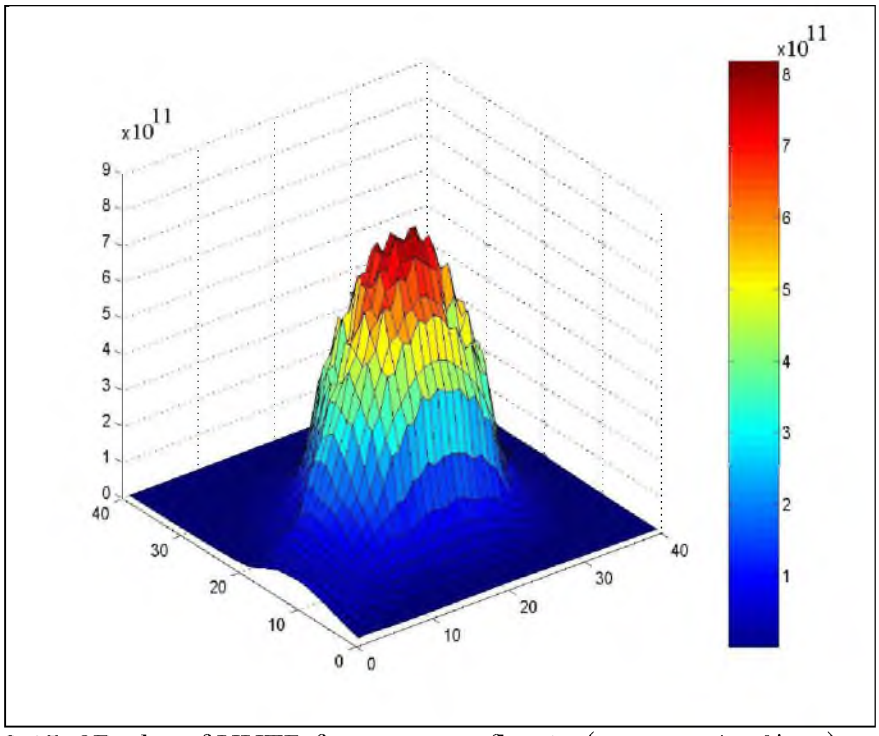

Figure 6-15. 3D plot of UUTR fast neutron flux in (neutrons/cm^2*sec) at 150kW reactor power for neutron energies above 100keV

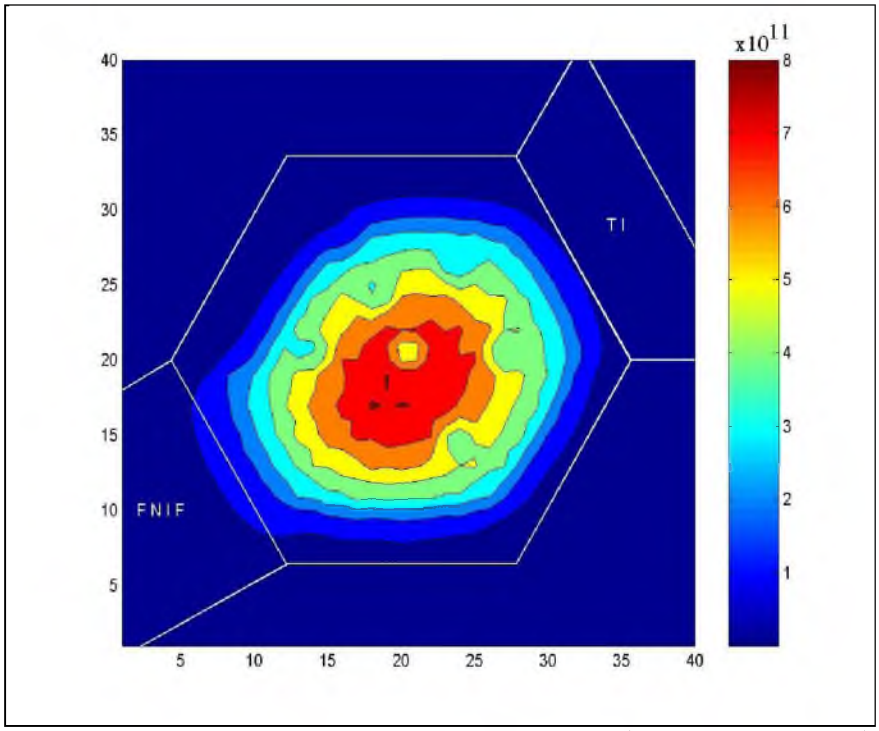

Figure 6-16. Contour plot of UUTR fast neutron flux in (neutrons/cm^2*sec) at 150kW reactor power for neutron energies above 100keV

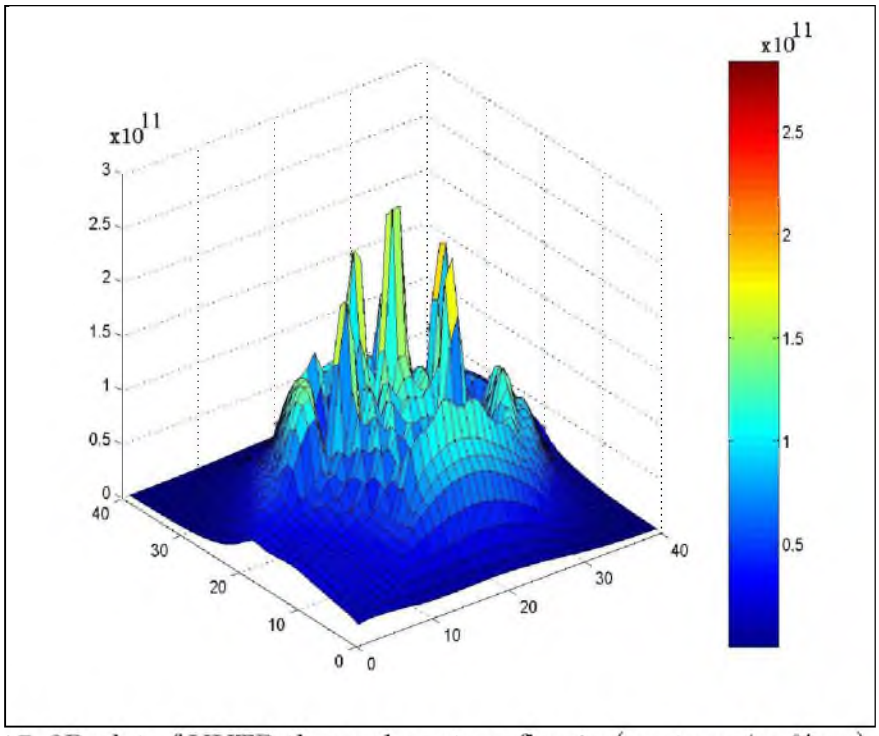

Figure 6-17. 3D plot of UUTR thermal neutron flux in (neutrons/cm^2*sec) at 150kW reactor power for neutron energies below 0.025eV

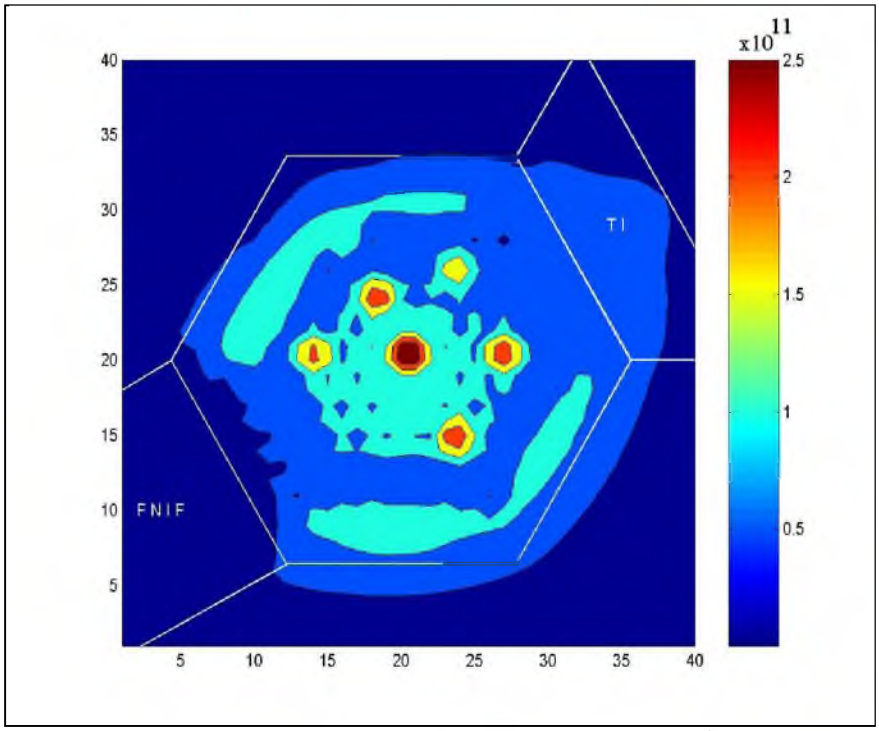

Figure 6-18. Contour plot of UUTR thermal neutron flux in (neutrons/cm^2*sec) at 150kW reactor power for neutron energies below 0.025eV

CHAPTER 7

UUTR MAXIMUM PRACTICAL POWER

7.1. Introduction

Reactivity insertion experiments in Chapter 4 examined the relationship between reactivity insertion and reactor power. In Chapter 5, the negative temperature coefficient of fuel was measured. MCNP5 numerical calculations in Chapter 6 calculated the worth of each control rod and the negative temperature coefficient. These studies allowed for a confident estimate of the maximum achievable reactor power. In this chapter, the maximum practical power of the UUTR will be presented.

7.2. UUTR Reactor Performance

MCNP5 calculations show that the k_{eff} eigenvalue for the current UUTR configuration with all control rods withdrawn is 1.0650. This value, in addition to the negative temperature coefficient, can be used to numerically estimate the maximum practical reactor power [40]. Figure 7-1 shows a plot of reactor power as a function of MCNP5 calculated k_{eff} eigenvalue. In addition, this graph also superimposes the results from the reactivity insertion experiments. It is evident that the experimentally measured values of reactivity insertions as well as the MCNP5 numerical calculations of the k_{eff} (which numerically simulate reactivity insertion) show a linear relationship to reactor power [41].

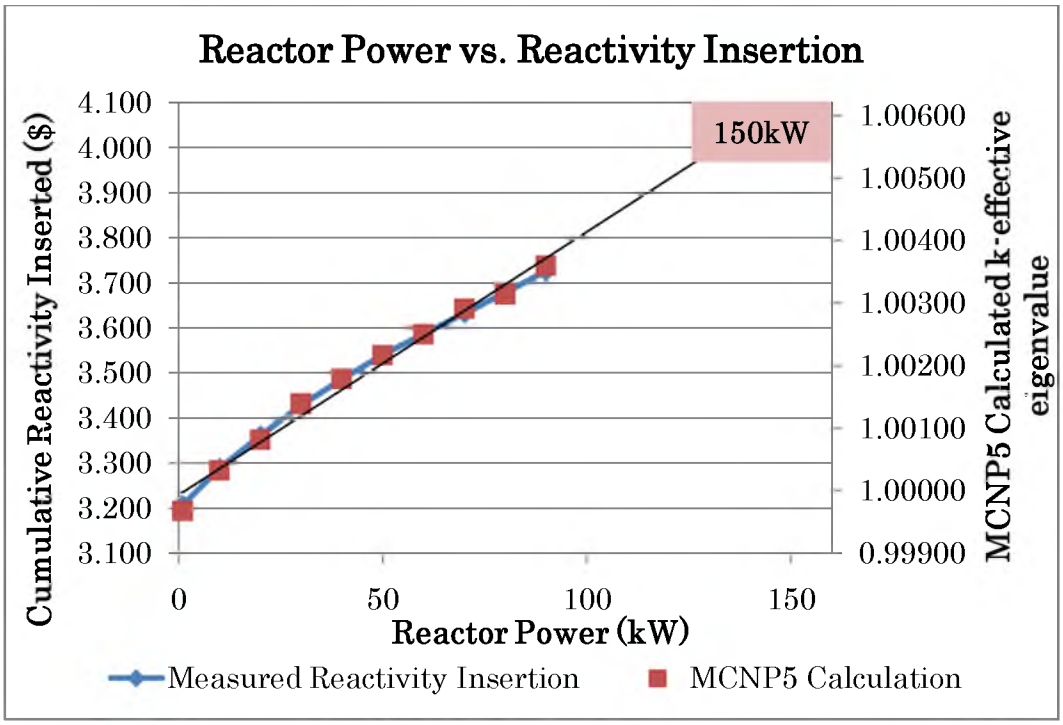

Figure 7-1. Extrapolated plot of reactor power vs. reactivity insertion

The trend in Figure 7-1 also confirms that the experimental values and the numerical calculations match closely to one another and can be used effectively to extrapolate for higher powers [33]. As evident in Figure 7-1, the maximum achievable reactor power is shown to be 150kW.

Table 7-1 and Table 7-2 show the reactor performance of the current UUTR for higher powers. It is known that the negative reactivity inserted by the negative temperature coefficient of the fuel is equal to the positive reactivity inserted through the withdrawal of the control rods. Therefore, for each consecutive withdrawal of the control rod, the positive reactivity inserted will be offset by the negative reactivity inserted due to the fuel temperature coefficient. This trend will continue until the maximum achievable reactor power is reached at 150kW.

Table 7-1. Negative temperature coefficient for C-4 fuel pin

"C-4" Fuel Pin (C-Ring)					
Reactor Power (kW)	Average Cumulative Reactivity Inserted ($)	"C-4" Fuel Pin Temperature (°C)	ΔT_{C-4} (°C)	$\Delta\rho$ ($)	α_{C-4}($/K)
1	3.207	27.2			
10	3.289	39.4	12.2	0.082	-0.00673
20	3.362	54.0	14.6	0.072	-0.00494
30	3.429	62.8	8.8	0.068	-0.00770
40	3.486	71.8	9.0	0.057	-0.00630
50	3.541	80.2	8.4	0.055	-0.00649
60	3.587	88.2	8.0	0.046	-0.00578
70	3.633	94.2	6.0	0.046	-0.00768
80	3.679	104.2	10.0	0.046	-0.00458
90	3.727	112.8	8.6	0.048	-0.00564
100*	3.778	121.0	8.2	0.050	-0.00614
110*	3.827	129.0	8.0	0.049	-0.00614
120*	3.876	137.0	8.0	0.049	-0.00614
130*	3.931	146.0	9.0	0.055	-0.00614
140*	3.980	154.0	8.0	0.049	-0.00614
150*	4.035	163.0	9.0	0.055	-0.00614

* extrapolated value

Table 7-2. Negative temperature coefficient for D-11 fuel pin

"D-11" Fuel Pin (D-Ring)					
Reactor Power (kW)	Average Cumulative Reactivity Inserted ($)	"D-11" Fuel Pin Temperature (°C)	ΔT_{D-11} (°C)	$\Delta\rho$ ($)	α_{D-11} ($/K)
1	3.207	27.8			
10	3.289	37.4	9.6	0.082	-0.00855
20	3.362	46.6	9.2	0.072	-0.00784
30	3.429	55.6	9.0	0.068	-0.00753
40	3.486	62.8	7.2	0.057	-0.00787
50	3.541	69.8	7.0	0.055	-0.00779
60	3.587	77.4	7.6	0.046	-0.00608
70	3.633	84.4	7.0	0.046	-0.00658
80	3.679	91.0	6.6	0.046	-0.00695
90	3.727	97.8	6.8	0.048	-0.00713
100*	3.779	105.0	7.2	0.052	-0.00722
110*	3.830	112.0	7.0	0.051	-0.00722
120*	3.888	120.0	8.0	0.058	-0.00722
130*	3.938	127.0	7.0	0.051	-0.00722
140*	3.989	134.0	7.0	0.051	-0.00722
150*	4.046	142.0	8.0	0.058	-0.00722

*extrapolated value

The estimated fuel temperatures for higher powers are derived by extrapolating fuel pin temperature vs. reactor power. This is shown in Figure 5-1 and in the equation:

$$P(\text{kW}) = 1.38 * T_{D\text{-}11} - 45.98 \quad (7.1)$$

$$P(\text{kW}) = 1.201 * T_{C\text{-}4} - 45.22 \quad (7.2)$$

where:

P = UUTR power in kW

$T_{C\text{-}4}$ = Temperature in the "C-4" fuel pin in °C

$T_{D\text{-}11}$ = Temperature in the "D-11" fuel pin in °C

Once the fuel pin temperature has been determined at higher power, the negative reactivity inserted due to the temperature change can then be derived by:

$$T_{(\text{C-4})\text{f}} - T_{(\text{C-4})\text{i}} * \alpha_{C\text{-}4}(\$) = \rho_f(\$) - \rho_i(\$) \quad (7.3)$$

$$T_{(\text{D-11})\text{f}} - T_{(\text{D-11})\text{i}} * \alpha_{D\text{-}11}(\$) = \rho_f(\$) - \rho_i(\$) \quad (7.4)$$

where:

$T_{(\text{C-4})\text{f}}$ = Temperature of "C-4" fuel pin after power increase

$T_{(\text{C-4})\text{i}}$ = Temperature of "C-4" fuel pin before power increase

$T_{(\text{D-11})\text{f}}$ = Temperature of "D-11" fuel pin after power increase

$T_{(\text{D-11})\text{i}}$ = Temperature of "D-11" fuel pin before power increase

$\alpha_{C\text{-}4}$ = Temperature coefficient of "C-4" fuel pin

$\alpha_{D\text{-}11}$ = Temperature coefficient of "D-11" fuel pin

ρ_f = Cumulative reactivity inserted into the core contributed by all control rods after power increase.

ρ_i = Cumulative reactivity inserted into the core contributed by all control rods before power increase.

7.3. Discussion

Experimental measurements as well as numerical MCNP5 calculation are used to extrapolate for the maximum achievable UUTR power. It is shown that the maximum achievable power with the current control rod system is 150kW.

CHAPTER 8

UUTR POWER UPGRADE

8.1. Introduction

The maximum practical power of the current UUTR core configuration is 150kW. An additional control rod is necessary for reactor powers above 150kW. In this chapter, three reactor designs for a potential power upgrade are assessed. Reactor designs for powers of 300kW, 400kW, and 500kW are evaluated.

8.2. Power Upgrade

The design requirement for the power upgrade is to design a reactor core which is capable of reaching higher powers up to 500kW. In addition, the neutron flux shape across the reactor core needs to be without irregularities and similar to the current UUTR core configuration. The power peaking factors of the fuel are required to be equal or better (lower is better) than the current core design. Also, it is crucial to keep the shut down margin of the upgraded reactor equal or higher than the current UUTR core configuration.

8.3. Reactor Performance

MCNP5 is used to numerically estimate the k_{eff} for each upgraded reactor power up to 500kW. Since the temperature coefficient has been measured and numerically benchmarked, it can now be used to extrapolate the k_{eff} for higher

powers. Table 8-1 shows the k_{eff} required in order to reach a certain power level. The trend is linear, as shown in Figure 8-1.

The fuel temperature is proportional to reactor power. Table 8-2 shows the "C-4" and "D-11" fuel temperatures for reactor powers ranging from 100kW to 500kW. There is a linear trend that can be noted. This is because temperature and power are proportional to one another. Figure 8-2 shows the temperature of fuel pins "C4" and "D11" at each corresponding reactor power levels.

Table 8-1. Reactor power vs. k_{eff}

Reactor Power (kW)	k_{eff}
100	1.00401
150	1.00600
200	1.00798
250	1.00996
300	1.01194
350	1.01392
400	1.01590
450	1.01789
500	1.01987
550	1.02185

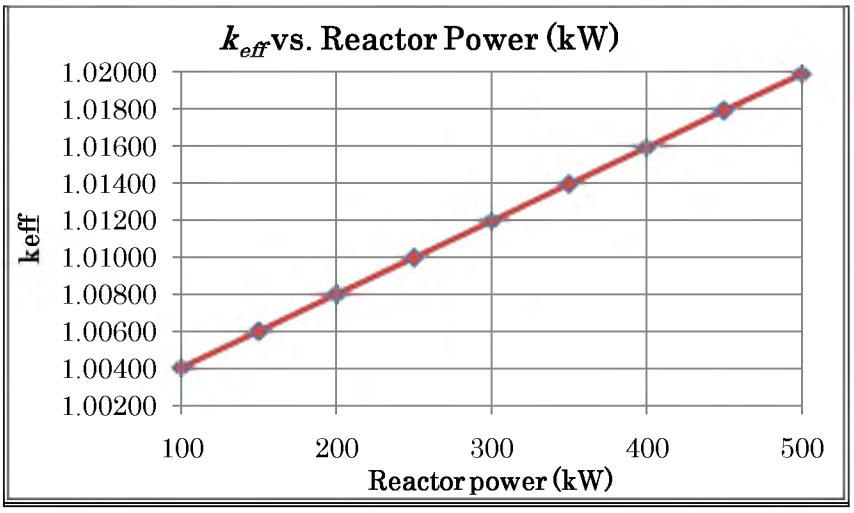

Figure 8-1. MCNP5 calculated reactor power vs. k_{eff}

Table 8-2. Reactor power vs. fuel pin temperature

Reactor Power (kW)	C-4 Fuel Temperature (°C)	D-11 Fuel Temperature (°C)
100	121	106
150	162	142
200	204	178
250	245	214
300	287	250
350	329	286
400	370	323
450	412	359
500	453	395

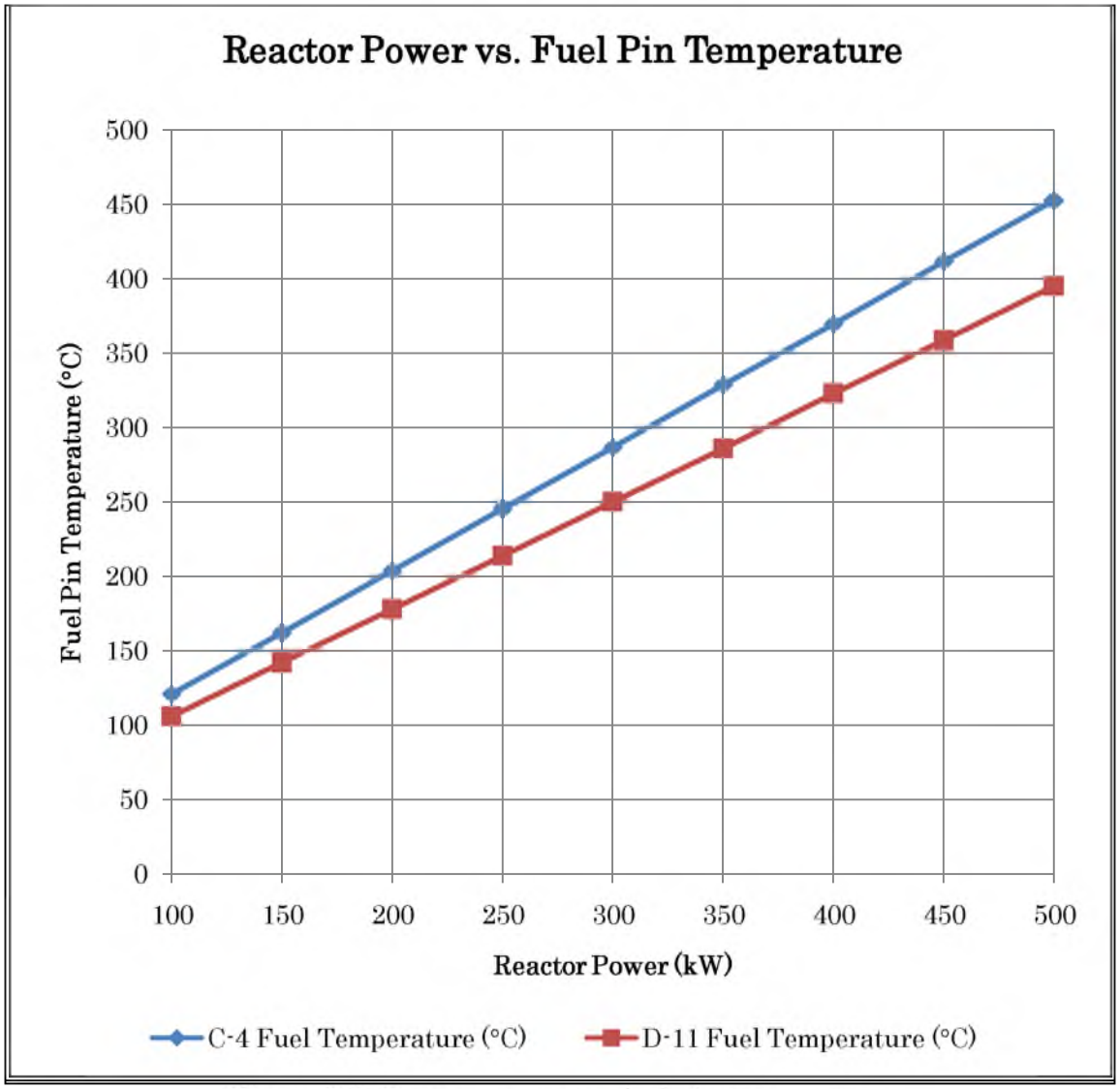

Figure 8-2. Reactor power vs. fuel pin temperature

8.4. Power Upgrade Design for 300kW

The first proposal suggests a design that has four control rods. The regulation, shim, and safety control rods are located in "D1", "D7", and "D13", respectively. Additionally, a safety 2 control rod is added into the "C-11". The "C-11" is vacant in the current UUTR core configuration.

A total of four new stainless steel clad elements are added into the core. A first new stainless steel clad fuel element is added into the currently vacant slot "E-21". The heavy water element is moved from "F-25" into "G-29"; concurrently, a second new stainless steel element is placed into "F-25". The heavy water element is moved from "F-24" into "G-28"; at the same time, a third new stainless steel element is placed into "F-24". The heavy water element is moved from "F-23" into "G-27"; in tandem, a fourth new stainless steel element is placed into "F-23". Figure 8-3 shows the graphical representation of the upgraded core.

8.4.1. Neutronics Parameters

The reactor core parameters are calculated using the MCNP5. Table 8-3 summarizes calculated k_{eff} for each corresponding control rod position. All k_{eff}MCNP5 calculations are done with 120 million particles on a Pentium Quad 2 Core Q6600.

IN position corresponds to fully inserted control rod. OUT position corresponds to fully withdrawn control rod. All k_{eff} simulations are done with 120 million particles. The $k_{eff}$with all control rods withdrawn is 1.01466 +/- 0.00016, which makes this reactor design ideally suitable for a 300kW reactor power.

Additional reactor core parameters are calculated using the MCNP5. Table 8-4 and Figure 8-4 summarize calculated excess reactivity, shutdown margin, and control rod worth.

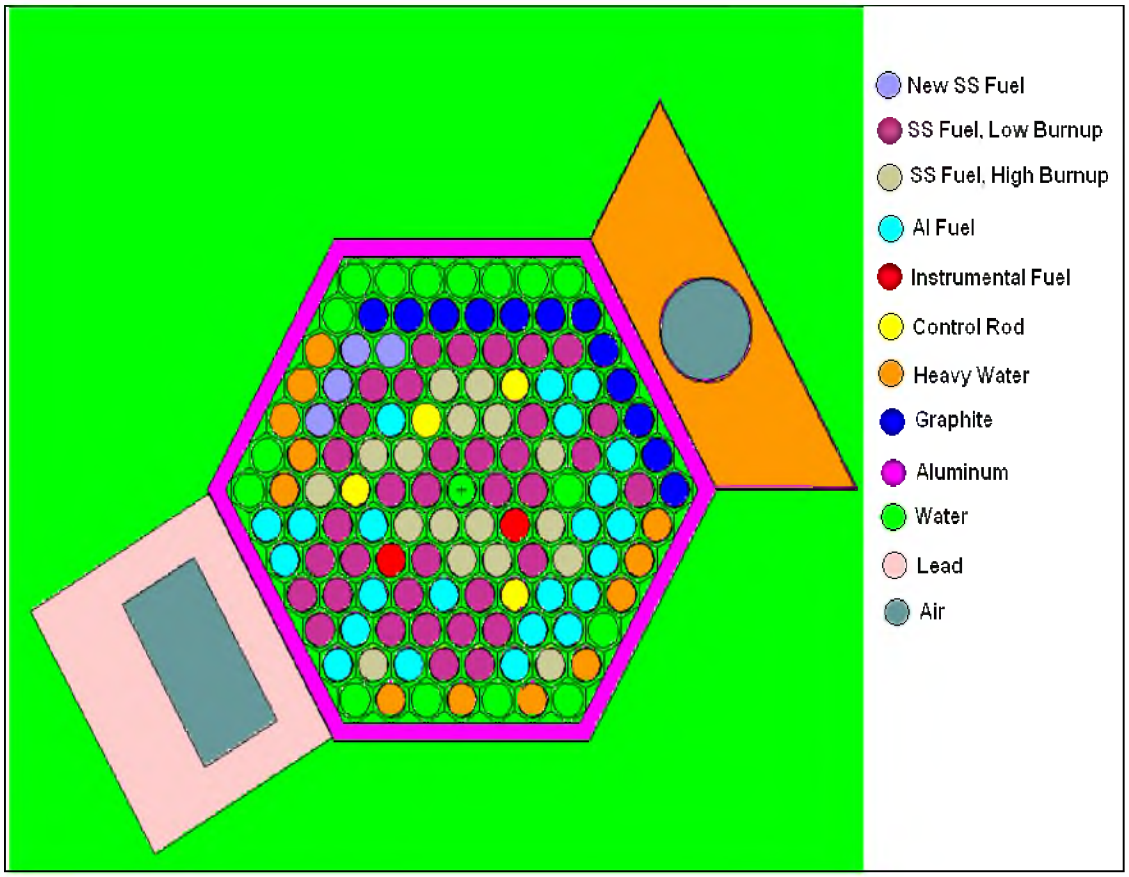

Figure 8-3. Schematics of the upgrade core design for 300kW reactor power

Table 8-3. MCNP5 calculated k_{eff} for each corresponding control rod position of the 300kW core design

Safety 2 control rod	Safety control rod	Shim control rod	Regulation control rod	k_{eff}			CPU Time (hours)
OUT	IN	IN	IN	0.98427	+/-	0.00017	23.1
IN	OUT	IN	IN	0.98679	+/-	0.00017	23.2
IN	IN	OUT	IN	0.98300	+/-	0.00017	23.1
IN	OUT	OUT	OUT	1.00071	+/-	0.00017	23.2
OUT	IN	OUT	OUT	1.00142	+/-	0.00014	23.2
OUT	OUT	IN	OUT	1.00171	+/-	0.00016	23.2
OUT	OUT	OUT	IN	1.01285	+/-	0.00015	23.1
OUT	**OUT**	**OUT**	**OUT**	**1.01466**	**+/-**	**0.00016**	23.4
OUT	OUT	OUT	OUT	1.00720	+/-	0.00015	22.8
			β_{eff}	0.00735	+/-	0.00016	

Table 8-4. MCNP5 calculated excess reactivity, shut down margin, and control rod worth of the 300kW core design

MCNP5 Simulation	ρ (Δk/k)			ρ ($)		
Safety 2 control rod	0.01374	+/-	0.00023	1.8686	+/-	0.0513
Safety control rod	0.01303	+/-	0.00021	1.7723	+/-	0.0479
Shim control rod	0.01274	+/-	0.00022	1.7330	+/-	0.0484
Regulation control rod	0.00176	+/-	0.00021	0.2395	+/-	0.0295
Total Rod Worth	**0.04127**	**+/-**	**0.00088**	**5.61344**	**+/-**	**0.1771**
Excess Reactivity	0.01445	+/-	0.00044	1.9651	+/-	0.0221
Shut Down Margin	0.01598	+/-	0.00043	2.1737	+/-	0.0188

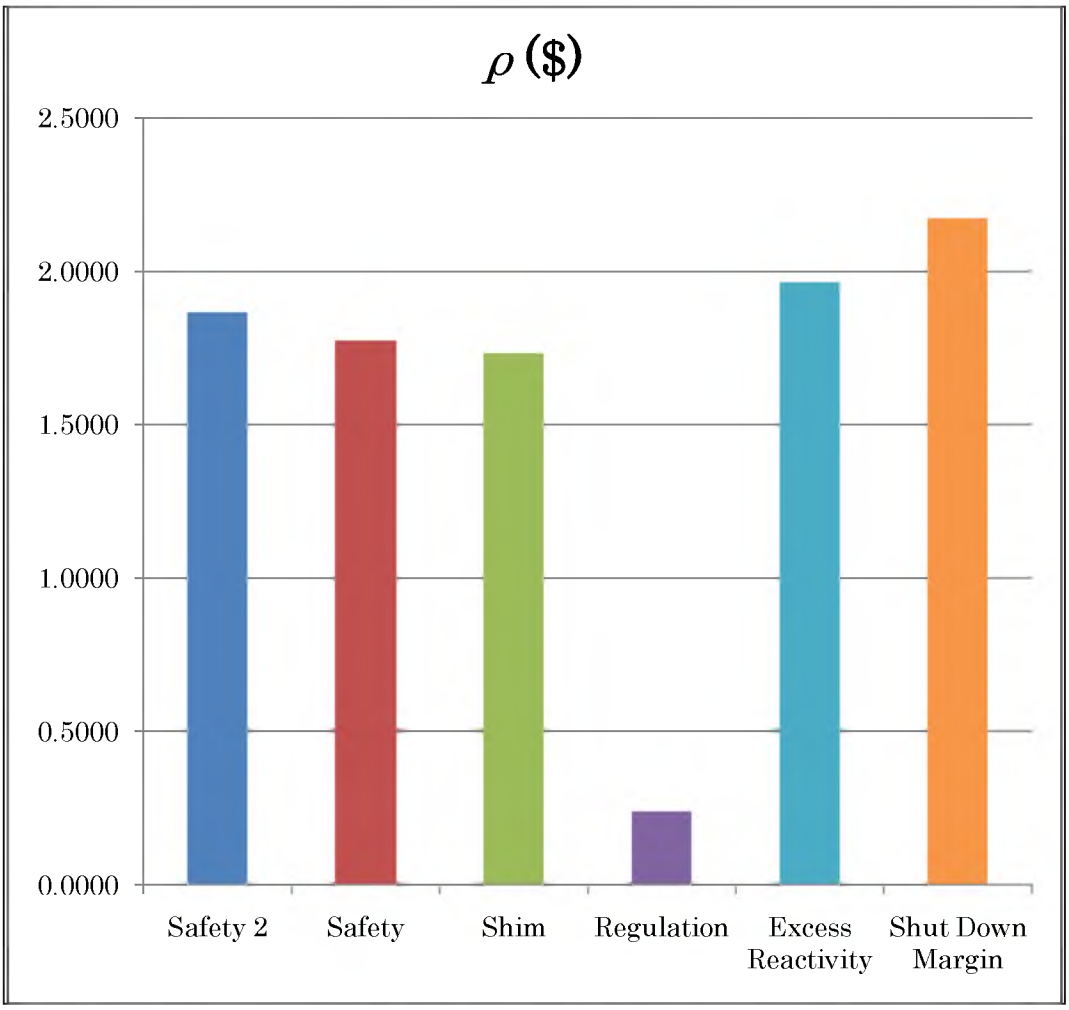

Figure 8-4. Reactivity worth of each control rod, excess reactivity, and shut down margin of the 300kW core design

8.4.2. MCNP5 Core Analysis at 300kW

Core analysis of the proposed upgrade at 300kW reactor power is shown in this subsection. Table 8-5 represents the fuel element power distribution per fuel ring at 300kW reactor power. Figure 8-5 shows the peaking factors of the UUTR core at 300kW reactor power. Figure 8-6 shows the 3D pin power distribution of the core at 300kW. Figure 8-7 shows the top view of pin power distribution in kilowatts at 300kW reactor power. Matlab program is used to plot the flux [38]. Figure 8-8 shows the 3D view of the total neutron flux distribution at a reactor power of 300kW. Figure 8-9 is a contour view of the total neutron flux distribution of the UUTR at a reactor power of 300kW. Figure 8-10 shows the 3D view of the fast neutron flux distribution at a reactor power of 300kW. Figure 8-11 is a contour view of the fast neutron flux distribution of the UUTR at a reactor power of 300kW. Figure 8-12 shows the 3D view of the thermal neutron flux distribution at a reactor power of 300kW. Figure 8-13 is a contour view of the thermal neutron flux distribution of the UUTR at a reactor power of 300kW.

Table 8-5. Fuel element power distribution per fuel ring at 300kW reactor power

Ring	Number of Fuel Pins	Maximum Power Per Fuel Pin P_{max} (kW/pin)	Minimum Power Per Fuel Pin P_{min} (kW/pin)	Average Power Per Fuel Pin P_{avg} (kW/pin)	Ratio (P_{max} / P_{min})	Ratio (P_{max} / P_{avg})
B	6	5.854	5.487	5.735	1.067	1.021
C	11	5.411	4.348	4.966	1.244	1.090
D	14	5.082	3.721	4.323	1.366	1.176
E	24	4.242	2.615	3.394	1.622	1.250
F	22	3.375	2.186	2.664	1.544	1.267
G	5	2.300	1.884	2.076	1.221	1.108
Total	82	5.854	1.884	3.659	3.107	1.600

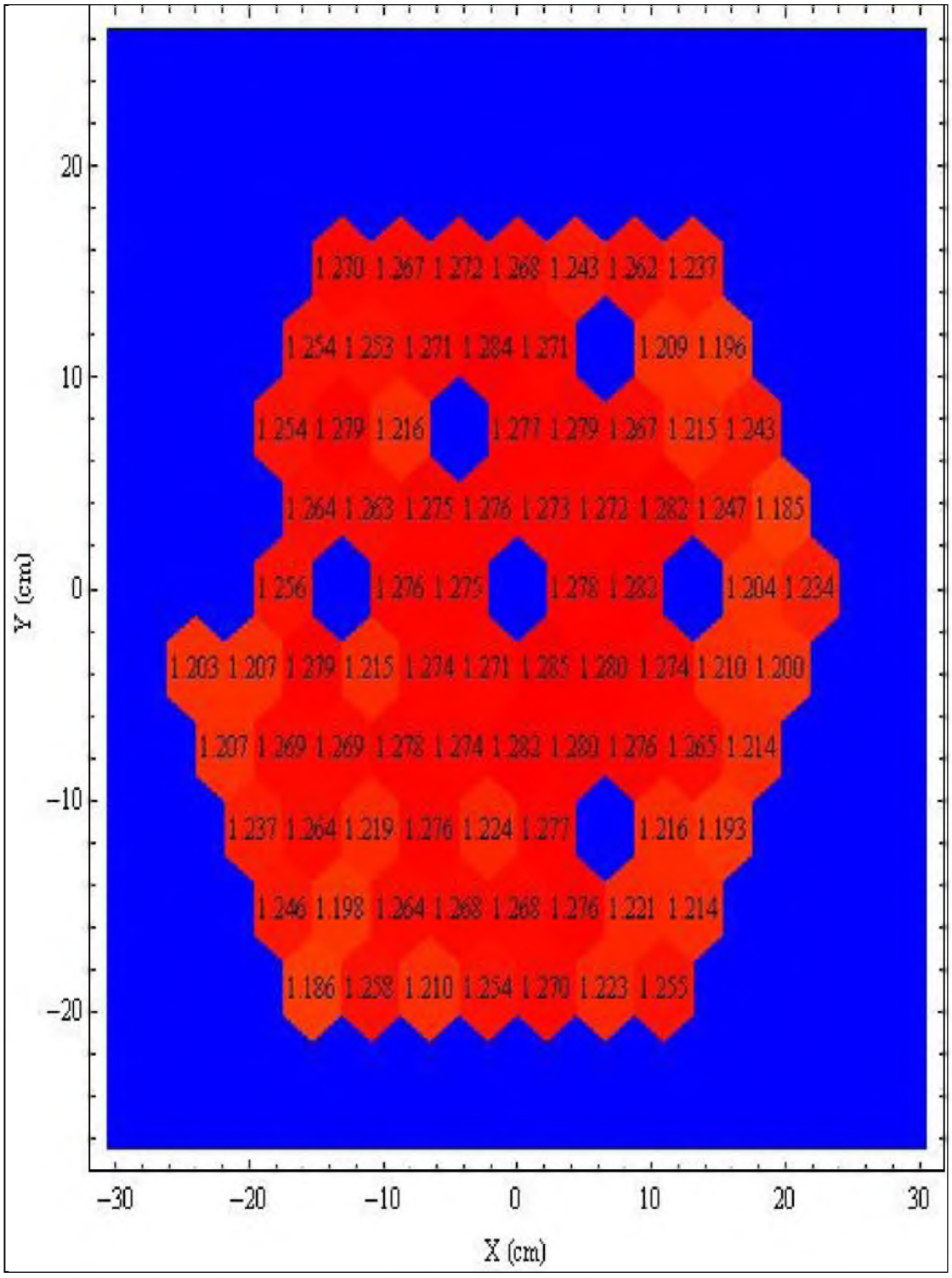

Figure 8-5. Peaking factors of core design at 300kW reactor power

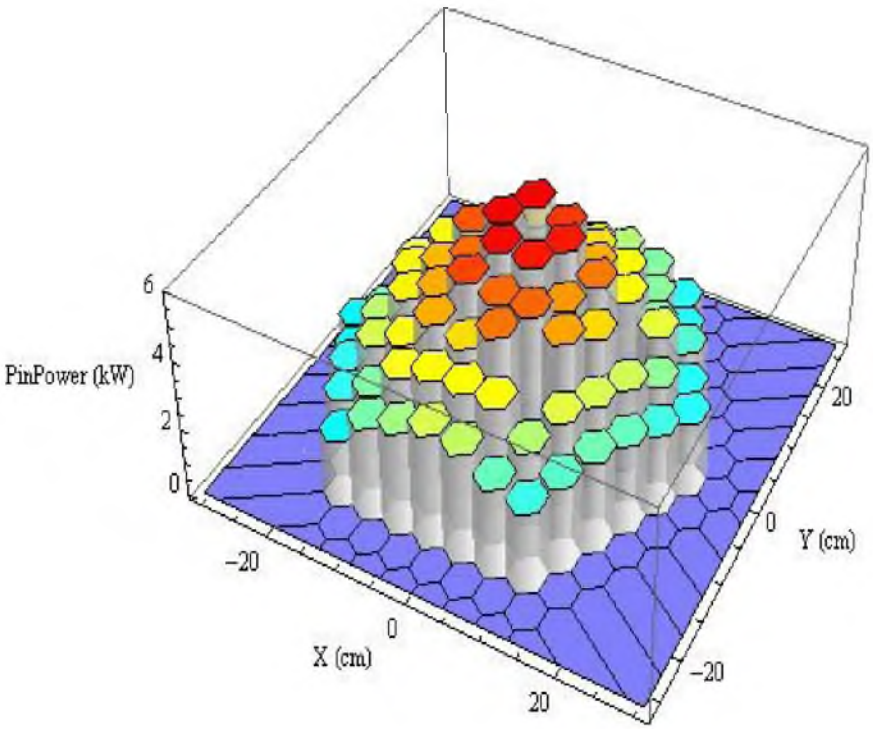

Figure 8-6. 3D view of pin power distribution in kilowatts at 300kW reactor power

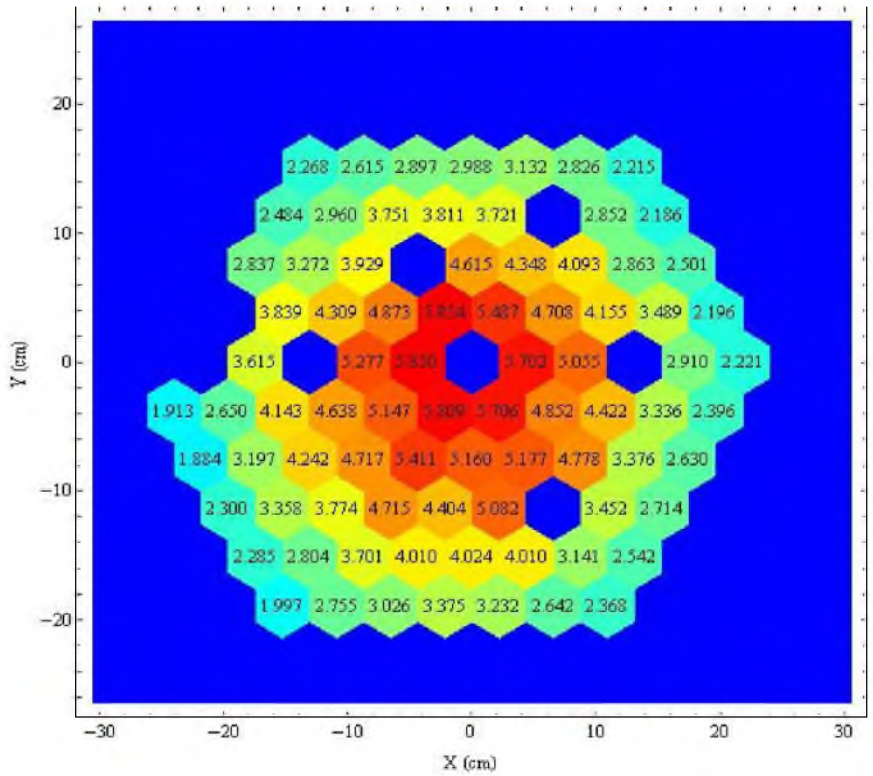

Figure 8-7. Top view of pin power distribution in kilowatts at 300kW reactor power

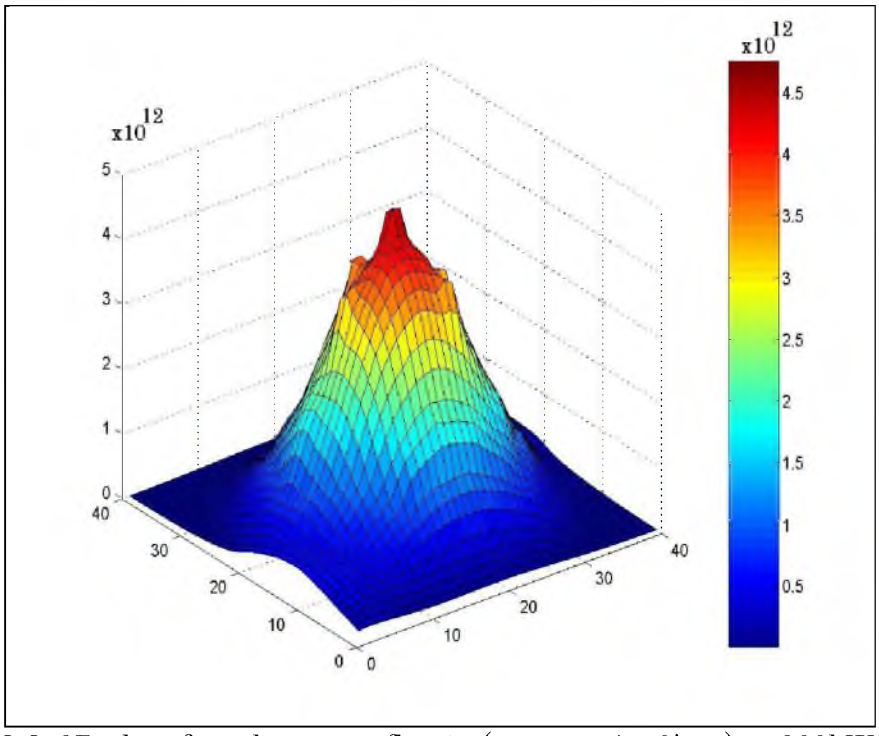

Figure 8-8. 3D plot of total neutron flux in (neutrons/cm^2*sec) at 300kW reactor power for all neutron energies

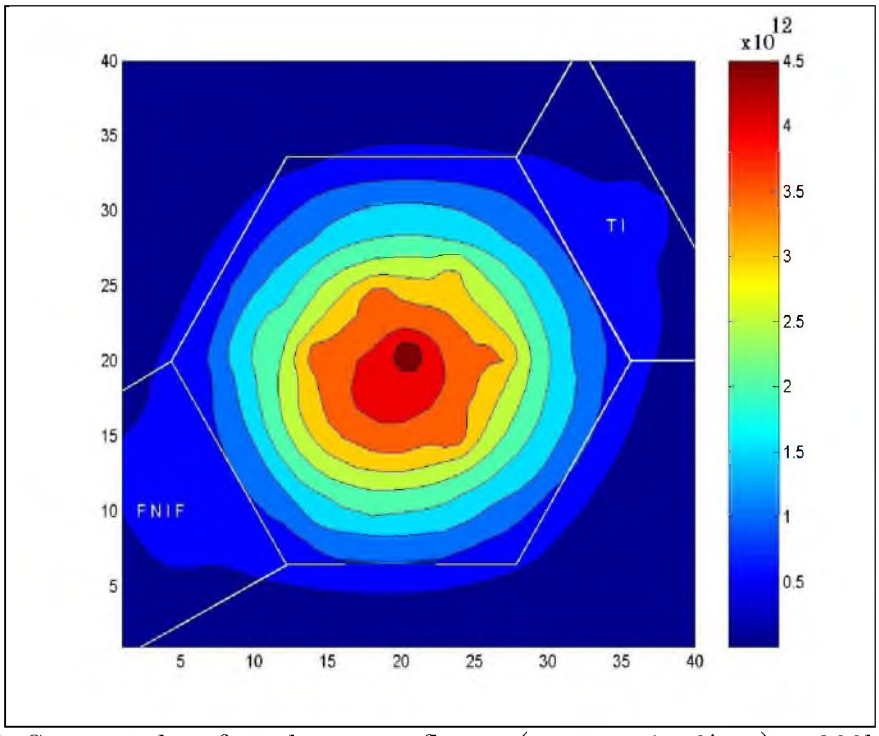

Figure 8-9. Contour plot of total neutron flux in (neutrons/cm^2*sec) at 300kW reactor power for all neutron energies

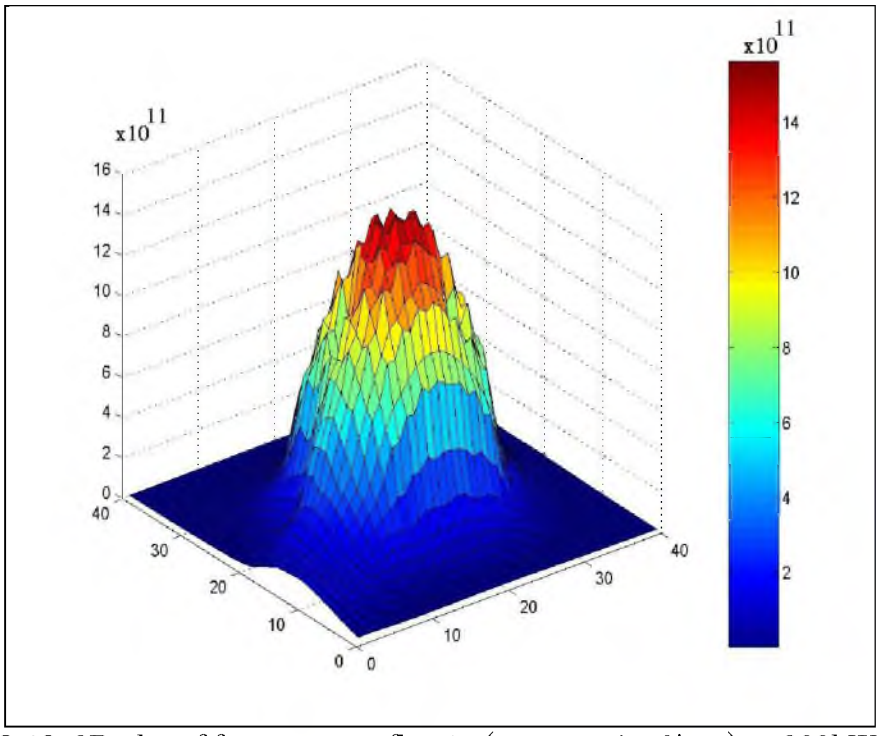

Figure 8-10. 3D plot of fast neutron flux in (neutrons/cm^2*sec) at 300kW reactor power for neutron energies above 100keV

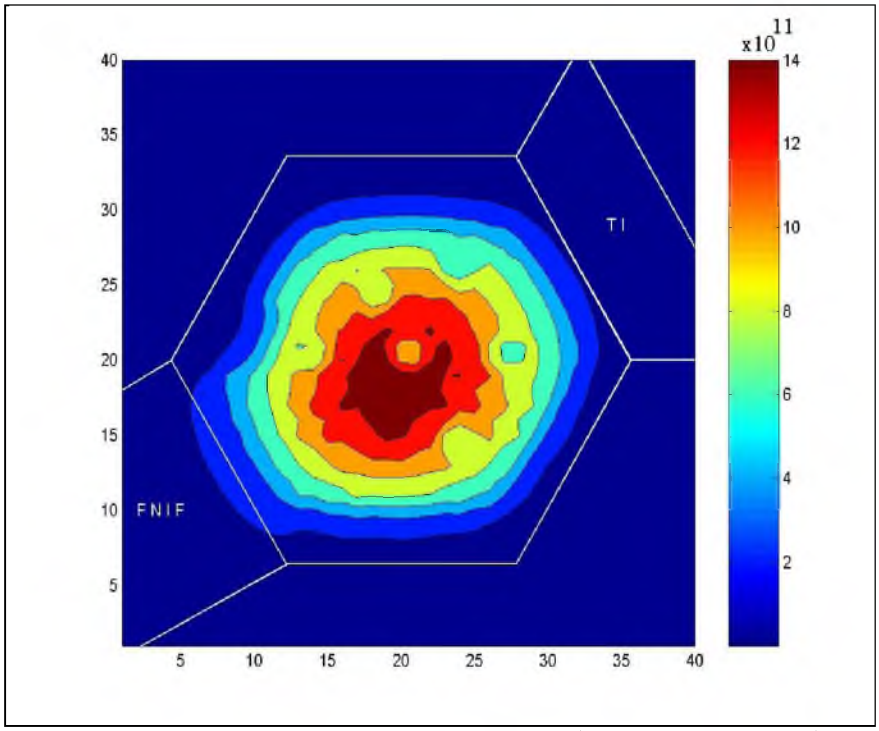

Figure 8-11. Contour plot of fast neutron flux in (neutrons/cm^2*sec) at 300kW reactor power for neutron energies above 100keV

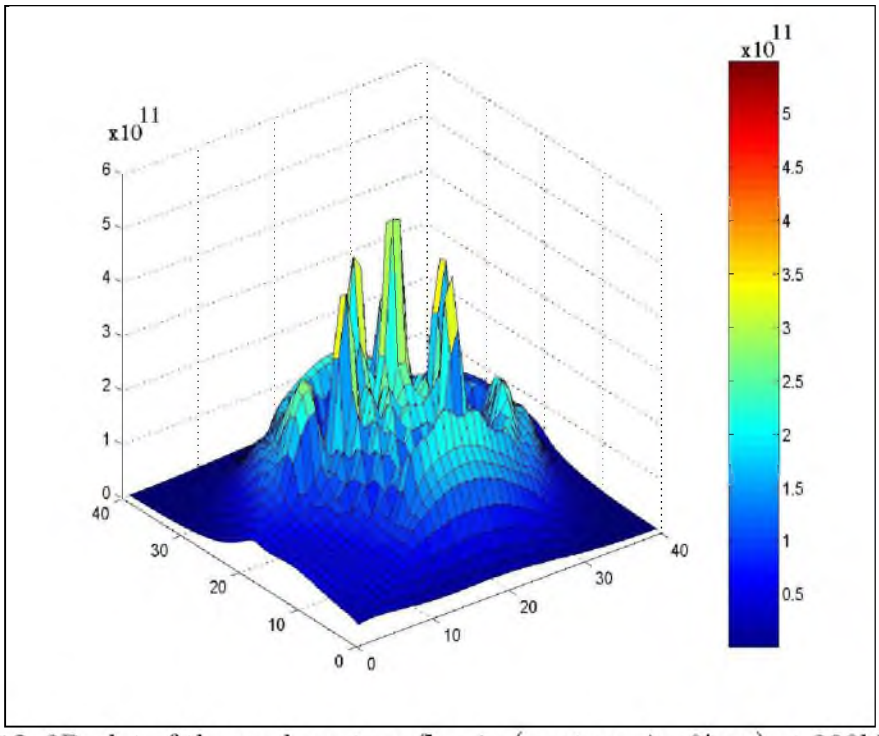

Figure 8-12. 3D plot of thermal neutron flux in (neutrons/cm^2*sec) at 300kW reactor power for neutron energies below 0.025eV

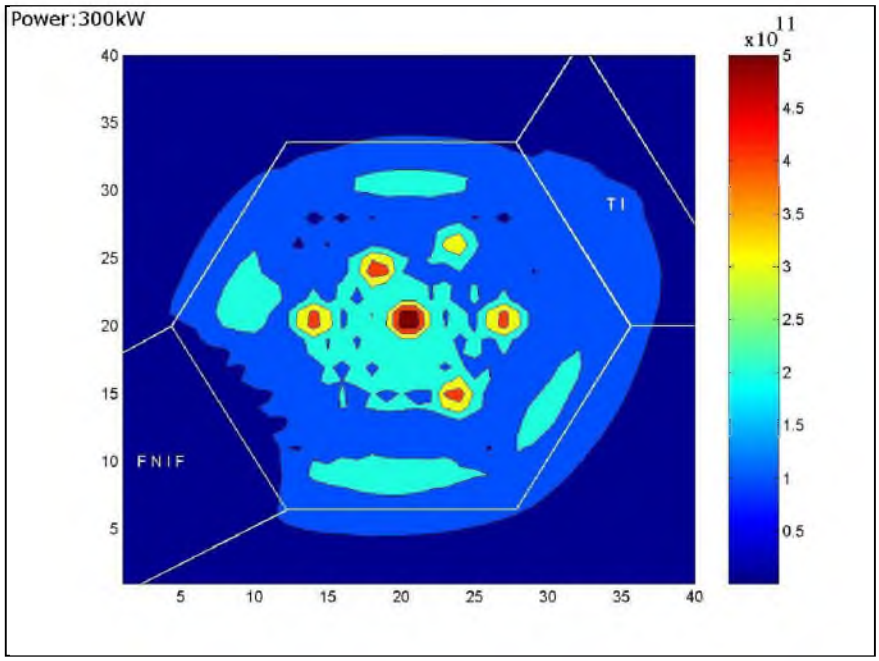

Figure 8-13. Contour plot of thermal neutron flux in (neutrons/cm^2*sec) at 300kW reactor power for neutron energies below 0.025eV

Figure 8-14 shows the power density profile of the fuel element with the highest power at each corresponding reactor power of 100kW, 150kW, 300kW, 400kW, and 500kW. The axial power of each fuel element is shown to be the highest at the center of the rod because the core neutron flux is the highest along the centerline of the core.

8.5. Power Upgrade Design for 400kW

The second proposal suggests a design that has four control rods. The regulation, shim, and safety control rods are located in the "D1", "D7", and "D13", respectively. Additionally, a safety 2 control rod is added into the "C-11". The "C-11" is vacant in the current UUTR core configuration.

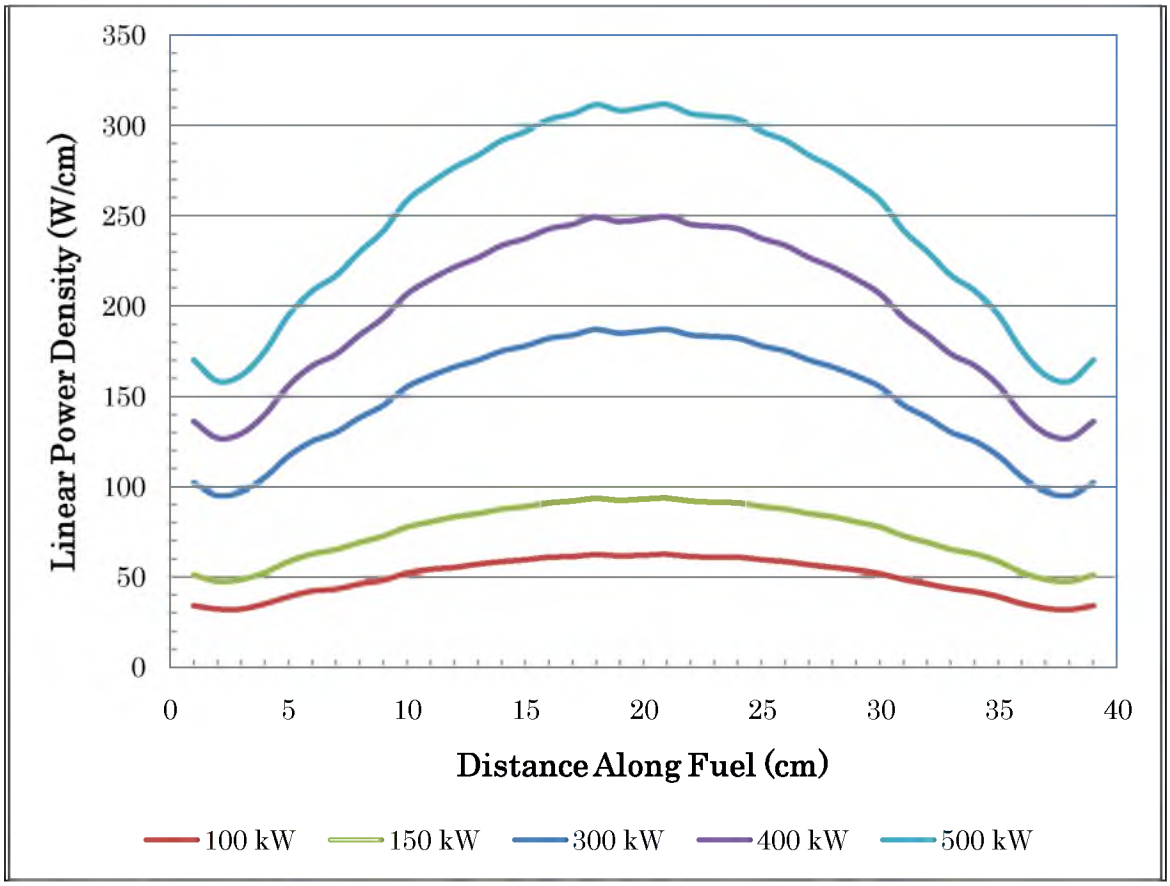

Figure 8-14. Axial power profile of the fuel element with the highest power at 100kW, 150kW, 300kW, 400kW, and 500kW reactor power.

A total of six new stainless steel clad elements are added into the core. A first new stainless steel clad fuel element is added into the currently vacant slot "E-21". The heavy water element is moved from "F-25" into "G-29"; concurrently, a second new stainless steel element is placed into "F-25". The heavy water element is moved from "F-24" into "G-28"; at the same time, a third new stainless steel element is placed into "F-24". The heavy water element is moved from "F-23" into "G-27"; in tandem, a fourth new stainless steel element is placed into the "F-23". The heavy water element is moved from "F-22" into "G-26"; concurrently, a fifth new stainless steel element is placed into "F-22". The heavy water element is moved from "F-21" into "G-25"; at the same time, a sixth new stainless steel clad fuel element is placed into "F-21". Schematics of the upgrade core design for 400kW reactor power is shown in Figure 8-15.

8.5.1. Neutronics Parameters

The reactor core parameters are calculated using the MCNP5. Table 8-6 summarizes calculated k_{eff} for each corresponding control rod position. All k_{eff} MCNP5 calculations are done with 120 million particles on a Pentium Quad 2 Core Q6600.

IN position corresponds to fully inserted control rod. OUT position corresponds to fully withdrawn control rod. All k_{eff} simulations are done with 120 million particles. The k_{eff} with all control rods withdrawn is 1.01963 +/- 0.00016, which makes this reactor design ideally suitable for a 400kW reactor power.

Additional reactor core parameters are calculated using the MCNP5. Table 8-7 and Figure 8-16 summarize the calculated excess reactivity, shutdown margin, and control rod worth.

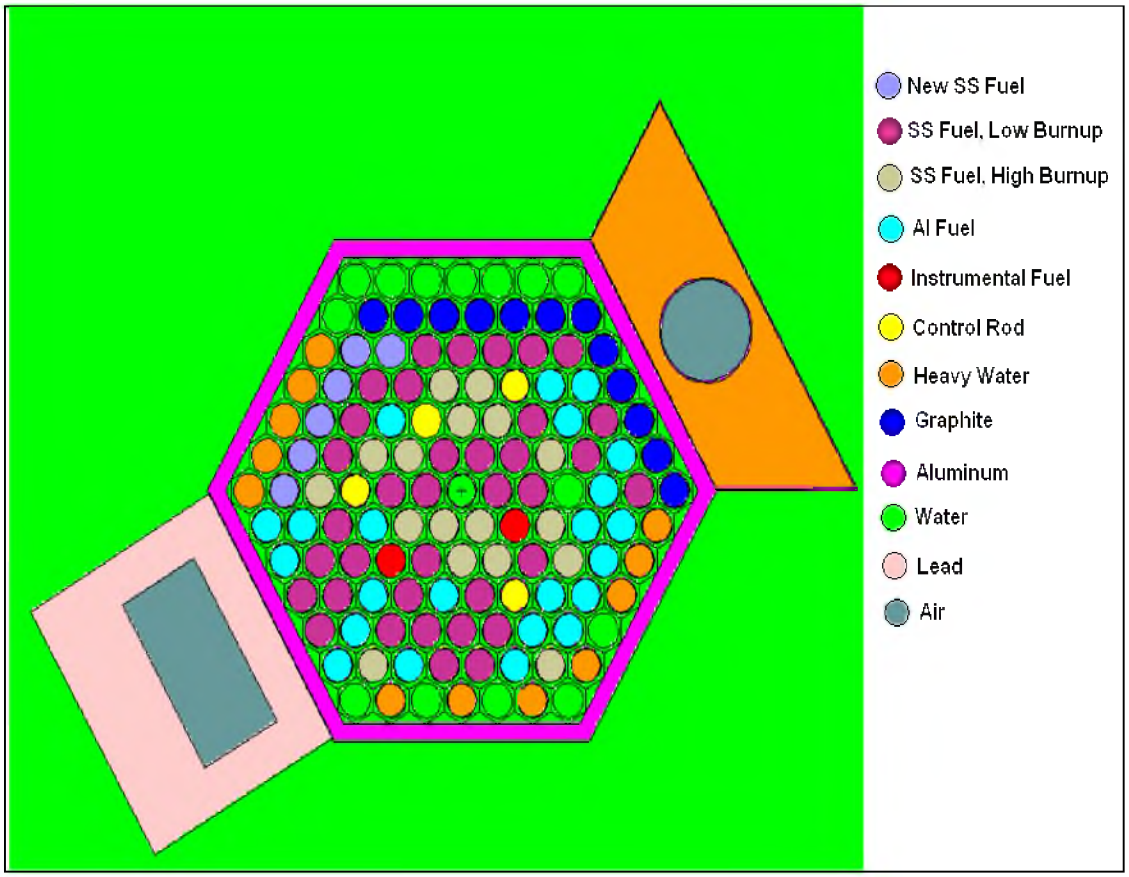

Figure 8-15. Schematics of the upgrade core design for 400kW reactor power

Table 8-6. MCNP5 calculated k_{eff} for each corresponding control rod position of the 400kW core design

Safety 2 control rod	Safety control rod	Shim control rod	Regulation control rod	k_{eff}			CPU Time (hours)
OUT	IN	IN	IN	0.98840	+/-	0.00017	23.1
IN	OUT	IN	IN	0.98963	+/-	0.00017	23.2
IN	IN	OUT	IN	0.98894	+/-	0.00017	23.1
IN	OUT	OUT	OUT	1.00542	+/-	0.00017	23.2
OUT	IN	OUT	OUT	1.00718	+/-	0.00014	23.2
OUT	OUT	IN	OUT	1.00572	+/-	0.00016	23.2
OUT	OUT	OUT	IN	1.01741	+/-	0.00015	23.1
OUT	**OUT**	**OUT**	**OUT**	**1.01963**	**+/-**	**0.00016**	23.4
OUT	OUT	OUT	OUT	1.01214	+/-	0.00015	22.8
			β_{eff}	0.00735	+/-	0.00016	

Table 8-7. MCNP5 calculated excess reactivity, shut down margin, and control rod worth of the 400kW core design

MCNP5 Simulation	ρ (Δk/k)			ρ ($)		
Safety 2 control rod	0.01386	+/-	0.00023	1.8870	+/-	0.0515
Safety control rod	0.01212	+/-	0.00021	1.6504	+/-	0.0457
Shim control rod	0.01356	+/-	0.00022	1.8466	+/-	0.0502
Regulation control rod	0.00214	+/-	0.00021	0.2913	+/-	0.0295
Total Rod Worth	**0.04169**	**+/-**	**0.00087**	**5.67524**	**+/-**	**0.1768**
Excess Reactivity	0.01925	+/-	0.00043	2.6208	+/-	0.0166
Shut Down Margin	0.01174	+/-	0.00043	1.5977	+/-	0.0256

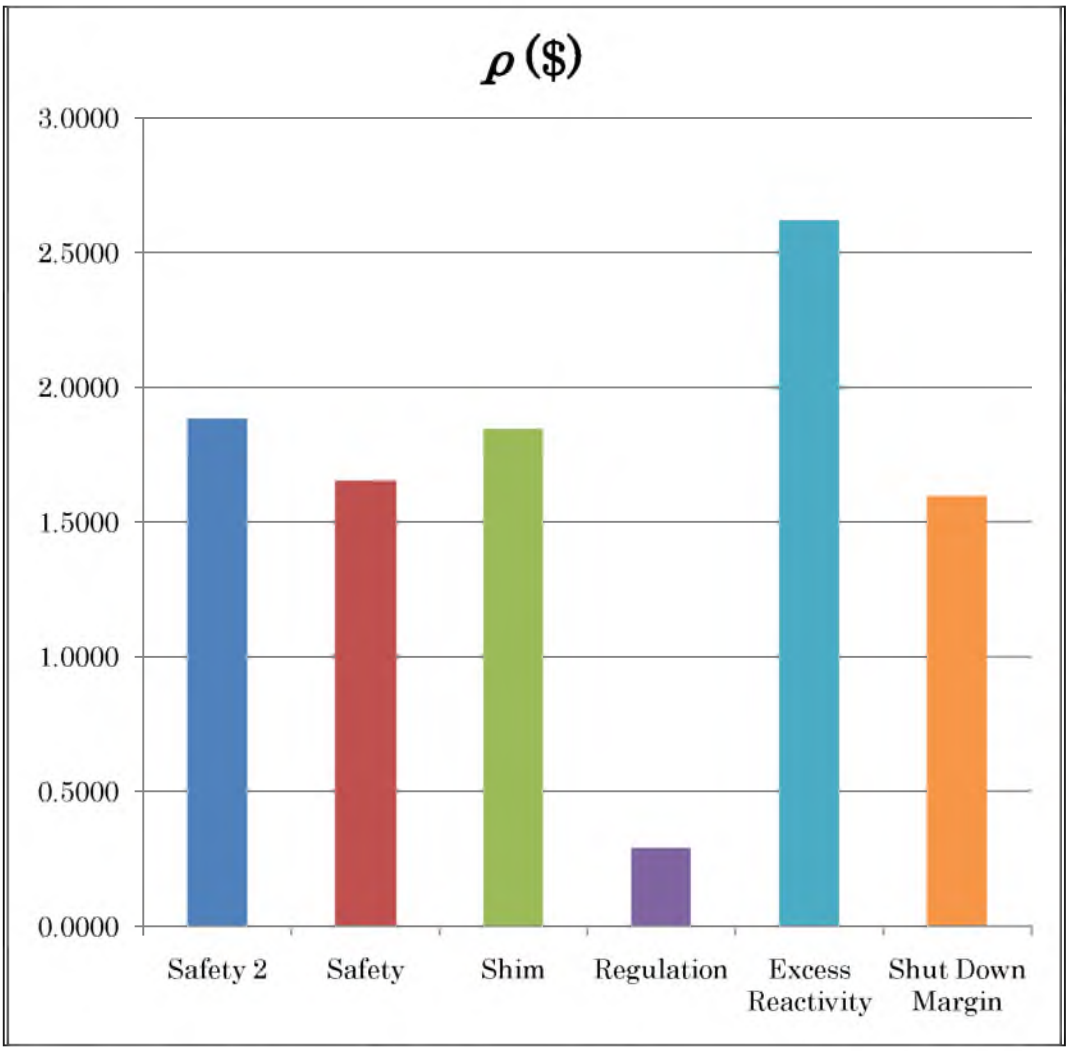

Figure 8-16. Reactivity worth of each control rod, excess reactivity, and shut down margin of the 400kW core design

8.5.2. MCNP5 Core Analysis at 400kW

Core analysis of the proposed upgrade at 400kW reactor power is shown in this subsection through upcoming figures and tables. Table 8-8 represents the fuel element power distribution per fuel ring at 400kW reactor power. Figure 8-17 shows the peaking factors of the UUTR core at 400kW reactor power. Figure 8-18 shows the 3D pin power distribution of the core at 400kW. Figure 8-19 shows the top view of pin power distribution in kilowatts at 400kW reactor power. Matlab program is used to plot the flux [38]. Figure 8-20 shows the 3D view of the total neutron flux distribution at a reactor power of 400kW. Figure 8-21 is a top view of the total neutron flux distribution of the UUTR at a reactor power of 400kW. Figure 8-22 shows the 3D view of the fast neutron flux distribution at a reactor power of 400kW. Figure 8-23 is a top view of the fast neutron flux distribution of the UUTR at a reactor power of 400kW. Figure 8-24 shows the 3D view of the thermal neutron flux distribution at a reactor power of 400kW. Figure 8-25 is a top view of the thermal neutron flux distribution of the UUTR at a reactor power of 400kW.

Table 8-8. Fuel element power distribution per fuel ring at 400kW reactor power

Ring	Number of Fuel Pins	Maximum Power Per Fuel Pin P_{max} (kW/pin)	Minimum Power Per Fuel Pin P_{min} (kW/pin)	Average Power Per Fuel Pin P_{avg} (kW/pin)	Ratio (P_{max} / P_{min})	Ratio (P_{max} / P_{avg})
B	6	7.698	7.116	7.463	1.082	1.031
C	11	7.088	5.655	6.480	1.253	1.094
D	14	6.516	4.849	5.670	1.344	1.149
E	24	5.751	3.487	4.446	1.649	1.294
F	24	4.524	2.766	3.493	1.636	1.295
G	5	3.181	2.442	2.808	1.303	1.133
Total	84	7.698	2.442	4.762	3.152	1.617

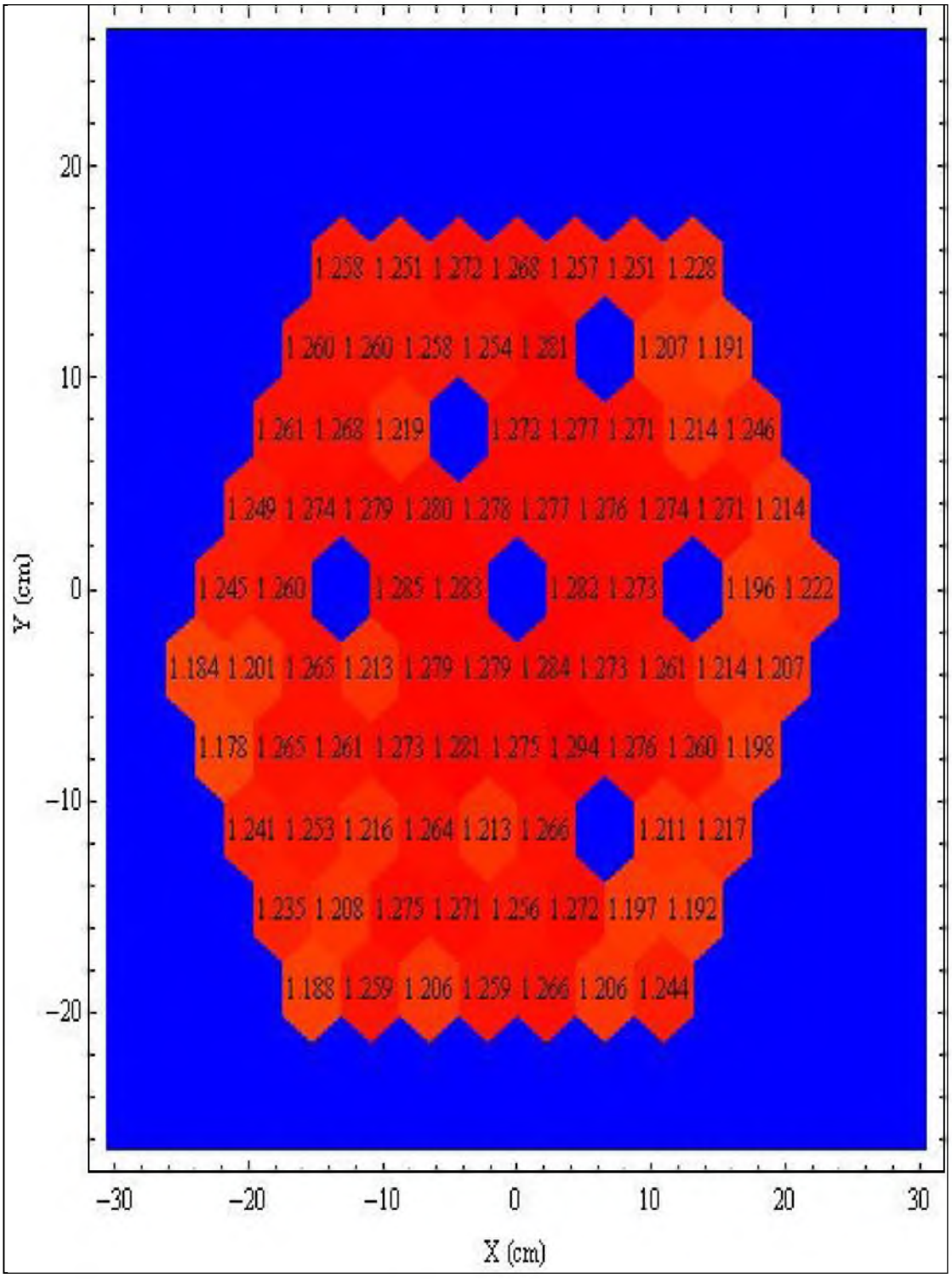

Figure 8-17. Peaking factors of core at 400kW reactor power

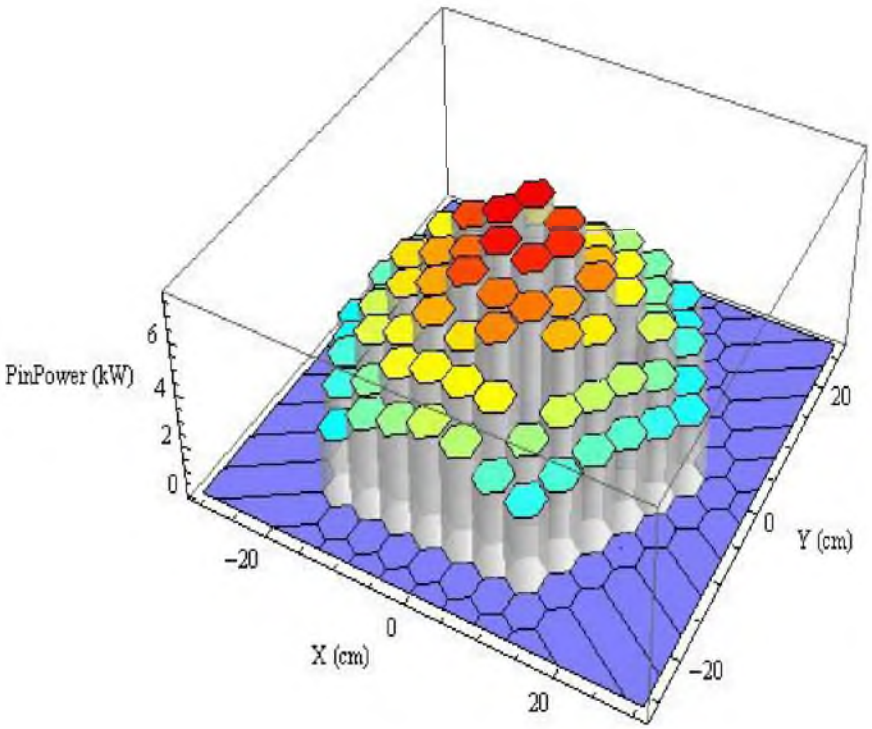

Figure 8-18. 3D view of pin power distribution in kilowatts at 400kW reactor power

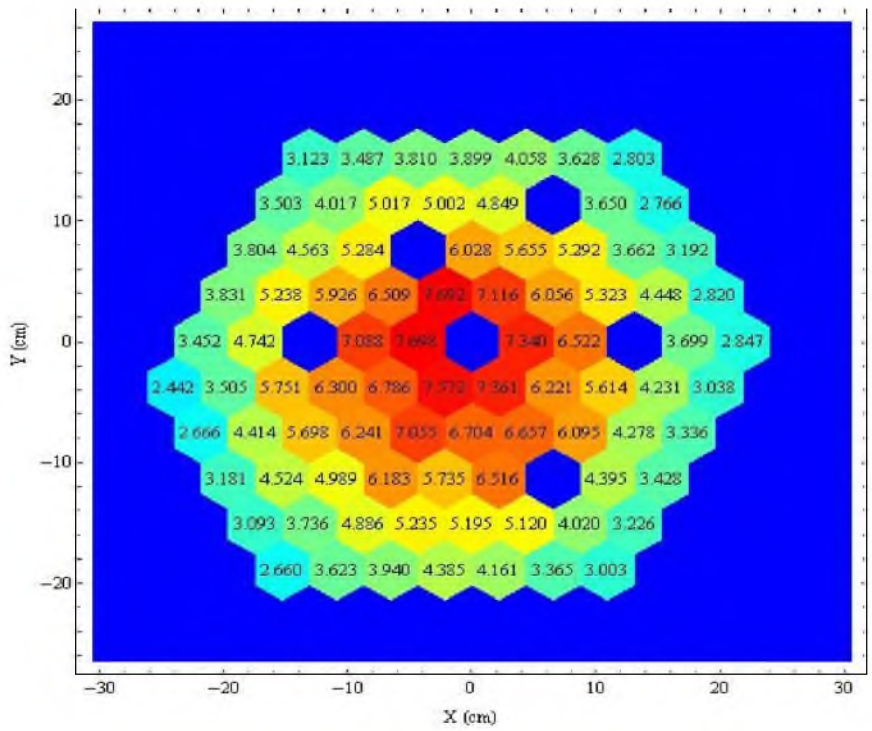

Figure 8-19. Top view of pin power distribution in kilowatts at 400kW reactor power

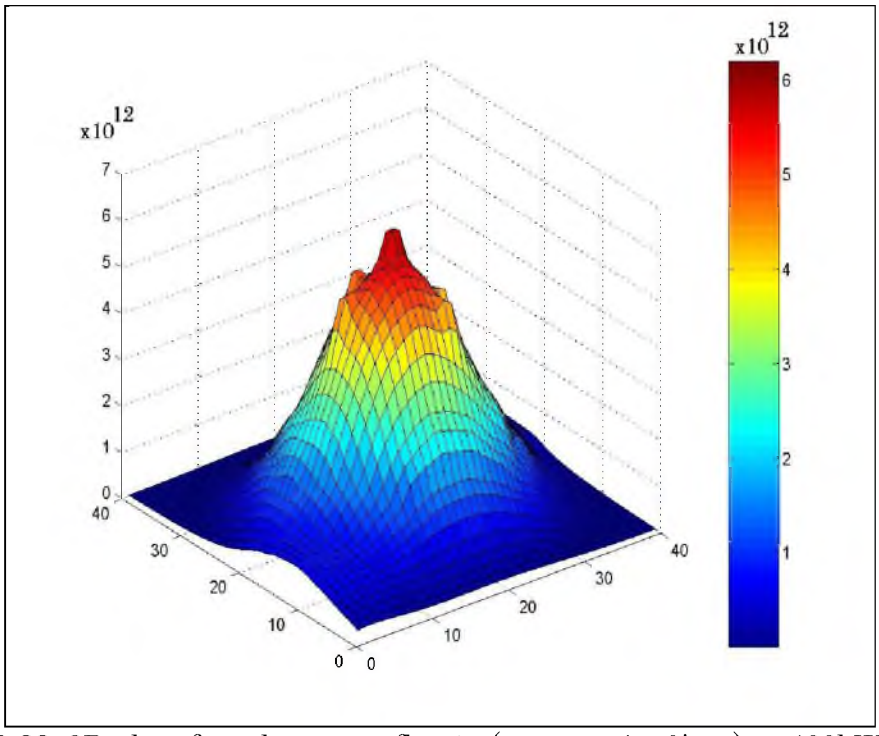

Figure 8-20. 3D plot of total neutron flux in (neutrons/cm^2*sec) at 400kW reactor power for all neutron energies

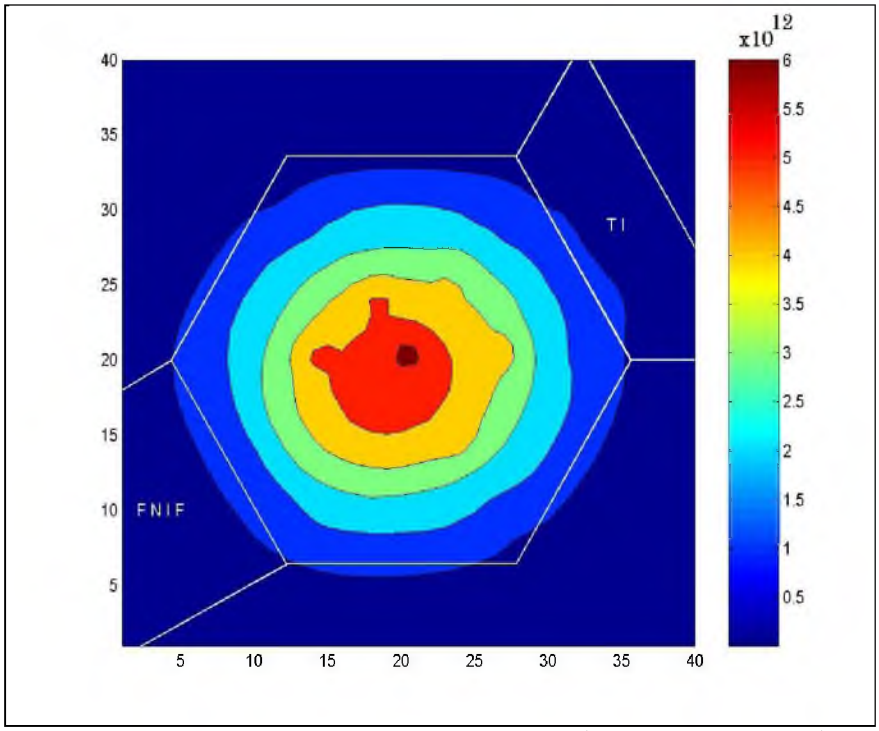

Figure 8-21. Contour plot of total neutron flux in (neutrons/cm^2*sec) at 400kW reactor power for all neutron energies

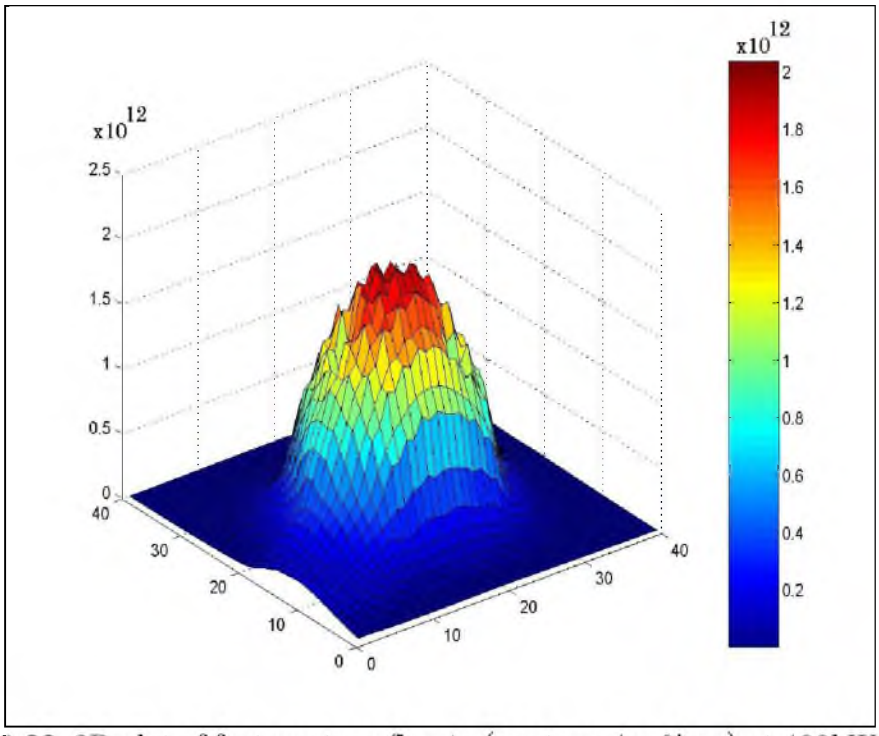

Figure 8-22. 3D plot of fast neutron flux in (neutrons/cm^2*sec) at 400kW reactor power for neutron energies above 100keV

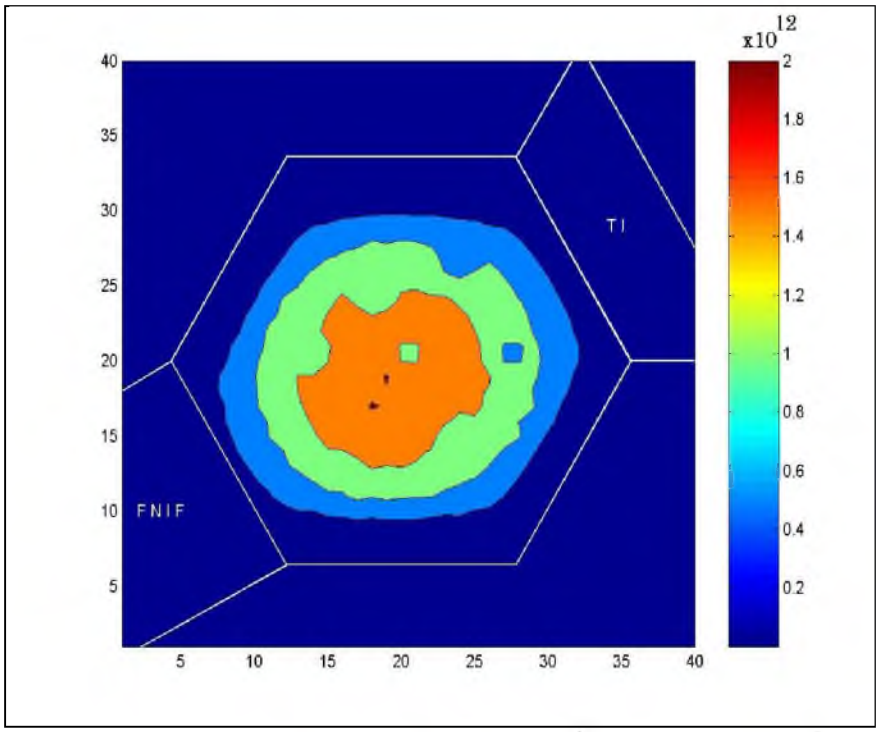

Figure 8-23. Contour plot of fast neutron flux in (neutrons/cm^2*sec) at 400kW reactor power for neutron energies above 100keV

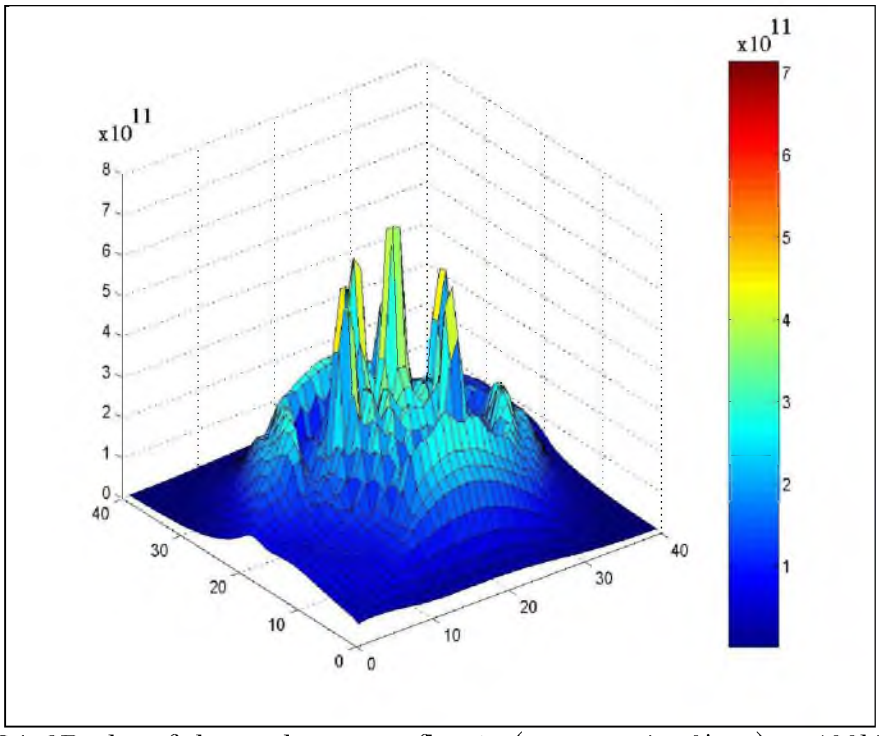

Figure 8-24. 3D plot of thermal neutron flux in (neutrons/cm^2*sec) at 400kW reactor power for neutron energies below 0.025eV

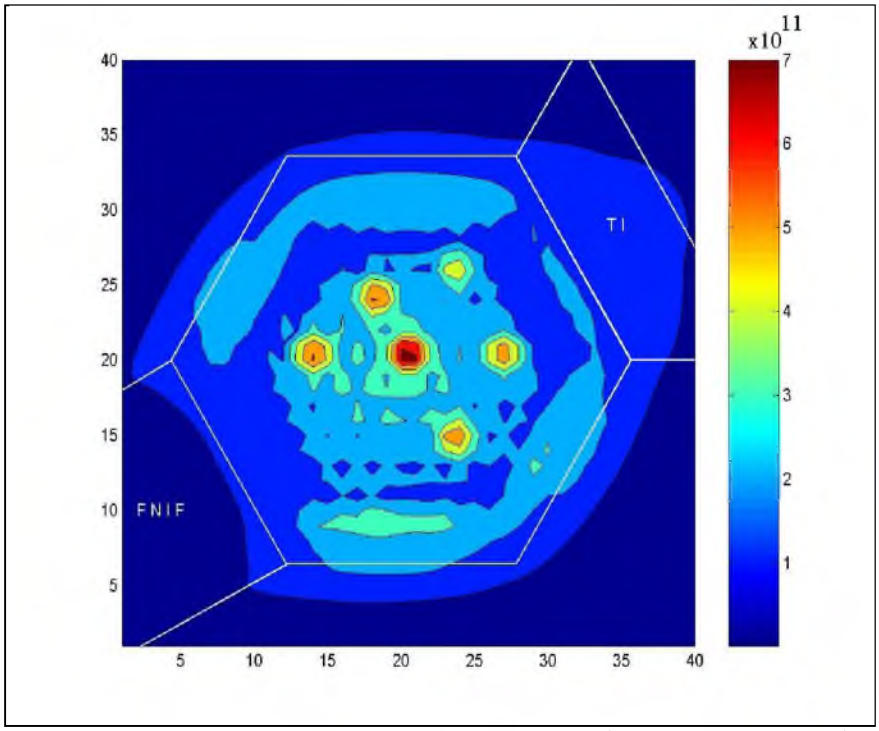

Figure 8-25. Contour plot of thermal neutron flux in (neutrons/cm^2*sec) at 400kW reactor power for neutron energies below 0.025eV

8.6. Power Upgrade Design for 500kW

The third proposal suggests a design that has four control rods. The regulation, shim, and safety are located in "D1", "D7", and "D13", respectively. Additionally, a safety 2 control rod is added into "C-11". The "C-11" is vacant in the current UUTR core configuration. Figure 8-26 shows the core design for 500kW.

A total of six graphite reflectors are moved from "F-1", "F-26", "F-27", "F-28", "F-29", and "F-30" into "G-1", "G-32", "G-33", "G-34", "G-35", and "G-36". A total of five heavy water elements are moved from "F-21", "F-22", "F-23", "F-24", and "F-25" into "G-25", "G-26", "G-27", "G-28", and "G-29". Nine new stainless steel clad elements are placed into "F-4", "F-7", "F-9", "F-11", "F-16", "F-20", "F-22", "F-24", and "F-26"; fuel elements which have been in these corresponding positions already are taken out prior to the placement of new fuel. The stainless steel clad low burn up is placed into "F-25". Two stainless steel clad high burn ups are placed into "F-23" and "F-27". Aluminum clad fuel elements are placed into "E-21", "F-21", and "F-28".

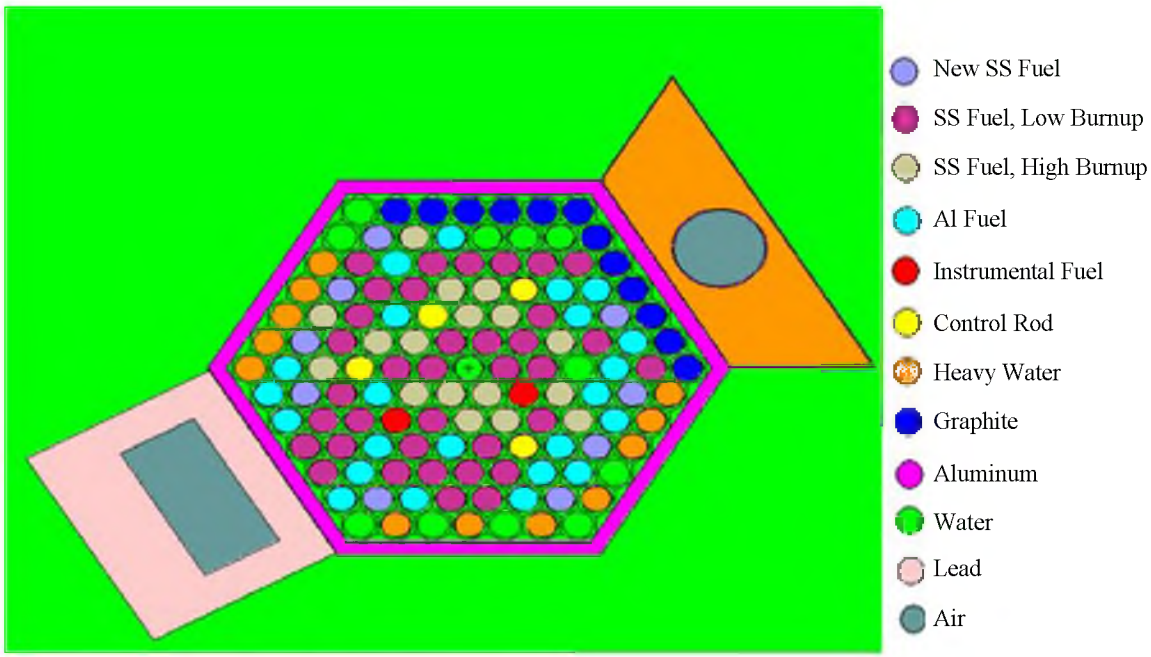

Figure 8-26. Schematics of the upgrade core design for 500kW reactor power

8.6.1. Neutronics Parameters

The reactor core parameters are calculated using the MCNP5. Table 8-9 summarizes calculated k_{eff} for each corresponding control rod position. All k_{eff} MCNP5 calculations are done with 120 million particles on a Pentium Quad 2 Core Q6600.

IN position corresponds to fully inserted control rod. OUT position corresponds to fully withdrawn control rod. All k_{eff} simulations are done with 120 million particles. The k_{eff} with all control rods withdrawn is 1.02355 +/- 0.00016, which makes this reactor design ideally suitable for a 500kW maximum power.

Additional reactor core parameters are calculated using the MCNP5. Table 8-10 and Figure 8-27 summarize the calculated excess reactivity, shutdown margin, and control rod worth.

Table 8-9. MCNP5 calculated k_{eff} for each corresponding control rod position of the 500kW core design

Safety 2 control rod	Safety control rod	Shim control rod	Regulation control rod	k_{eff}			Computation Time
OUT	IN	IN	IN	0.99270	+/-	0.00017	23.2
IN	OUT	IN	IN	0.99312	+/-	0.00017	23.2
IN	IN	OUT	IN	0.99288	+/-	0.00017	23.1
IN	OUT	OUT	OUT	1.00858	+/-	0.00017	23.2
OUT	IN	OUT	OUT	1.01173	+/-	0.00014	23.2
OUT	OUT	IN	OUT	1.00929	+/-	0.00016	23.2
OUT	OUT	OUT	IN	1.02153	+/-	0.00015	23.0
OUT	**OUT**	**OUT**	**OUT**	**1.02355**	**+/-**	**0.00016**	23.4
OUT	OUT	OUT	OUT	1.01597	+/-	0.00015	22.8
			β_{eff}	0.00741	+/-	0.00016	

Table 8-10. MCNP5 calculated excess reactivity, shut down margin, and control rod worth of the 500kW core design

MCNP5 Simulation	ρ (Δk/k)			ρ ($)		
Safety 2 control rod	0.01450	+/-	0.00023	1.9581	+/-	0.0522
Safety control rod	0.01141	+/-	0.00021	1.5413	+/-	0.0433
Shim control rod	0.01380	+/-	0.00022	1.8640	+/-	0.0500
Regulation control rod	0.00193	+/-	0.00021	0.2609	+/-	0.0289
Total Rod Worth	**0.04165**	**+/-**	**0.00086**	**5.62425**	**+/-**	**0.1744**
Excess Reactivity	0.02301	+/-	0.00043	3.1069	+/-	0.0139
Shut Down Margin	0.00735	+/-	0.00042	0.9930	+/-	0.0408

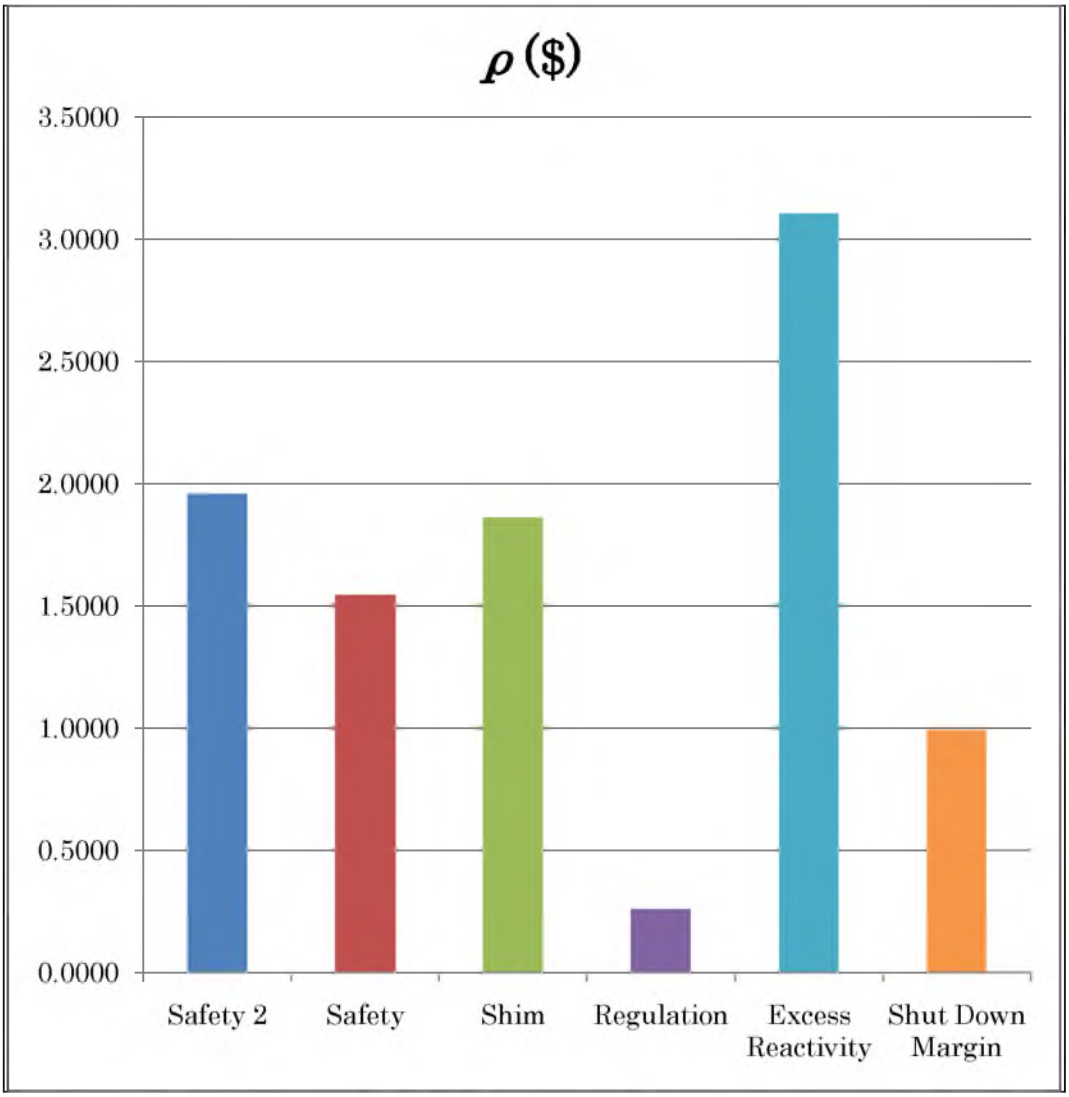

Figure 8-27. Reactivity worth of each control rod, excess reactivity, and shut down margin of the 500kW core design

8.6.2. MCNP5 Core Analysis at 500kW

Core analysis of the proposed upgrade at 500kW reactor power is shown in this subsection. Table 8-11 represents the fuel element power distribution per fuel ring at 500kW reactor power. Figure 8-28 shows the peaking factors of the UUTR core at 500kW reactor power. Figure 8-29 shows the 3D pin power distribution of the core at 500kW. Figure 8-30 shows the top view of pin power distribution in kilowatts at 500kW reactor power. Matlab program is used to plot the flux [38]. Figure 8-31 shows the 3D view of the total neutron flux distribution at a reactor power of 500kW. Figure 8-32 is a top view of the total neutron flux distribution of the UUTR at a reactor power of 500kW. Figure 8-33 shows the 3D view of the fast neutron flux distribution at a reactor power of 500kW. Figure 8-34 is a top view of the fast neutron flux distribution of the UUTR at a reactor power of 500kW. Figure 8-35 shows the 3D view of the thermal neutron flux distribution at a reactor power of 500kW. Figure 8-36 is a top view of the thermal neutron flux distribution of the UUTR at a reactor power of 500kW.

Table 8-11. Fuel element power distribution per fuel ring at 500kW reactor power

Ring	Number of Fuel Pins	Maximum Power Per Fuel Pin P_{max} (kW/pin)	Minimum Power Per Fuel Pin P_{min} (kW/pin)	Average Power Per Fuel Pin P_{avg} (kW/pin)	Ratio (P_{max} / P_{min})	Ratio (P_{max} / P_{avg})
B	6	9.491	8.719	9.118	1.089	1.041
C	11	8.680	6.945	7.896	1.250	1.099
D	14	7.861	6.112	6.962	1.286	1.129
E	24	7.077	3.923	5.442	1.804	1.300
F	27	5.512	3.343	4.199	1.649	1.313
G	5	3.866	2.967	3.397	1.303	1.138
Total	87	9.491	2.967	5.747	3.199	1.651

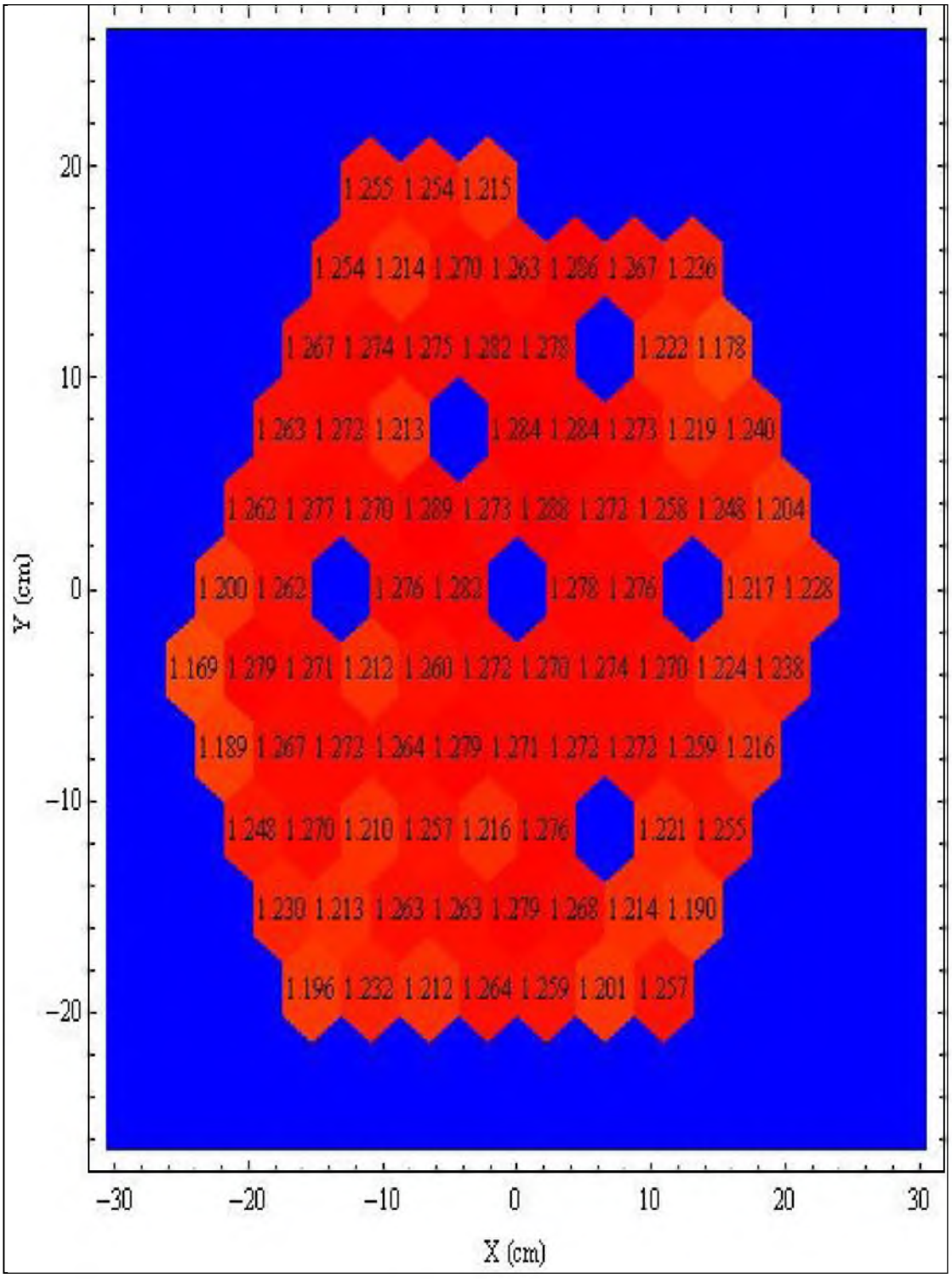

Figure 8-28. Peaking factors of core at 500kW reactor power

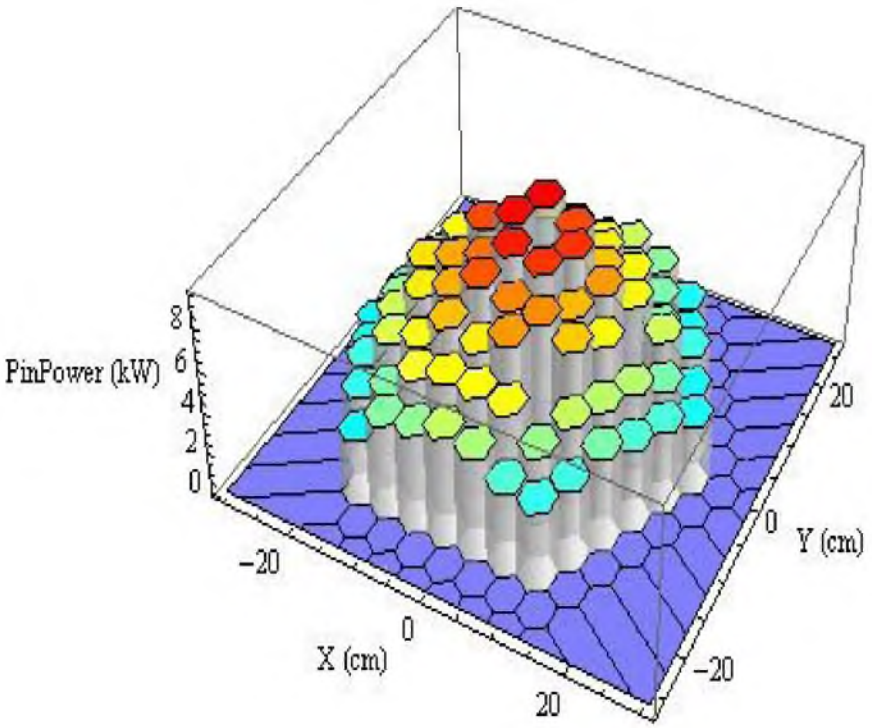

Figure 8-29. 3D view of pin power distribution in kilowatts at 500kW reactor power

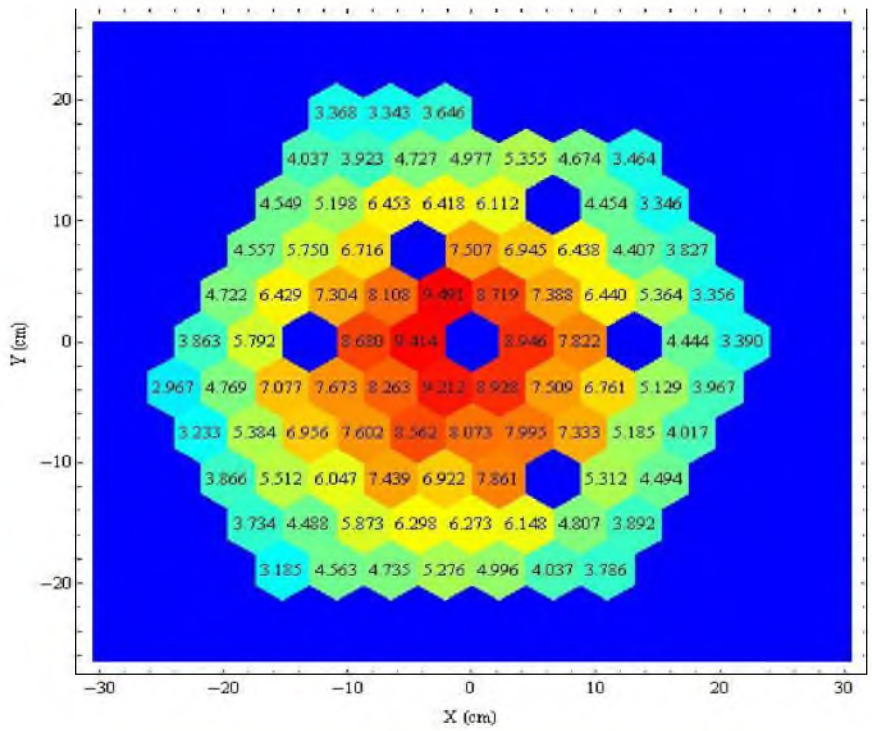

Figure 8-30. Top view of pin power distribution in kilowatts at 500kW reactor power

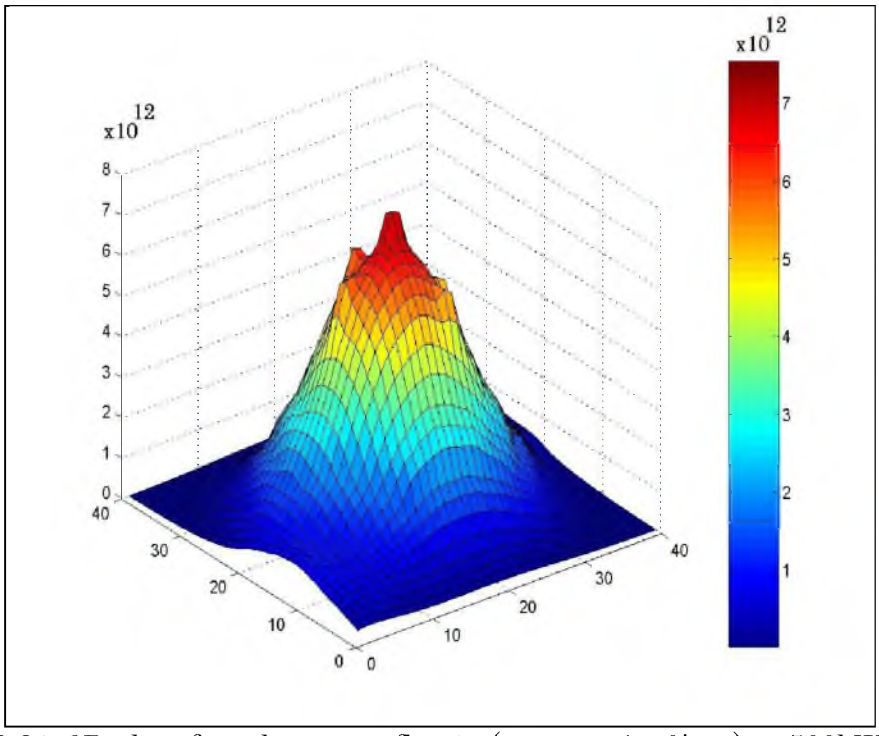

Figure 8-31. 3D plot of total neutron flux in (neutrons/cm^2*sec) at 500kW reactor power for all neutron energies

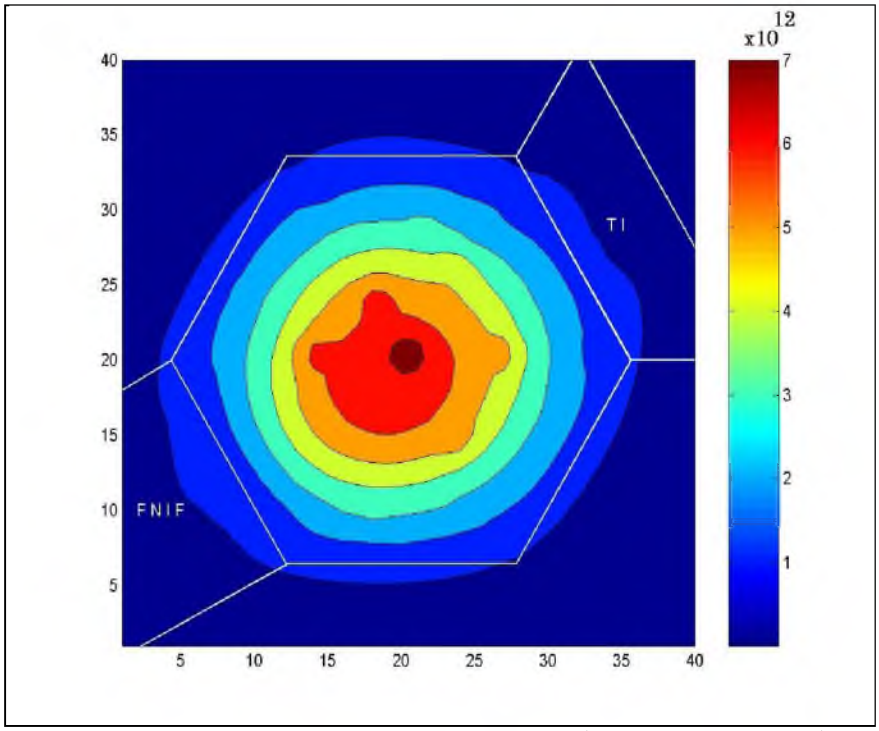

Figure 8-32. Contour plot of total neutron flux in (neutrons/cm^2*sec) at 500kW reactor power for all neutron energies

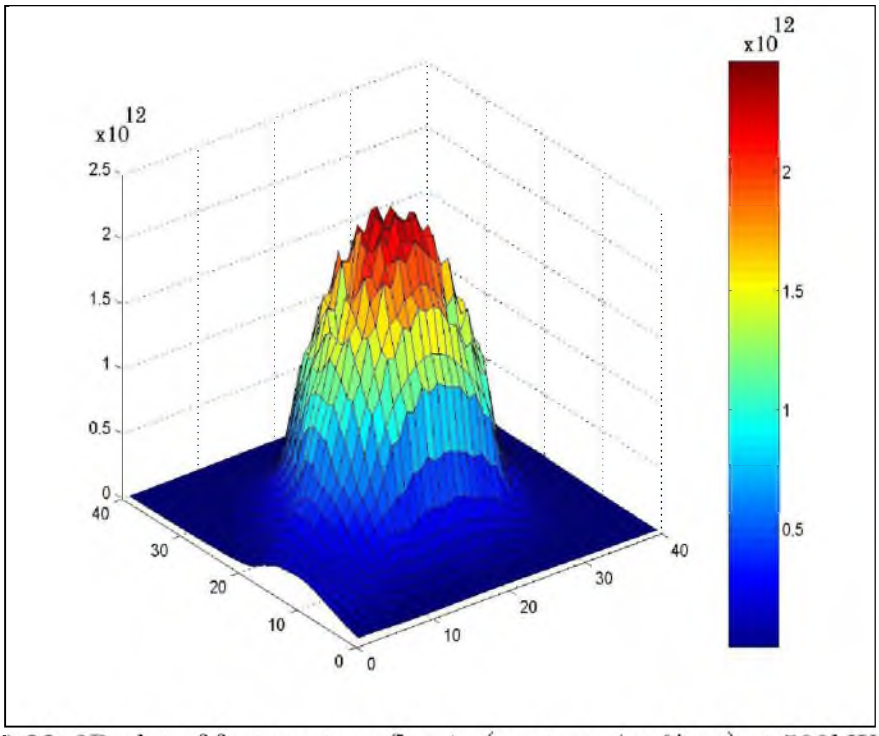

Figure 8-33. 3D plot of fast neutron flux in (neutrons/cm^2*sec) at 500kW reactor power for neutron energies above 100keV

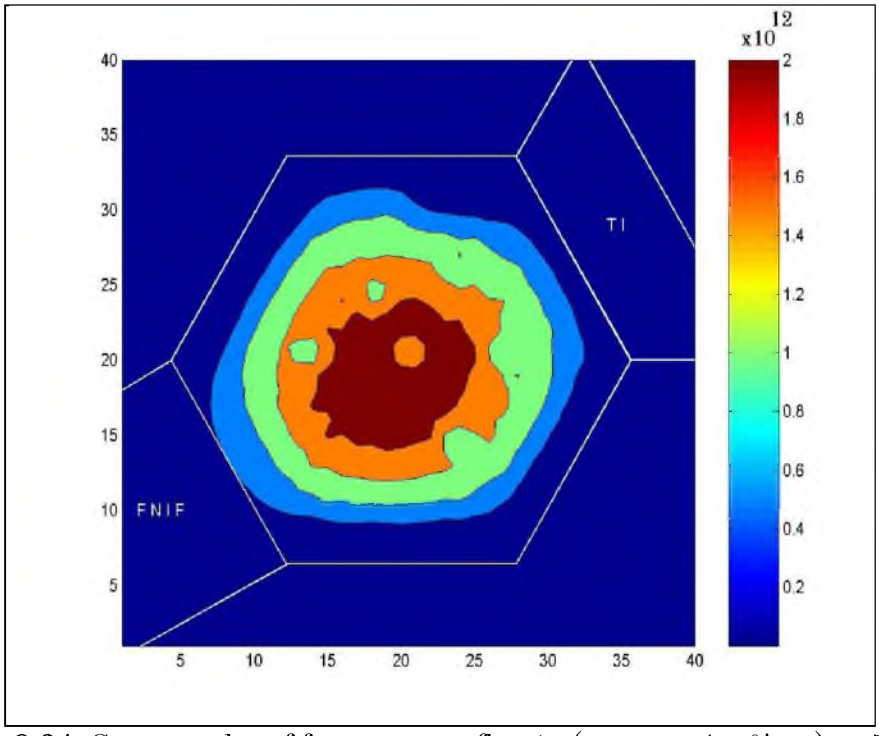

Figure 8-34. Contour plot of fast neutron flux in (neutrons/cm^2*sec) at 500kW reactor power for neutron energies above 100keV

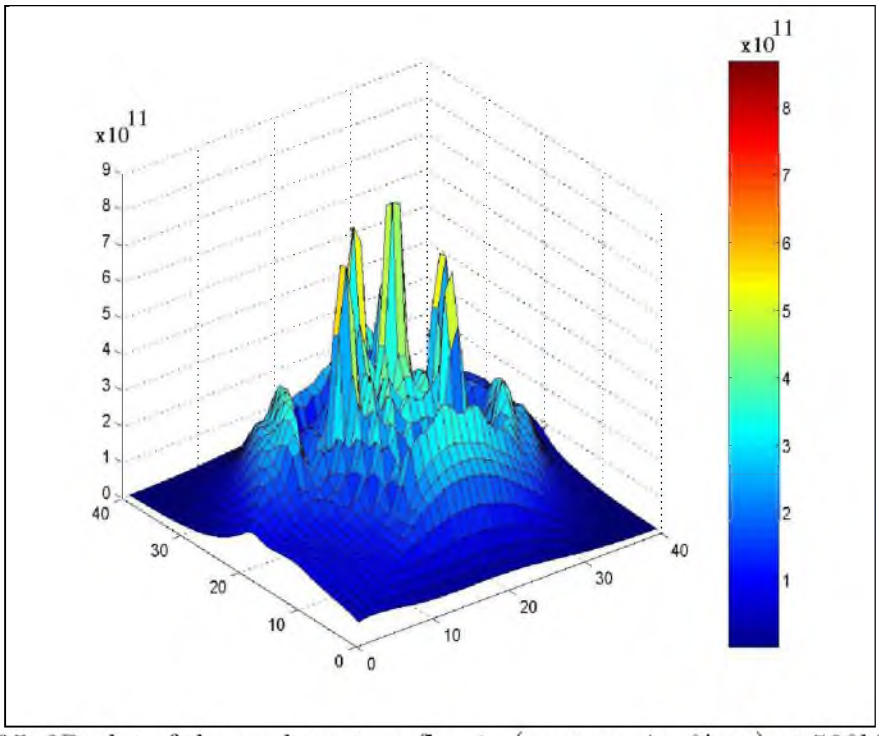

Figure 8-35. 3D plot of thermal neutron flux in (neutrons/cm^2*sec) at 500kW reactor power for neutron energies below 0.025eV

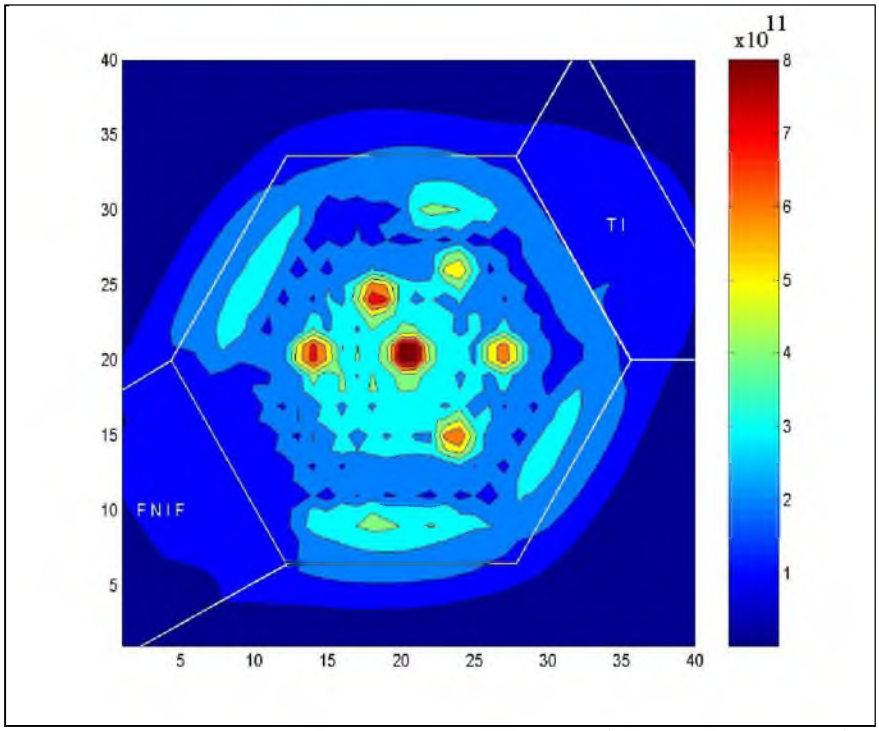

Figure 8-36. Contour plot of thermal neutron flux in (neutrons/cm^2*sec) at 500kW reactor power for neutron energies below 0.025eV

8.7. Discussion

The three reactor upgrade designs will now be compared to the current UUTR configuration. Table 8-12 shows the neutron population across the core as well as the maximum flux at the Central Irradiation Facility (C.I.) in (neutrons/cm^2*sec). This essentially shows the total number of neutrons which are in the core at each corresponding power level. There is a linear trend between total core neutron population and reactor power. In addition, Table 8-12 compares the control rod systems of each core design.

Table 8-12. Summary of all control rod systems

-	Current UUTR 100kW	300kW	400kW	500kW
Number of Fuel Elements	78	82	84	87
Safety 2 control rod ($)	N/A	1.869 +/- 0.0513	1.887 +/- 0.0515	1.958 +/- 0.0522
Safety control rod ($)	1.911 +/- 0.0211	1.772 +/- 0.0479	1.650 +/- 0.0457	1.541 +/- 0.0433
Shim control rod ($)	1.450 +/- 0.0167	1.733 +/- 0.0484	1.847 +/- 0.0502	1.864 +/- 0.0500
Regulation control rod ($)	0.298 +/- 0.0456	0.240 +/- 0.0295	0.291 +/- 0.0295	0.261 +/- 0.0289
Excess Reactivity ($)	0.823 +/- 0.0089	1.965 +/- 0.0221	2.621 +/- 0.0166	3.107 +/- 0.0139
Shut Down Margin ($)	0.950 +/- 0.0089	2.174 +/- 0.0188	1.598 +/- 0.0256	0.993 +/- 0.0408
CI* Flux φ(in 10^{12})	1.5	4.5	5.9	7.0

Figure 8-37 shows a graph representation of all control rod systems. The bars represent the dollar worth of all control rods, the shut down margin, and excess reactivity on the primary vertical axis on the left. The line graph shows the neutron flux in (neutrons/cm^{2}*sec) on the secondary vertical axis on the right.

For higher powers, the safety 2 control rod becomes the control rod with the highest value. Also, the safety control rod has a little less worth for higher powered reactors as compared to the current UUTR. This is because the fuel element configuration is different from the fuel configuration of the current UUTR. This alters the neutron flux in the core, which in turn changes the worth of each control rod.

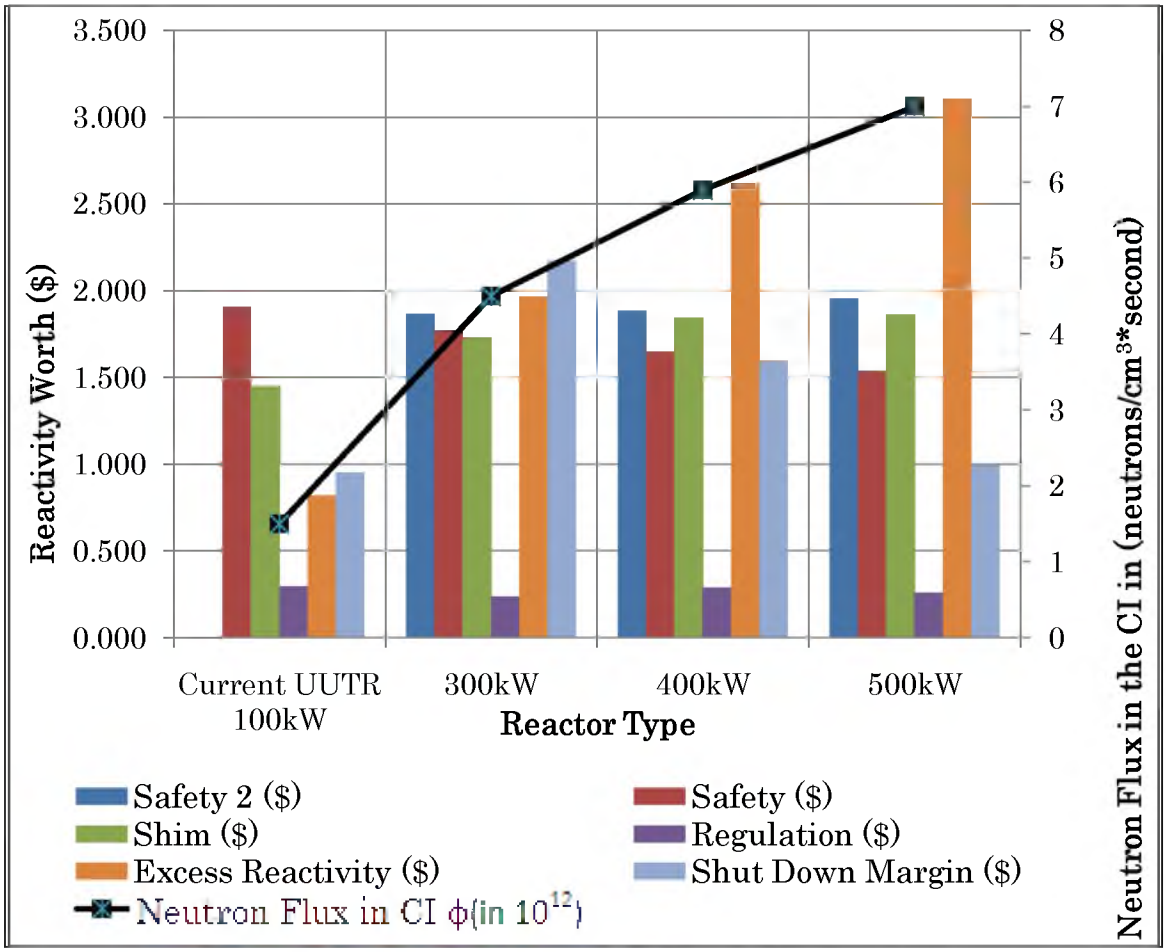

Figure 8-37. Graph summary of all control rod systems

The maximum power in kW per fuel in is shown in Table 8-13. A linear trend can be noted between reactor power and power of each fuel pin per ring. Table 8-13 and Figure 8-38 illustrate the fuel pin that has the maximum power per ring. Generally, the fuel pins with the highest power are located in the "B-Ring" while the fuel pins with the lowest power are located in the "G-Ring". This is to be expected because the highest neutron flux is in the center.

Table 8-13. Maximum power per fuel pin for each reactor power level

-	Current UUTR 100kW	300kW	400kW	500kW
Ring	Maximum Power Per Fuel Pin P_{max} (kW/pin)			
B	2.019	5.854	7.698	9.491
C	1.891	5.411	7.088	8.680
D	1.811	5.082	6.516	7.861
E	1.443	4.242	5.751	7.077
F	1.207	3.375	4.524	5.512
G	0.788	2.300	3.181	3.866

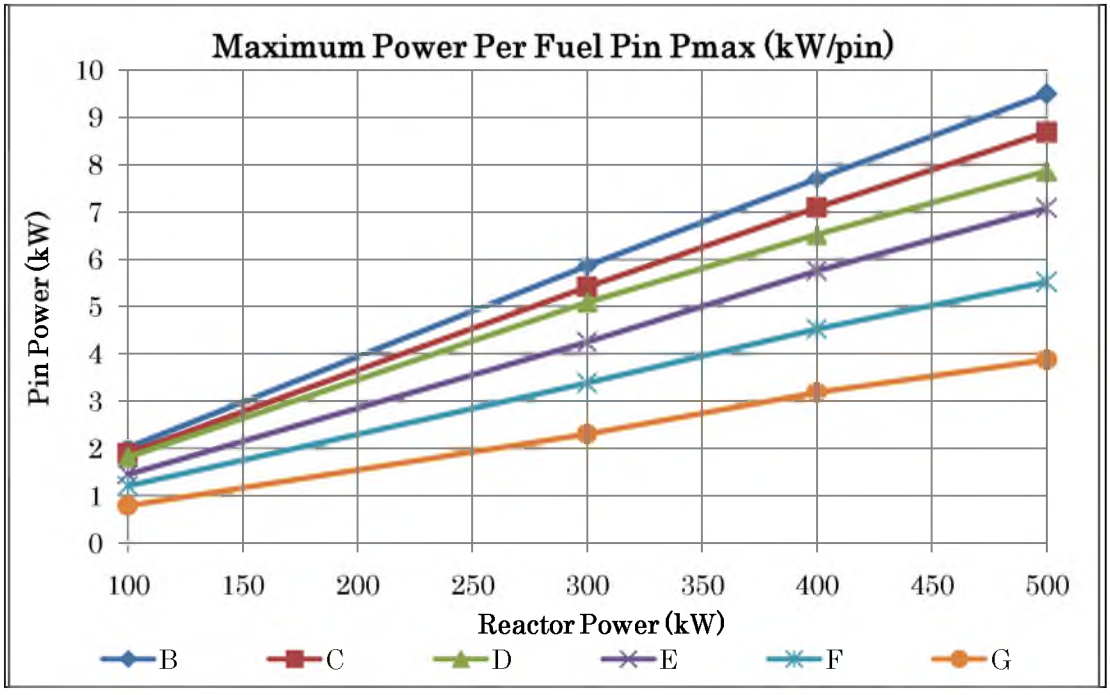

Figure 8-38. Maximum power per fuel pin in kW

The minimum power in kW per fuel in is shown in Table 8-14. A linear trend can be noted between reactor power and power of each fuel pin per ring. Table 8-14 and Figure 8-39 illustrate the fuel pin that has the minimum power per ring. Generally, the fuel pins with the highest power are located in the "B-Ring" while the fuel pins with the lowest power are located in the "G-Ring". This is to be expected because the highest neutron flux is in the center.

Table 8-14. Minimum power per fuel pin for each reactor power level

-	Current UUTR 100kW	300kW	400kW	500kW
Ring	Minimum Power Per Fuel Pin P_{min} (kW/pin)			
B	1.886	5.487	7.116	8.719
C	1.497	4.348	5.655	6.945
D	1.196	3.721	4.849	6.112
E	0.934	2.615	3.487	3.923
F	0.764	2.186	2.766	3.343
G	0.612	1.884	2.442	2.967

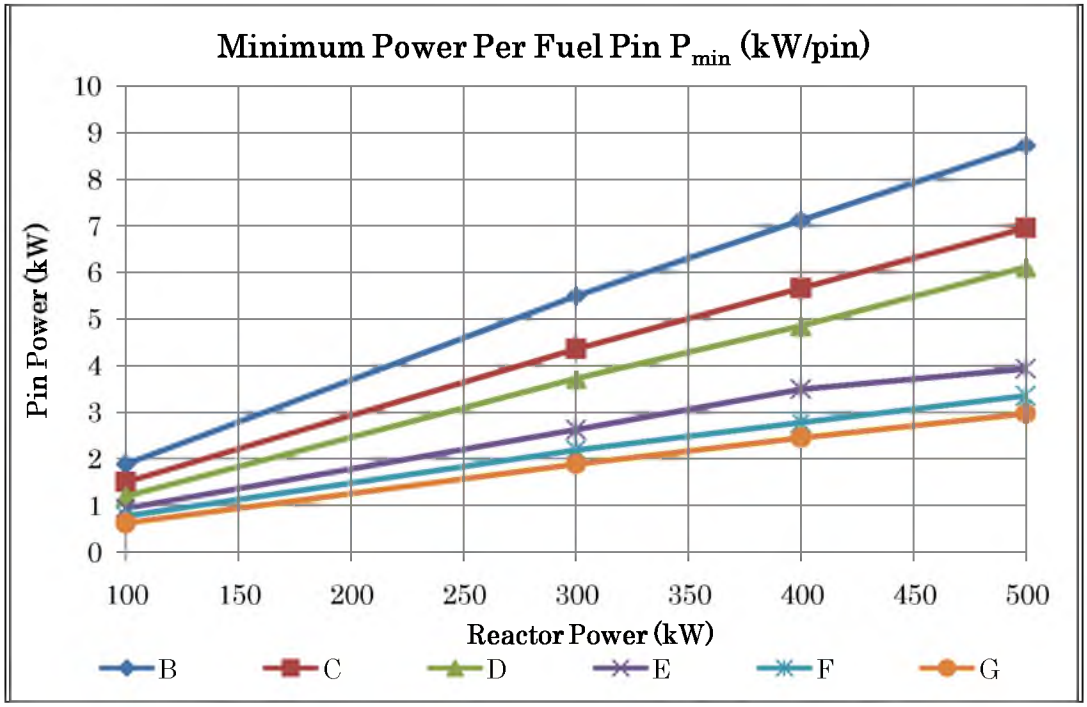

Figure 8-39. Minimum power per fuel pin in kW

The average power in kW per fuel in is shown in Table 8-15. A linear trend can be noted between reactor power and power of each fuel pin per ring. Table 8-15 and Figure 8-40 illustrate the average power per fuel pin per ring. Generally, the fuel pins with the highest power are located in the "B-Ring" while the fuel pins with the lowest power are located in the "G-Ring". This is to be expected because the highest neutron flux is in the center.

Table 8-15. Average power per fuel pin for each reactor power level

-	Current UUTR 100kW	300kW	400kW	500kW
Ring	Average Power Per Fuel Pin P_{avg} (kW/pin)			
B	1.980	5.735	7.463	9.118
C	1.717	4.966	6.480	7.896
D	1.474	4.323	5.670	6.962
E	1.179	3.394	4.446	5.442
F	0.947	2.664	3.493	4.199
G	0.700	2.076	2.808	3.397

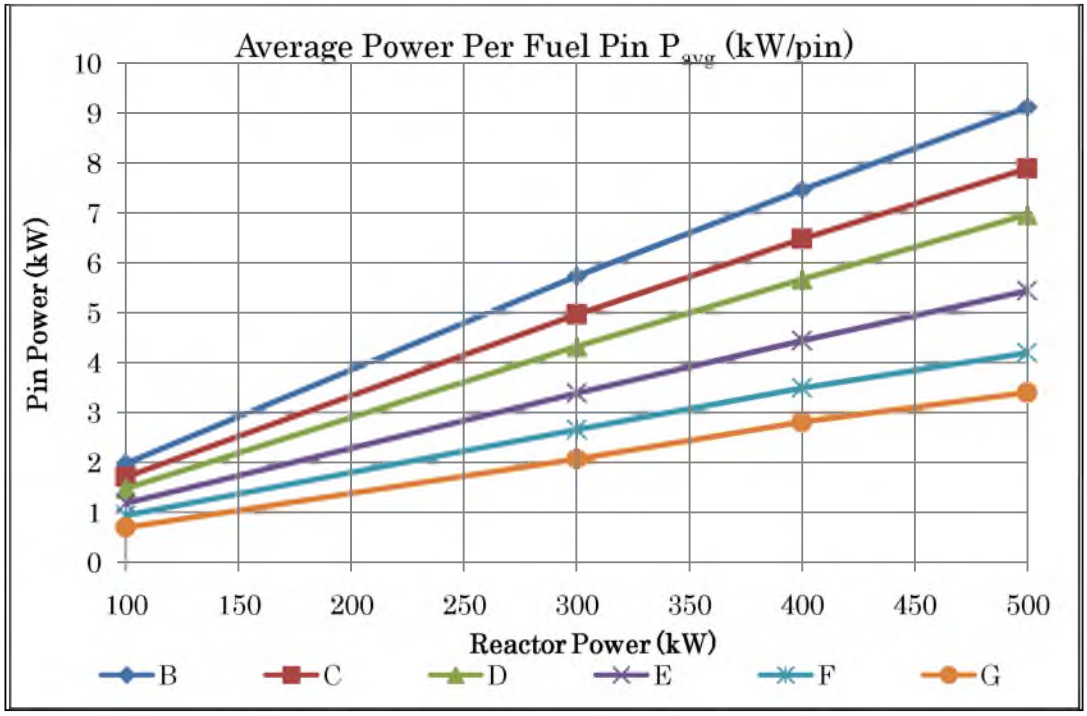

Figure 8-40. Average power per fuel pin in kW

Table 8-16 shows the ratio of the fuel pin with the highest power vs. the fuel pin with the lowest power per reactor power level per ring. The values in Table 8-16 and Figure 8-41 show that the power per ring is not symmetric. However, since pin power is proportional to neutron flux, this is expected. The pin power ratio is always the same for the same reactor design regardless the power level. Table 8-16 and Figure 8-41 show similar power ratios for each reactor design, which is preferable.

Table 8-16. Ratio of maximum pin power and minimum pin power per ring

-	Current UUTR 100kW	300kW	400kW	500kW
Ring	Ratio (P_{max} / P_{min})			
B	1.071	1.067	1.082	1.089
C	1.263	1.244	1.253	1.250
D	1.514	1.366	1.344	1.286
E	1.545	1.622	1.649	1.804
F	1.580	1.544	1.636	1.649
G	1.288	1.221	1.303	1.303

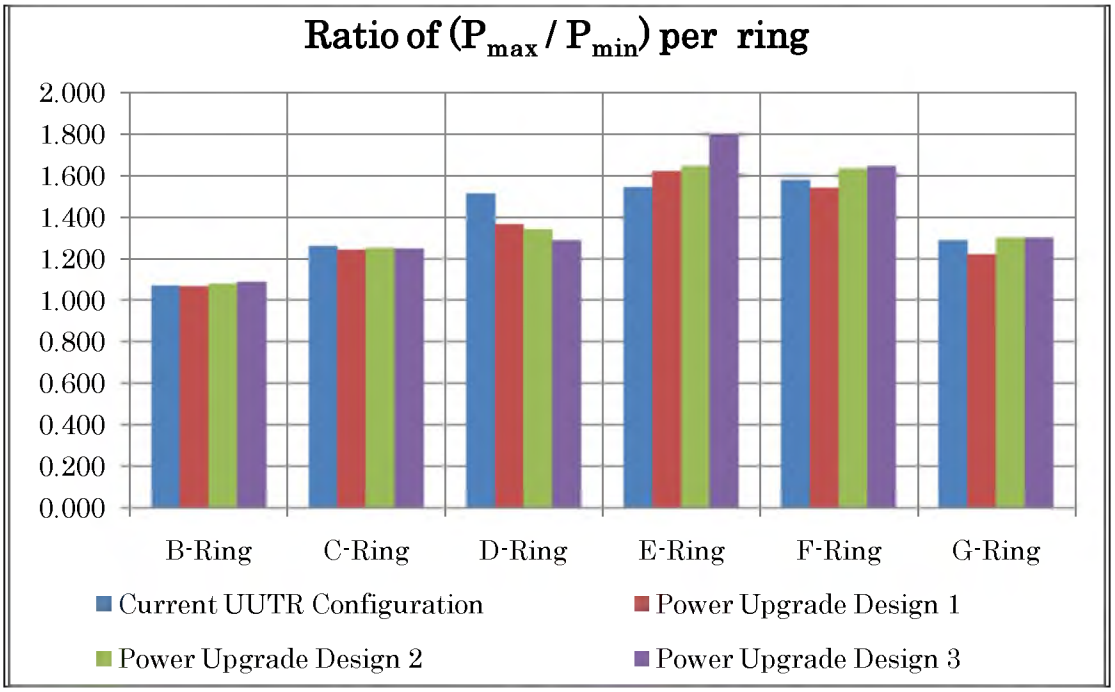

Figure 8-41. Power ratio between the fuel pin with the highest power and fuel pin with the lowest power per ring

Table 8-17 shows the ratio of the fuel pin with the highest power vs. the fuel pin with the lowest power per reactor power level per ring. The values in Table 8-17 and Figure 8-42 show that the power per ring is not symmetric. However, since pin power is proportional to neutron flux, this is expected. The pin power ratio is always the same for the same reactor design regardless the power level. Table 8-17 and Figure 8-42 show similar power ratios for each reactor design, which is preferable.

Table 8-17. Ratio of maximum pin power and average pin power per ring

-	Current UUTR 100kW	300kW	400kW	500kW
Ring	Ratio (P_{max} / P_{avg})			
B	1.020	1.021	1.031	1.041
C	1.101	1.090	1.094	1.099
D	1.229	1.175	1.149	1.129
E	1.224	1.250	1.294	1.300
F	1.275	1.267	1.295	1.313
G	1.126	1.108	1.133	1.138

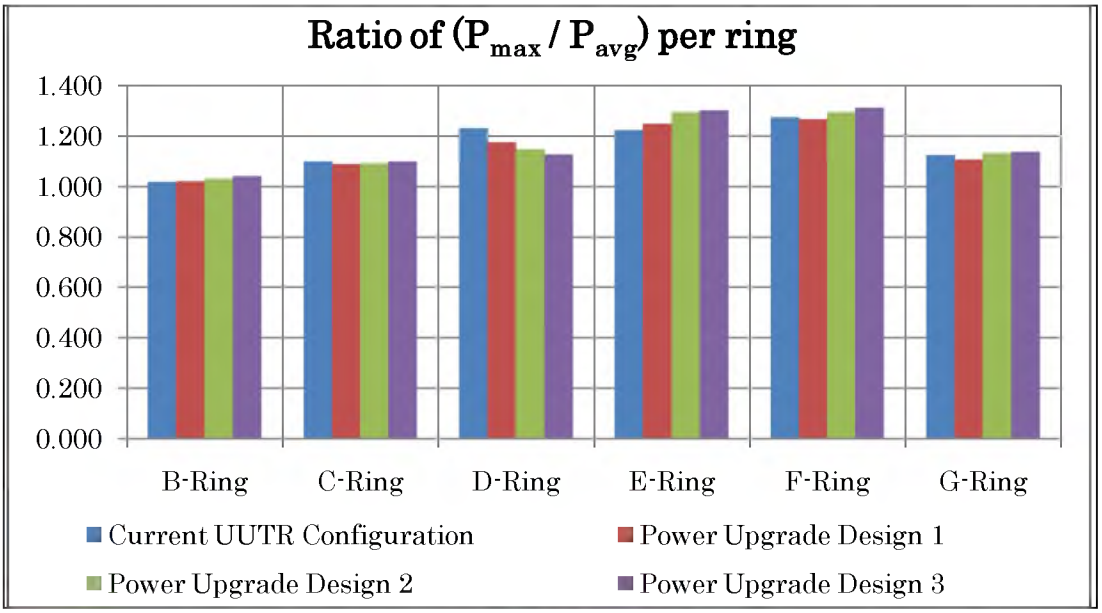

Figure 8-42. Power ratio between the fuel pin with the highest power and average fuel pin power per ring

CHAPTER 9

ECONOMICAL ANALYSIS

9.1. Introduction

The core objective of this thesis is to propose a feasible reactor power upgrade. In this chapter, the economical and monetary requirements associated with a reactor power upgrade are discussed.

9.2. Estimated Cost of Power Upgrade

The two most expensive components associated with adding the fourth control rod are the control rod itself and the control rod drive mechanism. In addition, the current control rod bridge plate is designed to hold up to three control rods (Figure 2-2); therefore, a new control rod bridge plate as well as the plate holder bars will have to be designed and manufactured. The wiring will not require major resources as the reactor console is two meters away from the control rod; however, it will be labor intensive because one would have to disassemble the reactor console to connect the control rod drive buttons to the control rod drive. There will be no major modifications expected for the reactor console because the console is equipped to operate up to a total of five control rods and the control buttons are already in place. There is also the labor associated with the upgrade.

The control rod system assembly which consists of the control rod and the control rod drive costs about $75,000, plus $1,500 shipping [42]. The cost of a new control rod bridge and bridge plate holding bars have been estimated by telephone

conversations with local machine shops to cost approximately $3,000 each [43].The cost of labor required to wire the electromechanical components has been based on previous average labor costs that were done on the University of Utah Nuclear Engineering Facilities and estimated to be $100 per hour. All work will require at least two technicians to be present at any time. The time required to install a fourth control rod has been estimated and confirmed by General Atomics to be about four weeks. Table 9-1 roughly identifies all the required components for the power upgrade. Since an additional control rod is required for reactor powers beyond 150kW, the cost of upgrading the current UUTR to 300kW, 400kW, or 500kW will be the same and is estimated to cost $115,500.

Table 9-1. Estimated Cost of Materials of the most expensive components

Component	Cost
Safety 2 Control Rod	$50,000
Control Rod Drive	$25,000
Shipping of Control Rod Assembly	$1,500
Control Rod Bridge Plate	$3,000
Bridge Plate Holding Bars	$3,000
Wires and Electrical Components	$1,000
Cost of Physical Labor (320 men-hours at $100/hr)	$32,000
Total	**$115,500**

CHAPTER 10

SOURCES OF ERROR

10.1. Introduction

The MCNP5 computer code is a stochastic, nondeterministic approach which introduces variance and therefore error into the solution [44, 45]. There is also an error introduced when measurements are taken during tests and experiments. In addition, a propagation of error exists which occurs during calculations involving two or more values.

10.2. Quantification of Error

The quantification of error is of importance in this thesis. Here, the relative error is defined by the following equation [46]:

$$\delta x = \frac{\Delta x}{x} \tag{10.1}$$

$$\sigma_{x\,(\%)} = \delta x * 100\% \tag{10.2}$$

where:

δx = relative error of a measurement

Δx = absolute error of a measurement

x = measured value

σ_x *(%)* = relative error percent

Table 10-1 shows a relative error of 5% in reactor power. This is because during thermal power calibration at the UUTR, the maximum allowable variance is no more than 5kW out of 100kW, which brings this relative error to 5%. The relative error in the control rod position is estimated by examining the reactor console output fluctuations during reactor operations. It can be noted that the control rod position output indicator on the reactor console fluctuates within a fraction of a percentage point due to electrical noise in the range of 0.2%. The relative error in fuel pin temperature is due to the allowed four degrees Celsius per 200 degrees Celsius variance in fuel temperature, which is an error of 2%. The relative error in the control rod worth measurement is derived by the standard deviation of all control rod measurements in the past 10 years, which is 7% (Table 3-1). The relative error in the MCNP5 k_{eff} calculation is derived from the variance of the MCNP5 k_{eff} result. The MCNP5 control rod calculations have a relative error of 2.5% due to propagation of error. The MCNP5 calculated neutron flux has a 5% relative error associate with it. Table 10-1 shows the potential sources of relative error [3, 5].

Table 10-1. Estimated sources of relative errors

System	Relative Error
Reactor Power	5.00%
Control Rod Position	0.20%
Fuel Pin Temperature	2.00%
Control Rod Worth Measurements	7.00%
MCNP5 k_{eff} Calculations	0.01%
MCNP5 Control Rod Worth Calculations	2.50%
MCNP5 Calculated Neutron Flux	5.00%

10.3. Propagation of Error

Uncertainty in the MCNP5 control rod worth comes from more than one source. The error in the MCNP5 k_{eff} calculation is a statistical error and therefore adding the errors would result in an overestimation of error in the final result. Table 10-2 shows the Error Propagation in Arithmetic Calculations [45, 46]. Table 10-2 also shows the type of calculation, example of calculation, and the standard deviation of x.

Table 10-2. Error propagation in arithmetic calculations

Type of Calculation	Example	Standard Deviation of x
Addition or Subtraction	$x = p + q - r$	$s_x = \sqrt{s_p^2 + s_q^2 + s_r^2}$
Multiplication or Division	$x = \frac{p \cdot q}{r}$	$s_x = x\sqrt{\left(\frac{s_p}{p}\right)^2 + \left(\frac{s_q}{q}\right)^2 + \left(\frac{s_r}{r}\right)^2}$
Exponentiation	$x = p^y$	$s_x = y \cdot x \frac{s_p}{p}$
Logarithm	$x = \log_{10} p$	$s_x = 0.434 \frac{s_p}{p}$
Natural Logarithm	$x = \ln p$	$s_x = \frac{s_p}{p}$
Antilogarithm	$x = \text{antilog}_{10} p$	$s_x = 2.303 \cdot x \cdot s_p$
Natural Antilogarithm	$x = e^p$	$s_x = e \cdot s_p$

The control rod worth is calculated by determining the reactivity change between all control rods out and the measuring control rod in through the following equation:

$$\Delta\rho = \frac{k_2 - k_1}{k_2 * k_1} \tag{10.3}$$

$$\rho(\$) = \frac{\Delta\rho}{\beta_{eff}} \tag{10.4}$$

where:

$k_2 = k_{eff}$ with all control rods out

$k_1 = k_{eff}$ with the measuring control rod in

$\Delta\rho$ = change in reactivity

$\rho(\$)$ = Dollar worth reactivity of the measuring control rod

The example error calculation of the MCNP5 calculated control rod worth goes as follows:

$$(k_2 +/- \Delta_{k2}) - (k_1 +/- \Delta_{k1}) = L \tag{10.5}$$

$$\Delta_L = \sqrt{\Delta_{k2}^2 + \Delta_{k1}^2} \tag{10.6}$$

$$(k_2 +/- \Delta_{k2}) * (k_1 +/- \Delta_{k2}) = M \tag{10.7}$$

$$\Delta_M = M * \sqrt{\left(\frac{\Delta_{k2}}{k2}\right)^2 + \left(\frac{\Delta_{k1}}{k1}\right)^2} \tag{10.8}$$

$$\Delta\rho = \frac{L}{M} \tag{10.9}$$

$$\Delta_{\Delta\rho} = \Delta\rho * \sqrt{\left(\frac{\Delta_M}{M}\right)^2 + \left(\frac{\Delta_L}{L}\right)^2} \tag{10.10}$$

$$\rho(\$) = \frac{\Delta\rho}{\beta_{eff}} \tag{10.11}$$

$$\Delta_{\rho\$} = \rho(\$) * \sqrt{\left(\frac{\Delta_{\Delta\rho}}{\Delta\rho}\right)^2 + \left(\frac{\Delta_{\beta eff}}{\beta_{eff}}\right)^2} \quad (10.12)$$

where:

Δk_2 = variance in k_2

Δk_1 = variance in k_1

L = subtraction result of $k_2 - k_1$

ΔL = variance in the subtraction result of $k_2 - k_1$

M = result of multiplication of $k_2 * k_1$

ΔM = variance in the result of multiplication of $k_2 * k_1$

$\Delta\rho$ = change in reactivity which is the result due to division of L by M

$\Delta_{\Delta\rho}$ = variance in the result due to division of L by M

β_{eff} = effective delayed neutron fraction

$\Delta_{\beta eff}$ = variance in the effective delayed neutron fraction

$\rho(\$)$ = Dollar worth reactivity of the measuring control rod which is the result of dividing $\Delta\rho$ by β_{eff}

$\Delta\rho(\$)$ = variance in the Dollar worth reactivity of the measuring control rod

CHAPTER 11

CONCLUSION AND FUTURE WORK

11.1. Conclusion

The objectives of this thesis were to investigate the current UUTR "24B" core configuration by determining the highest attainable power level with the existing control rod system. This was done by experimentally and numerically determining the worth of each control rod, the core excess reactivity, and the shut down margin as well as the negative temperature coefficient. The highest attainable power turned out to be 150kW. Additionally,MCNP5 calculations determining the control rod worth, the core excess reactivity, the shut down margins, and temperature coefficient of the fuel were used to derive a feasible power upgrade, leading to a maximum reactor power of up to 500kW. Such an upgrade, however, would require an additional control rod system at a total cost of $115,000.

11.2. Recommendations for Future Work

Higher reactor power would certainly increase the neutron flux. This would enable new types of experiments which otherwise could not have been feasible with a lower neutron flux such as, but not limited to:

- Single Event Effects studies, which are macro-scale events caused by a single high energy neutron interacting with electronic components, could become an option due to an increased neutron flux.

- Boron-neutron capture therapy, a promising cancer treatment radiation therapy, could be made possible with the increased thermal flux as a result of a power upgrade.
- An underwater neutron radiography facility would become a feasible option as a result of the increased thermal flux.
- Prompt gamma neutron activation analysis, a real-time elemental analysis technique which utilizes thermal neutrons, could become an option due to the increased neutron flux.
- Fast neutron activation analysis studies could be implemented to further study elemental composition of samples.
- Fast neuron pencil beam could be used for studies such as radiation damage to materials, electronics, and organisms.
- Ultra cold neutrons are neutrons having energies of several Kelvin. Neutrons of such energy are hard to make and require a very high neutron flux. A higher flux would make an ultra cold neutron facility a prospect.

However, a cost-benefit-risk analysis will have to be performed in order to fully understand the impacts of such a power upgrade.

APPENDIX A

MCNP5 INPUT FILE FOR CRITICALITY CALCULATIONS

```
TRIGA 3D Model
c New SS Fuel
100   1   -5.636 -2 11 -12                u=1   imp:n=1 $Fuel Meat
101   2   -1.70  -2 12 -14                u=1   imp:n=1 $Up Graphite
102   2   -1.70  -2 13 -11                u=1   imp:n=1 $Down Graphite
103   3   -7.92  (-1 15 -16) (2:-13:14)   u=1   imp:n=1 $Cladding
104   4   -1.0   1:-15:16 92 -93           u=1   imp:n=1 $H2O
c Old SS Fuel
110 like 100 but mat=12 rho=-5.636        u=2   imp:n=1 $Fuel Meat
111 like 101 but                          u=2   imp:n=1 $Up Graphite
112 like 102 but                          u=2   imp:n=1 $Down Graphite
113 like 103 but                          u=2   imp:n=1 $Cladding
114 like 104 but                          u=2   imp:n=1 $H2O
c Al Fuel
120   5   -6.143 -3 21 -22                u=3   imp:n=1 $Fuel Meat
121   2   -1.70  -3 22 -24                u=3   imp:n=1 $Up Graphite
122   2   -1.70  -3 23 -21                u=3   imp:n=1 $Down Graphite
123   6   -2.70  (-1 25 -26) (3:-23:24)   u=3   imp:n=1 $Cladding
124   4   -1.0   1:-25:26 92 -93                 u=3   imp:n=1 $H2O
c Instrumental Fuel
130 like 110 but                          u=4   imp:n=1 $Fuel Meat
131 like 111 but                          u=4   imp:n=1 $Up Graphite
132 like 112 but                          u=4   imp:n=1 $Down Graphite
133 like 113 but                          u=4   imp:n=1 $Cladding
134 like 114 but                          u=4   imp:n=1 $H2O
c Graphite
140   2   -1.70   -3 23 -24               u=6   imp:n=1 $Graphite
143   like 123 but                        u=6   imp:n=1 $Cladding
144   like 124 but                        u=6   imp:n=1 $H2O
c Heavy Water
150   7   -1.056  -3 23 -24               u=7   imp:n=1 $D2O
153   like 123 but                        u=7   imp:n=1 $Cladding
154   like 124 but                        u=7   imp:n=1 $H2O
c Water
160   4   -1.0    -1 92 -93               u=8   imp:n=1 $H2O
161   4   -1.0     1 92 -93               u=8   imp:n=1 $H2O
c Safety Control Rod
170   9   -2.52   -46 11 -93              u=10  imp:n=1 $B4C
171   6   -2.7     46 -47 11 -93          u=10  imp:n=1 $Al Cladding
172   4   -1.0    (47 -50 11 -93):(-50 -11 92)  u=10  imp:n=1 $H2O
173   6   -2.7     50 -1 92 -93           u=10  imp:n=1 $Al Tube
174   4   -1.0     1 92 -93               u=10  imp:n=1 $H2O
c Shim Control Rod
180   9   -2.52   -46 501 -93              u=11  imp:n=1 $B4C
181   6   -2.7     46 -47 501 -93          u=11  imp:n=1 $Al Cladding
182   4   -1.0    (47 -50 501 -93):(-50 -501 92)  u=11  imp:n=1 $H2O
183   6   -2.7     50 -1 92 -93           u=11  imp:n=1 $Al Tube
184   4   -1.0     1 92 -93               u=11  imp:n=1 $H2O
c Reg Control Rod
190   9   -2.52   -48 500 -93              u=12  imp:n=1 $B4C
191   6   -2.7     48 -49 500 -93          u=12  imp:n=1 $Al Cladding
192   4   -1.0    (49 -50 500 -93):(-50 -500 92)  u=12  imp:n=1 $H2O
193   6   -2.7     50 -1 92 -93           u=12  imp:n=1 $Al Tube
194   4   -1.0     1 92 -93               u=12  imp:n=1 $H2O
c Empty Control Rod
196   4   -1.0    -50 92 -93              u=5   imp:n=1 $H2O
197   6   -2.7     50 -1 92 -93           u=5   imp:n=1 $Al Tube
198   4   -1.0     1 92 -93               u=5   imp:n=1 $H2O
c Brand New SS Fuel, more U235
c 310 like 100 but mat=5  rho=-5.781        u=15   imp:n=1 $Fuel Meat
c 311 like 101 but                          u=15   imp:n=1 $Up Graphite
c 312 like 102 but                          u=15   imp:n=1 $Down Graphite
c 313 like 103 but                          u=15   imp:n=1 $Cladding
```

```
c 314 like 104 but                          u=15   imp:n=1 $H2O
c Lattice
200   4   -1.0   -101 102 -103 104 -105 106 92 -93    lat=2    u=9
                 fill=-7:7 -7:7 0:0
                 0 0 0 0 0 0 0 9 9 9 9 9 9 9 9
                  0 0 0 0 0 0 0 9 8 7 8 7 8 7 8 9
                   0 0 0 0 0 0 9 3 2 3 1 1 3 2 7 9
                    0 0 0 0 0 9 1 3 1 1 1 1 3 3 8 9
                     0 0 0 0 9 1 1 3 1 3 1 5 3 3 7 9
                      0 0 0 9 3 1 1 4 1 2 2 1 2 3 7 9
                       0 9 3 3 1 3 2 2 2 4 2 3 3 7 9
                        9 8 7 2 11 1 1 5 1 1 8 3 1 6 9
                         9 8 7 1 2 2 1 1 1 2 1 3 6 9 0
                          9 8 7 1 3 8 2 2 1 3 1 6 9 0 0
                           9 8 7 1 1 2 2 12 3 3 6 9 0 0 0
                            9 8 7 8 1 1 1 1 1 6 9 0 0 0 0
                             9 8 6 6 6 6 6 6 6 9 0 0 0 0 0
                              9 8 8 8 8 8 8 8 9 0 0 0 0 0 0
                               9 9 9 9 9 9 9 9 0 0 0 0 0 0 0 imp:n=1
201   4   -1.0   -111 112 -113 114 -115 116 92 -93  fill=9  imp:n=1 $Lattices
202   6   -2.7   (-121 122 -123 124 -125 126) 91 -94
                 (111:-112:113:-114:115:-116)               imp:n=1       $Al
Wall
203   6   -2.7   -111 112 -113 114 -115 116 91 -92          imp:n=1
$Lower Al Plate
204   6   -2.7   -111 112 -113 114 -115 116 93 -94 41 43 45 imp:n=1
$Upper Al Plate
206   4   -1.0   -131 94 -97 41 43 45 imp:n=1               $Top Water
207   4   -1.0   -131 96 -91                               imp:n=1
$Bottom Water
208   10  -2.30  -131 -96 95                               imp:n=1
$Bottom Concrete
301   9   -2.52  -40 93 -97      imp:n=1 $Safety Rod above core region
302   6   -2.7    40 -41 93 -97  imp:n=1
303   9   -2.52  -42 93 -97      imp:n=1 $Shim Rod above core region
304   6   -2.7    42 -43 93 -97  imp:n=1
305   9   -2.52  -44 93 -97      imp:n=1 $Reg Rod above core region
306   6   -2.7    44 -45 93 -97  imp:n=1
c FNIF
400   11  -0.00115   -141        imp:n=1 $ FNIF Air
401   8  -11.34  -140 141        imp:n=1 $ FNIF Pb
c Heavy water block
500   11  -0.00115   -159 160 -161 imp:n=1 $ Heavy water Air
501   6   -2.7   159 -158 160 -161 imp:n=1
502   7   -1.056 158 154 -155 156 157 160 -161  imp:n=1
503   6   -2.7   (-154:155:-156:-157)
                  150 -151 152 153 160 -161    imp:n=1
c
900   4   -1.0   -131 91 -94 140
                 (-150:151:-152:-153:-160:161)
                 (121:-122:123:-124:125:-126)               imp:n=1
$Water Arround Core
999   0           131:-95:97   imp:n=0

C Surface Cards
1     cz     1.873  $Outer Radius
2     cz     1.82   $Inner Radius
3     cz     1.79   $Inner Radius for Aluminum Container
11    pz   -19.05   $SS Fuel Meat Bottom (7.5 inch * 2)
12    pz    19.05   $SS Fuel Meat Top
13    pz   -29.21   $SS Fuel Graphite Bottom (4 inch)
14    pz    29.21   $SS Fuel Graphite Top
15    pz   -30.39   $SS Cladding Bottom (1.18 cm)
```

```
16    pz    30.39   $SS Cladding Top (1.18 cm)
21    pz   -17.78   $Al Fuel Meat Bottom (7 inch * 2)
22    pz    17.78   $Al Fuel Meat Top
23    pz   -27.94   $Al Fuel Graphite Bottom (4 inch)
24    pz    27.94   $Al Fuel Graphite Top
25    pz   -29.12   $Al Cladding Bottom (1.18 cm)
26    pz    29.12   $Al Cladding Top (1.18 cm)
40    c/z    6.555 -11.354 1.00  $Safety Control Rod
41    c/z    6.555 -11.354 1.11  $Safety Control Rod Cladding
42    c/z  -13.11    0.0   1.00  $Shim Control Rod
43    c/z  -13.11    0.0   1.11  $Shim Control Rod Cladding
44    c/z    6.555  11.354 0.200 $Reg Control Rod
45    c/z    6.555  11.354 0.318 $Reg Control Rod Cladding
46    cz     1.00   $ Safety and Shim Rod in Unit
47    cz     1.11   $ Safety and Shim Rod in Unit Cladding
48    cz     0.200  $ Reg Rod in Unit
49    cz     0.318  $ Reg Rod in Unit Cladding
50    cz     1.750  $ Inner radius of Al tube for control rod
91    pz   -33.43   $Lower Plate Bottom
92    pz   -30.89   $Lower Plate Top (1 inch)
93    pz    30.89   $Upper Plate Bottom
94    pz    32.79   $Upper Plate Top (0.75 inch)
95    pz   -55.0    $Concrete Bottom
96    pz   -43.09   $Water Bottom (2 inch)
97    pz    50.0    $Water Top
C Lattice Cells
101   px    2.185
102   px   -2.185
103   p     0.5   0.8660254  0   2.185
104   p     0.5   0.8660254  0  -2.185
105   p    -0.5   0.8660254  0   2.185
106   p    -0.5   0.8660254  0  -2.185
c Frame Boundary
111   p     1.732038    1   0    50.460
112   p     1.732038    1   0   -50.460
113   p     1.732038   -1   0    50.460
114   p     1.732038   -1   0   -50.460
115   py   25.230
116   py  -25.230
c Al Wall
121   p     1.732038    1   0    54.270
122   p     1.732038    1   0   -54.270
123   p     1.732038   -1   0    54.270
124   p     1.732038   -1   0   -54.270
125   py   27.135
126   py  -27.135
C Reflector Surfaces
131   cz   65.0       $ Water reflector
c 131   p     1.732038    1    0  83.259682
c 132   p     1.732038    1    0 -83.259682
c 133   p     1.732038   -1    0  83.259682
c 134   p     1.732038   -1    0 -83.259682
c 135   py   41.629841
c 136   py  -41.629841
c FNIF
140   BOX -15.88 -26.77 -30.48   -15.24 26.40 0  -22.00 -12.7 0   0 0 60.96
141   BOX -22.82 -24.91 -30.48   -10.16 17.60 0   -8.80  -5.1 0   0 0 60.96
c Heavy water beside core
150   p     1.732038    1   0    54.270  $ Al outer
151   p     1.732038    1   0    84.670
152   py    0.0
153   p     1.732038   -1   0     0.0
154   p     1.732038    1   0    54.670  $ Al outer
```

```
155   p     1.732038    1   0    84.270
156   py    0.2
157   p     1.732038   -1   0     0.4
158   c/z   30.08 17.37 5.7  $ Air tub Al wall
159   c/z   30.08 17.37 5.5  $ Air tub
160   pz   -30.0            $ Heavy water top
161   pz    30.0            $ Heavy water bottom
201 pz -18.5
202 pz -17.5
203 pz -16.5
204 pz -15.5
205 pz -14.5
206 pz -13.5
207 pz -12.5
208 pz -11.5
209 pz -10.5
210 pz -9.5
211 pz -8.5
212 pz -7.5
213 pz -6.5
214 pz -5.5
215 pz -4.5
216 pz -3.5
217 pz -2.5
218 pz -1.5
219 pz -0.5
220 pz 0.5
221 pz 1.5
222 pz 2.5
223 pz 3.5
224 pz 4.5
225 pz 5.5
226 pz 6.5
227 pz 7.5
228 pz 8.5
229 pz 9.5
230 pz 10.5
231 pz 11.5
232 pz 12.5
233 pz 13.5
234 pz 14.5
235 pz 15.5
236 pz 16.5
237 pz 17.5
238 pz 18.5
500 pz 5.8293   $Reg is 65.3 percent out
501 pz 0.3302   $Shim altered

mode n
kcode 300000 1.0 100 1500
ksrc   -15.2950   -18.9227     0.0000
       -10.9250   -18.9227     0.0000
        -6.5550   -18.9227     0.0000
        -2.1850   -18.9227     0.0000
         2.1850   -18.9227     0.0000
         6.5550   -18.9227     0.0000
        10.9250   -18.9227     0.0000
       -17.4800   -15.1381     0.0000
       -13.1100   -15.1381     0.0000
        -8.7400   -15.1381     0.0000
        -4.3700   -15.1381     0.0000
         0.0000   -15.1381     0.0000
         4.3700   -15.1381     0.0000
```

8.7400	-15.1381	0.0000
13.1100	-15.1381	0.0000
-19.6650	-11.3536	0.0000
-15.2950	-11.3536	0.0000
-10.9250	-11.3536	0.0000
-6.5550	-11.3536	0.0000
-2.1850	-11.3536	0.0000
2.1850	-11.3536	0.0000
10.9250	-11.3536	0.0000
15.2950	-11.3536	0.0000
-21.8500	-7.5691	0.0000
-17.4800	-7.5691	0.0000
-13.1100	-7.5691	0.0000
-8.7400	-7.5691	0.0000
-4.3700	-7.5691	0.0000
0.0000	-7.5691	0.0000
4.3700	-7.5691	0.0000
8.7400	-7.5691	0.0000
13.1100	-7.5691	0.0000
17.4800	-7.5691	0.0000
-24.0350	-3.7845	0.0000
-19.6650	-3.7845	0.0000
-15.2950	-3.7845	0.0000
-10.9250	-3.7845	0.0000
-6.5550	-3.7845	0.0000
-2.1850	-3.7845	0.0000
2.1850	-3.7845	0.0000
6.5550	-3.7845	0.0000
10.9250	-3.7845	0.0000
15.2950	-3.7845	0.0000
19.6650	-3.7845	0.0000
-17.4800	0.0000	0.0000
-8.7400	0.0000	0.0000
-4.3700	0.0000	0.0000
4.3700	0.0000	0.0000
8.7400	0.0000	0.0000
17.4800	0.0000	0.0000
21.8500	0.0000	0.0000
-15.2950	3.7845	0.0000
-10.9250	3.7845	0.0000
-6.5550	3.7845	0.0000
-2.1850	3.7845	0.0000
2.1850	3.7845	0.0000
6.5550	3.7845	0.0000
10.9250	3.7845	0.0000
15.2950	3.7845	0.0000
19.6650	3.7845	0.0000
-13.1100	7.5691	0.0000
-8.7400	7.5691	0.0000
0.0000	7.5691	0.0000
4.3700	7.5691	0.0000
8.7400	7.5691	0.0000
13.1100	7.5691	0.0000
17.4800	7.5691	0.0000
-10.9250	11.3536	0.0000
-6.5550	11.3536	0.0000
-2.1850	11.3536	0.0000
2.1850	11.3536	0.0000
10.9250	11.3536	0.0000
15.2950	11.3536	0.0000
-4.3700	15.1381	0.0000
0.0000	15.1381	0.0000
4.3700	15.1381	0.0000

```
          8.7400    15.1381     0.0000
         13.1100    15.1381     0.0000
m1      1001.66c    -0.015896   $ new SS meat, H/Zr=1.6. 0.59% burn-up
       40000.66c    -0.899104
       92235.66c    -0.016728
       92238.66c    -0.068272
mt1     h/zr.60t
        zr/h.60t
m2      6000.66c     1.0        $ graphite
mt2     grph.60t
m3      6000.66c    -0.0004     $ ss cladding
       14000.60c    -0.0046
       24000.50c    -0.190
       25055.66c    -0.009
       26000.50c    -0.699
       28000.50c    -0.097
m4      1001.66c     2.0        $ H2O
        8016.66c     1.0
mt4     lwtr.60t
m5      1001.66c    -0.010   $ Al meat, H/Zr=1.0, 8.91% burnup
       40000.66c    -0.905
       92235.66c    -0.01533
       92238.66c    -0.06967
mt5     h/zr.60t
        zr/h.60t
m6     13027.66c     1.0        $ Al
m7      1001.66c     0.64       $ D20 (68% atom)
        1002.66c     1.36
        8016.66c     1.00
mt7     lwtr.60t
        hwtr.60t
m8     82000.50c     1.0        $ Pb
m9      5010.66c    -0.1566     $ b4c
        5011.66c    -0.6264
        6000.66c    -0.217
m10     1001.66c    -0.00619    $ Concrete
        6000.66c    -0.17520
        8016.66c    -0.41020
       11023.66c    -0.00027
       12000.66c    -0.03265
       13027.66c    -0.01083
       14000.60c    -0.03448
       19000.66c    -0.00114
       20000.66c    -0.32130
       26000.50c    -0.00778
m11     7014.66c     0.0000381259 $Air
        8016.66c     0.0000095012
       18000.59c     0.0000001664
m12     1001.66c    -0.015896   $ Old SS meat, H/Zr=1.6, 8.77% burnup
       40000.66c    -0.899104
       92235.66c    -0.015354
       92238.66c    -0.069646
mt12    h/zr.60t
        zr/h.60t
c
c New SS Fuel (u=1)
f17:n  (100<200[2  -5 0]<201)  (100<200[3  -5 0]<201)
       (100<200[-2 -4 0]<201)  (100<200[0  -4 0]<201)  (100<200[1 -4 0]<201)
       (100<200[2  -4 0]<201)  (100<200[3  -4 0]<201)
       (100<200[-3 -3 0]<201)  (100<200[-2 -3 0]<201)  (100<200[0 -3 0]<201)
       (100<200[2  -3 0]<201)
       (100<200[-3 -2 0]<201)  (100<200[-2 -2 0]<201)  (100<200[0 -2 0]<201)
       (100<200[3  -2 0]<201)
```

```
       (100<200[-3 -1 0]<201)
       (100<200[-2  0 0]<201)  (100<200[-1  0 0]<201)  (100<200[1  0 0]<201)
       (100<200[2   0 0]<201)  (100<200[5   0 0]<201)
       (100<200[-4  1 0]<201)  (100<200[-1  1 0]<201)  (100<200[0  1 0]<201)
       (100<200[1   1 0]<201)  (100<200[3   1 0]<201)
       (100<200[-4  2 0]<201)  (100<200[1   2 0]<201)  (100<200[3  2 0]<201)
       (100<200[-4  3 0]<201)  (100<200[-3  3 0]<201)
       (100<200[-3  4 0]<201)  (100<200[-2  4 0]<201)  (100<200[-1 4 0]<201)
       (100<200[0   4 0]<201)  (100<200[1   4 0]<201)
FS17 -201 -202 -203 -204 -205 -206 -207 -208 -209 -210 -211 -212 -213 -214
     -215 -216 -217 -218 -219 -220 -221 -222 -223 -224 -225 -226 -227 -228
     -229 -230 -231 -232 -233 -234 -235 -236 -237 -238
fq17 s
c
c Old SS Fuel (u=2)
f27:n  (110<200[0  -5 0]<201)  (110<200[5 -5 0]<201)
       (110<200[1  -2 0]<201)  (110<200[2 -2 0]<201)  (110<200[4 -2 0]<201)
       (110<200[-1 -1 0]<201)  (110<200[0 -1 0]<201)  (110<200[1 -1 0]<201)
       (110<200[3  -1 0]<201)
       (110<200[-4  0 0]<201)
       (110<200[-3  1 0]<201)  (110<200[-2 1 0]<201)  (110<200[2  1 0]<201)
       (110<200[-1  2 0]<201)  (110<200[0  2 0]<201)
       (110<200[-2  3 0]<201)  (110<200[-1 3 0]<201)
FS27 -201 -202 -203 -204 -205 -206 -207 -208 -209 -210 -211 -212 -213 -214
     -215 -216 -217 -218 -219 -220 -221 -222 -223 -224 -225 -226 -227 -228
     -229 -230 -231 -232 -233 -234 -235 -236 -237 -238
fq27 s
c
c Al Fuel (u=3)
f37:n  (120<200[-1 -5 0]<201)  (120<200[1 -5 0]<201)  (120<200[4 -5 0]<201)
       (120<200[-1 -4 0]<201)  (120<200[4 -4 0]<201)  (120<200[5 -4 0]<201)
       (120<200[-1 -3 0]<201)  (120<200[1 -3 0]<201)  (120<200[4 -3 0]<201)
       (120<200[5  -3 0]<201)
       (120<200[-4 -2 0]<201)  (120<200[5 -2 0]<201)
       (120<200[-5 -1 0]<201)  (120<200[-4 -1 0]<201) (120<200[-2 -1 0]<201)
       (120<200[4  -1 0]<201)  (120<200[5 -1 0]<201)
       (120<200[4   0 0]<201)
       (120<200[4   1 0]<201)
       (120<200[-3  2 0]<201)  (120<200[2  2 0]<201)
       (120<200[1   3 0]<201)  (120<200[2  3 0]<201)
FS37 -203 -204 -205 -206 -207 -208 -209 -210 -211 -212 -213 -214
     -215 -216 -217 -218 -219 -220 -221 -222 -223 -224 -225 -226 -227 -228
     -229 -230 -231 -232 -233 -234 -235 -236
fq37 s
c
c Instrumented Fuel (u=4)
f47:n  (130<200[-1 -2 0]<201)  (130<200[2 -1 0]<201)
FS47 -201 -202 -203 -204 -205 -206 -207 -208 -209 -210 -211 -212 -213 -214
     -215 -216 -217 -218 -219 -220 -221 -222 -223 -224 -225 -226 -227 -228
     -229 -230 -231 -232 -233 -234 -235 -236 -237 -238
fq47 s
c
f54:n  400   $ FNIF
E54 0 1E-9 5E-9 2.5E-8 1E-7 6.25E-7 2E-6 1E-5 1E-4 1E-3 0.01 0.1
      1 2 4 7 10 15 20
FS54  -217 -218 -219 -220 -221
fq54 s e
f64:n  500   $ TI
E64 0 1E-9 5E-9 2.5E-8 1E-7 6.25E-7 2E-6 1E-5 1E-4 1E-3 0.01 0.1
      1 2 4 7 10 15 20
FS64  -217 -218 -219 -220 -221
fq64 s e
c Mesh tally
```

```
FMESH84:n GEOM=rec ORIGIN=-40 -40 -40
          IMESH=40 IINTS=40
          JMESH=40 JINTS=40
          KMESH=40 KINTS=40
          EMESH=2.5E-8 6.25E-7 0.1 20 EINTS=1 1 1 1  OUT=ij
c CI
F94:n (196<200[0 0 0]<201)
E94 0 1E-9 5E-9 2.5E-8 1E-7 6.25E-7 2E-6 1E-5 1E-4 1E-3 0.01 0.1
      1 2 4 7 10 15 20
FS94  -217 -218 -219 -220 -221
fq94 s e
print
```

APPENDIX B

SAMPLE CALCULATION OF ERROR PROPAGATION

$k_1 = 0.99174$

$\Delta_{k1} = 0.00004$

$k_2 = 1.00650$

$\Delta_{k2} = 0.00004$

$\beta_{eff} = 0.00774$

$\Delta_{\beta eff} = 0.00008$

$$(k_2 +/- \Delta_{k2}) - (k_1 +/- \Delta_{k1}) = L \quad \text{(B.1)}$$

$$(1.00652 +/- 0.00004) - (0.99174 +/- 0.00004) = 0.01476 \quad \text{(B.2)}$$

$$\Delta_L = \sqrt{\Delta_{k2}^2 + \Delta_{k1}^2} \quad \text{(B.3)}$$

$$\sqrt{0.00004^2 + 0.00004^2} = 0.00006 \quad \text{(B.4)}$$

$$(k_2 +/- \Delta_{k2}) * (k_1 +/- \Delta_{k2}) = M \quad \text{(B.5)}$$

$$(1.00650 +/- 0.00004) * (0.99174 +/- 0.00004) = 0.99819 \quad \text{(B.6)}$$

$$0.99819 * \sqrt{\left(\frac{0.00004}{1.00650}\right)^2 + \left(\frac{0.00004}{0.99174}\right)^2} = 0.00006 \quad \text{(B.7)}$$

$$\Delta\rho = \frac{0.01476}{0.99819} = 0.01479 \quad \text{(B.8)}$$

$$\Delta_{\Delta\rho} = \Delta\rho * \sqrt{\left(\frac{\Delta_M}{M}\right)^2 + \left(\frac{\Delta_L}{L}\right)^2} \quad \text{(B.9)}$$

$$0.01479 * \sqrt{\left(\frac{0.00006}{0.99819}\right)^2 + \left(\frac{0.00006}{0.01476}\right)^2} = 0.00006 \quad \text{(B.10)}$$

$$\rho(\$) = \frac{\Delta\rho}{\beta_{eff}} \quad \text{(B.11)}$$

$$\rho(\$) = \frac{0.01479}{0.00774} = \$1.9105 \quad \text{(B.12)}$$

$$\Delta_{\rho\$} = \rho(\$) * \sqrt{\left(\frac{\Delta_{\Delta\rho}}{\Delta\rho}\right)^2 + \left(\frac{\Delta_{\beta eff}}{\beta_{eff}}\right)^2} \quad \text{(B.13)}$$

$$\Delta_{\rho\$} == \$1.9105 * \sqrt{\left(\frac{0.00006}{0.01476}\right)^2 + \left(\frac{0.00008}{0.00774}\right)^2} = 0.0211 \quad \text{(B.14)}$$

REFERENCES

1. General Atomics Electronic Systems, TRIGA Nuclear Reactors, 2012. Web,http://www.ga-esi.com/triga/

2. Sandquist G. M.. U.S. Nuclear Regulatory Commission Training for Research and Training Reactor Inspectors. World Academy of Science, Engineering and Technology 81 **2011**

3. Bess JD. Designing A High-Flux Trap In The University Of Utah TRIGA Reactor. Masters Thesis. University of Utah, 2005

4. University of Utah - Submission of Safety Analysis Report, Technical Specifications and Responses to NRC RAIs. 2010. Document #ML10321004. http://pbadupws.nrc.gov/docs/ML1032/ML103210041.pdf

5. Utah Nuclear Engineering Program, Internal Document. UNEP–SL–Surveillance Procedures and Log.2000 – 2012.

6. Reed Robert Burn, Introduction to Nuclear Reactor Operations, Detroit Edison Company, University of Michigan, 1988

7. Murphy C, Pedersen K, Measurement of Shut Down Margin. Iowa State University and Universidad de Puerto Rico

8. Kimura CY. Reactor Physics Experiments On A TRIGA Mark One Reactor. Masters Thesis. University of Utah, 1979

9. US Department of Energy, DOE Fundamentals Handbook, Nuclear Physics and Reactor Theory.DOE-HDBK-1019. 1993.

10. General Atomics. Kinetic Behavior of TRIGA Reactors, Document GA-7882. Conference on Utilization of Research Reactors, Mexico City, May, 1967.

11. Elmer E. Lewis. Nuclear Reactor Physics. Academic Press, 2008

12. Gacuci, DG. Handbook of Nuclear Engineering. Springer, 2010.

13. Utah Nuclear Engineering Program, Internal Document. Reactor Operation Log Books #33, #34, #35, #36, #37, and #38. 2000 – 2012.

14. Utah Nuclear Engineering Program, Internal Document. UNEP–STL–Start up and Termination Procedures and Logs. 2000 – 2012.

15. Rose Mary Gomes do Prado Souza, Amir Zacarias Mesquita, Fausto Maretti Júnior,Paulo Fernando de Oliveira and Luiz Otávio I. S. Câmara. REACTIVITY POWER COEFFICIENT DETERMINATION, OF THE IPR-R1 TRIGA REACTOR.3rd WORLD TRIGA USERS CONFERENCE August 22 to 25, 2006. Minascentro – Belo Horizonte, Minas Gerais, BRAZIL.

16. Duderstadt JJ, Hamilton LJ. Nuclear Reactor Analysis. John Wiley & Sons; 1976.

17. International Atomic Energy Agency, IAEA-TECDOC-351, RESEARCH REACTORS AND ALTERNATIVE DEVICES FOR RESEARCH, Report Of A Consultants' Meeting On Alternatives To Research Reactors As A Research Tool Organized By The International Atomic Energy Agency And Held In Uppsala, Sweden, 18-21 June 1984

18. Ravnik M. Determination of Research reactor safety parameters by Reactor Calculations. J. Stefan Institute, Ljubljana, Slovenia. Workshop on nuclear data and nuclear reactor; Physics design and safey 2000.

19. Berglund GR. Start Up Test for a TRIGA Mark I Test Reactor. Masters Thesis. University of Utah, 1977.

20. Nuclear Data For The Calculation Of Thermal Reactor Reactivity Coefficients, Proceedings Of An Advisory Group Meeting Organized By The International Atomic Energy Agency And Held In Vienna, 7-10 December 1987

21. Candalino RW. Engineering Analysis Of Low Enriched Uranium Fuel Using Improved Zirconium Hydride Cross Sections. Masters Thesis. Texas A&M University; August 2006

22. Shultis JK, Faw RE. Fundamentals of Nuclear Engineering. New York, New York: Marcel Dekker; 2002.

23. Michalek S, Hascik J,Farkas G. MCNP5 DELAYED NEUTRON FRACTION (β_{eff}) CALCULATION IN TRAINING REACTOR VR. Journal of ELECTRICAL ENGINEERING, VOL. 59, NO. 4, **2008**,pp 221-224

24. Cho NZ. Fundamentals and Recent Developments of Reactor Physics Methods. Nucl Eng Technol 37(1):25-78; **2005**.

25. Engle W.W., Williams L.R. Temperature and Void Reactivity Coefficient Calculations for the High Flux Isotope Reactor Safety Analysis Report. ORNL/TM-12386. Oak Ridge National Laboratory. **1994**.

26. Brown FB, Mosteller RD, Sood A. Verification of MCNP5. Nuclear Mathematical and Computational Science, Proceedings of the American Nuclear Society Mathematics & Computation Topical Meeting. Gatlinburg, Tennessee; American Nuclear Society; **2003**.

27. Choi H, Roh G, Park D. Benchmarking MCNP and WIMS/RFSP Against Measurement Data – II: Wolsong Nuclear Power Plant 2. Nucl Sci Eng 150(1):37-55; **2005**.

28. RSICC Computer Code Collection: MCNP5/MCNPX. Oak Ridge National Laboratory; 2012. http://www-rsicc.ornl.gov/

29. Jeraj R, Glumac B, Maučec M. MCNP Simulation of the TRIGA Mark II Benchmark Experiment. Proceedings of the International Conference for Nuclear Energy in Central Europe '96. Portorož, Slovenia; Nuclear Society of Slovenia; 1996: 66-73

30. Brown FB, Barrett RF, Booth TE, Bull JS, Cox LJ, Forster RA, Goorley TJ, Mosteller RD, Post SE, Prael RE, Selcow EC, Sood A, Sweezy J. MCNP Version 5. Proceedings of the American Nuclear Society 2002 Winter Meeting. Washington, DC; American Nuclear Society; 2002.

31. Sood A, Forster RA, Parsons KD. Analytical Benchmark Test Set for Criticality Code Verification. Prog Nucl Ene 42(1):55-106; **2003**.

32. ENDF/B-VII Evaluated Nuclear Data Fiel. BNL.2011.

33. Wagner JC, Sisolak JE, McKinney GW. MCNP: Criticality Safety Benchmark Problems. LA-12415. Los Alamos National Laboratories; **1993**.

34. Jeraj R, Peršič A, Žagar T, Ravnik M. Sensitivity Studies of the TRIGA Benchmark Critical Experiment. Proceedings of the International Conference for Nuclear Energy in Central Europe '99. Portorož, Slovenia; Nuclear Society of Slovenia, 1999:629-636.

35. Mosteller RD. Testing of the ENDF66 Nuclear Data Library with the MCNP Criticality Validation Suite. Proceedings of the 2003 Annual Meeting of the American Nuclear Society. San Diego, California; American Nuclear Society; 2003.

36. Razvi J.,Bolin J. M., Saurwein J. J., Whittemore W. L., General Atomics. DESIGN AND SAFETY CONSIDERATIONS FOR THE 10 MW(t) MULTIPURPOSE TRIGAREACTOR IN THAILAND. S. Proongmuang Office of Atomic Energy for Peace, Thailand

37. Žagar T, Peršič A, Jeraj R, Ravnik M. Simulation of the TRIGA Mark II Benchmark Experiment with Burned Fuel. Proceedings of the International Conference for Nuclear Energy in Central Europe '99. Portorož, Slovenia; Nuclear Society of Slovenia; 1999: 651-658

38. MATLAB 7.12. Natick, Massachusetts: The Mathworks, Inc.; 2012.

39. Brown FB, Sweezy JE, Hayes R. Monte Carlo Parameter Studies and Uncertainty Analysis with MCNP5. Proceedings of the PHYSOR 2004 Conference. Chicago, Illinois; **2004**.

40. J. Carew, L. Cheng, A. et. al. Physics And Safety Analysis For The NIST Research Reactor. BNL-71695-2003-IR. Brookhaven National Laboratory. **2003**.

41. Lamarsh JR, Baratta AJ. Introduction to Nuclear Engineering. 3rd ed. Reading, Massachusetts: Addison-Wesley Publishing; 2001.

42. Telephone communication between Dr. Dongok Choe at UNEP and Jason Yi, senior technical advisor at General Atomics, San Diego, CA. April 24, 2012.

43. Telephone communication between Avdo Cutic at UNEP and Steve Sampson at Extreme Machine, Logan UT. February, 9, 2012.

44. Booth TE. A Sample Problem for Variance Reduction in MCNP. LA-10363-MS. Los Alamos National Laboratories; **1985**.

45. Oberkampf W.L.; DeLand S.M.; Rutherford B.M.; Diegert K.V.; Alvin K.F. Error and uncertainty in modeling and simulation. Reliability Engineering and System Safety, Volume 75, Number 3, pp. 333-357(25) , March **2002**

46. John Robert Taylor. An Introduction to Error Analysis. University Science Books 1996